

Development of on-wafer calibration methods and planar Schottky diode characterisation at THz frequencies

Krista Dahlberg

Development of on-wafer calibration methods and planar Schottky diode characterisation at THz frequencies

Krista Dahlberg

A doctoral dissertation completed for the degree of Doctor of Science (Technology) to be defended, with the permission of the Aalto University School of Electrical Engineering, at a public examination held at the lecture hall S5 of the school on 24 September 2014 at 12.

Aalto University
School of Electrical Engineering
Department of Radio Science and Engineering

Supervising professor

Prof. Antti Räisänen

Thesis advisors

Dr. Juha Mallat

Dr. Kimmo Silvonen

Dr. Tero Kiuru

Preliminary examiners

Dr. Bertrand Thomas, Radiometer Physics GmbH, Germany

Adj. Prof. Klas Yhland, SP Technical Research Institute of Sweden,
Sweden

Opponent

Prof. Viktor Krozer, Goethe University of Frankfurt am Main, Germany

Aalto University publication series

DOCTORAL DISSERTATIONS 128/2014

© Krista Dahlberg

ISBN 978-952-60-5830-6

ISBN 978-952-60-5831-3 (pdf)

ISSN-L 1799-4934

ISSN 1799-4934 (printed)

ISSN 1799-4942 (pdf)

<http://urn.fi/URN:ISBN:978-952-60-5831-3>

Unigrafia Oy

Helsinki 2014

Finland



Author

Krista Dahlberg

Name of the doctoral dissertation

Development of on-wafer calibration methods and planar Schottky diode characterisation at THz frequencies

Publisher School of Electrical Engineering**Unit** Department of Radio Science and Engineering**Series** Aalto University publication series DOCTORAL DISSERTATIONS 128/2014**Field of research** Radio Engineering**Manuscript submitted** 9 May 2014**Date of the defence** 24 September 2014**Permission to publish granted (date)** 25 August 2014**Language** English **Monograph** **Article dissertation (summary + original articles)****Abstract**

This thesis focuses on development of on-wafer calibration methods for S-parameter measurements and Schottky diode characterisation at millimeter wave and terahertz frequencies. The radio frequency characteristics of components at the wafer level are obtained using on-wafer S-parameter measurements with a vector network analyzer. In general an error network including eight error terms is used to calibrate the on-wafer S-parameter measurements, but in measurement configurations affected by leakage the use of full 16-term error network can be profitable.

In this thesis a novel 16-term calibration method based on reciprocity conditions of the error network is introduced and demonstrated with simulations and practical on-wafer measurements. The developed calibration method enables the calibration of the full 16-term error network using only four calibration standards. The method is limited to second-tier calibration of reciprocal error networks with a pre-calibrated network analyzer, when the reciprocity assumption is valid. Also a novel method to determine Line-Reflect-Reflect-Match (LRRM) calibration standards for reciprocal 16-term error network is presented. The Line standard and the resistance of the Match standard need to be exactly known and the reactances of the two unknown lossless reflect standards (typically Short and Open) and the Match standard are solved using the raw S-parameter data of the calibration standard measurements. The accuracy of the known S-parameters or self-calibration results of the calibration standards can be verified as a by-product of the 16-term reciprocal calibration. LRRM is only one possible combination of the four calibration standards to solve the reciprocal 16-term error network. In this thesis all possible non-singular combinations are solved with a simulation approach.

Schottky diodes are significant components in the millimeter wave and terahertz frequency applications. Traditionally Schottky diodes are characterised by current-voltage, capacitance-voltage, and S-parameter measurements. The design of the millimeter wave and terahertz diode mixers relies heavily on the extracted parameters from the traditional characterisation measurements. However, the diode operation in the final application such as a mixer cannot be completely predicted by using the extracted parameters. In this thesis a novel mixer-based characterisation method of discrete planar Schottky diodes is presented. A fundamental mixer test jig for single-anode Schottky diodes and a subharmonic mixer test jig for antiparallel Schottky diodes are developed to characterize and compare the mixer operation of different diodes at 183 GHz.

Keywords calibration, mixer, on-wafer measurements, Schottky diode, S-parameter measurements**ISBN (printed)** 978-952-60-5830-6**ISBN (pdf)** 978-952-60-5831-3**ISSN-L** 1799-4934**ISSN (printed)** 1799-4934**ISSN (pdf)** 1799-4942**Location of publisher** Helsinki**Location of printing** Helsinki**Year** 2014**Pages** 174**urn** <http://urn.fi/URN:ISBN:978-952-60-5831-3>

Tekijä

Krista Dahlberg

Väitöskirjan nimi

On-wafer-kalibrointimenetelmien ja planaarien Schottky-diodien karakterisoinnin kehittäminen THz-taajuuksilla

Julkaisija Sähkötekniikan korkeakoulu**Yksikkö** Radiotieteen ja -tekniikan laitos**Sarja** Aalto University publication series DOCTORAL DISSERTATIONS 128/2014**Tutkimusala** Radiotekniikka**Käsikirjoituksen pvm** 09.05.2014**Väitöspäivä** 24.09.2014**Julkaisuluvan myöntämispäivä** 25.08.2014**Kieli** Englanti **Monografia** **Yhdistelmäväitöskirja (yhteenvedo-osa + erillisartikkelit)****Tiivistelmä**

Tämä väitöskirja käsittelee millimetriaalto- ja terahertsialueen on-wafer-sirontaparametrimittauksen kalibrointimenetelmien sekä Schottky-diodien karakterisoinnin kehittämistä. Piirianalysointilla tehdyillä on-wafer-sirontaparametrimittauksilla saadaan selvitettyä komponenttien radiotaajuiset ominaisuudet. Yleensä on-wafer-sirontaparametrimittauksen kalibroinnissa käytetään 8-termistä virhepiiriä, mutta mittausjärjestelmissä, joissa esiintyy mittausporttien välistä signaalin ohivuotoa, voi 16-termisen virhepiirin käyttö olla hyödyllistä.

Työssä esitellään uusi resiprookkisuusehtoihin perustuva 16-terminen kalibrointimenetelmä, jota havainnollistetaan simulaatioilla ja käytännön on-wafer-mittauksilla. Kalibrointimenetelmä mahdollistaa täyden 16-termisen virhepiirin kalibroinnin käyttämällä vain neljää kalibrointistandardia. Menetelmä rajoittuu resiprookkisen virhepiirin kalibrointiin esikalibroidulla piirianalysointilla, jolloin on perusteltua olettaa piiri resiprookkiseksi. Työssä on myös kehitetty uusi menetelmä määrittämään resiprookkisen 16-termisen virhepiirin Line-Reflect-Reflect-Match (LRRM) kalibrointistandardit. Siirtojohto-standardi sekä sovitetun päätteen resistanssi täytyvät olla täysin tunnettuja. Kahden tuntemattoman heijastusstandardin (tyypillisesti oikosulku ja avoin pääte) sekä sovitetun päätteen reaktanssit saadaan ratkaistua kalibrointistandardien S-parametrimittauksen raakadatasta. Kalibrointistandardien todellisten S-parametrien tai itsekalibrointitulosten tarkkuus voidaan tarkastaa 16-termisen resiprookkisen kalibroinnin sivutuotteena. LRRM on vain yksi mahdollinen neljän kalibrointistandardin kombinaatio, jolla resiprookkinen 16-terminen virhepiiri voidaan ratkaista. Tässä työssä on etsitty simuloinnin avulla kaikki mahdolliset ei-singulaariset kombinaatiot.

Schottky-diodit ovat tärkeitä komponentteja millimetriaalto- ja terahertsialueen sovelluksissa. Perinteisesti Schottky-diodit karakterisoidaan virta-jännite-, kapasitanssi-jännite- ja S-parametrimittauksilla. Millimetriaalto- ja terahertsialueen sekoitus suunnittelu pohjautuu perinteisistä mittauksista ekstraktoituihin parametreihin. Diodien toimintaa lopullisessa sovelluksessa kuten sekoittimissa ei voida kuitenkaan täysin ennustaa näiden ekstraktoitujen parametrien avulla. Työssä esitellään uusi sekoitintoimintaan perustuva erillisten planaarien Schottky-diodien karakterisointimenetelmä. Perustaja juinen sekoitintestialusta on kehitetty yksianodisten Schottky-diodien toiminnan karakterisointiin ja vertailuun, ja aliharmonen sekoitintestialusta vastakkaisuuntaisten Schottky diodien karakterisointiin ja vertailuun 183 GHz:n taajuudella

Avainsanat kalibrointi, on-wafer-mittaukset, Schottky-diodi, sekoitin, S-parametrimittaukset**ISBN (painettu)** 978-952-60-5830-6**ISBN (pdf)** 978-952-60-5831-3**ISSN-L** 1799-4934**ISSN (painettu)** 1799-4934**ISSN (pdf)** 1799-4942**Julkaisupaikka** Helsinki**Painopaikka** Helsinki**Vuosi** 2014**Sivumäärä** 174**urn** <http://urn.fi/URN:ISBN:978-952-60-5831-3>

Preface

My warmest thanks go to my supervisor, Professor Antti Räsänen, for giving me the opportunity to work on this interesting topic and for his guidance during the thesis work. I am very thankful to my instructors, Dr. Juha Mallat, Dr. Kimmo Silvonen, and Dr. Tero Kiuru, for shearing their remarkable expertise with me and for always having time to advise me. I have learned a lot from you. I also want to thank Dr. Tapani Närhi for his contribution to the work in this thesis.

I want to thank all my present and former colleagues at the Department of Radio Science and Engineering for the past years. Thank you Aleks, Antti, Eikka, Jari, Late, Olli, Pekka, Sampo, Subash, Timo, Tom, Tomas, Veli-Matti, Viki, Zhou, and many more.

The work included in this thesis has been supported by the Graduate School of Faculty of Electronics, Communications and Automation, European Space Agency (ESA), and Academy of Finland through its Centre of Excellence program SMARAD. I highly appreciate the financial support from Finnish Foundation for Technology Promotion, Finnish Society of Electronics Engineers, HPY Research Foundation, Jenny and Antti Wihuri Foundation, Nokia Foundation, and Emil Aaltonen Foundation.

I am grateful to the pre-examiners, Adj. Prof. Klas Yhland and Dr. Bertrand Thomas, for their valuable comments on the manuscript.

I would like to thank my parents and siblings for supporting and encouraging me during all these years.

Finally, my deepest thanks go to my spouse for your patience and endless support. Writing of this thesis would not have been possible without you.

Espoo, August 26, 2014,

Krista Dahlberg

Contents

Preface	7
Contents	9
List of Publications	11
Author's Contribution	13
List of Symbols	15
List of Abbreviations	19
1. Introduction	21
1.1 Motivation and scope of the thesis	21
1.2 Scientific contribution of the thesis.....	23
2. Calibration of on-wafer S-parameter measurements	25
2.1 Two-port (four-receiver) vector network analyzer	25
2.1.1 Switching error correction.....	27
2.1.2 Measurement configuration	27
2.2 Error correction and calibration standards	28
2.3 Error models and calibration methods	30
2.3.1 16-term error model.....	30
2.3.2 12-term error model.....	32
2.3.3 10- and 8-term error models	33
2.4 Selection of a suitable calibration method.....	35
3. Calibration of the reciprocal 16-term error network	37
3.1 Definition of the LRRM calibration standards	38
3.2 16-term calibration based on reciprocity conditions	42
3.3 Accuracy of the calibration standards.....	49
3.4 Combinations of calibration standards.....	52

3.5 Discussion and future work.....	55
4. Millimeter wave planar Schottky diodes and mixers	57
4.1 Schottky diode structure and characteristics	57
4.2 Traditional Schottky diode measurements.....	61
4.3 Millimeter wave Schottky diode mixers.....	64
4.3.1 Single-diode mixers	66
4.3.2 Subharmonic mixers.....	67
4.4 Waveguide-to-planar transmission line transitions	68
5. Mixer-based characterisation of Schottky diodes	71
5.1 Waveguide-to-suspended microstrip line transition.....	72
5.2 Fundamental mixer test jig.....	74
5.3 Subharmonic mixer test jig.....	80
5.4 Comparison of traditional Schottky diode characterisation and mixer-based characterisation	83
5.4.1 Fundamental mixer test jig	83
5.4.2 Subharmonic mixer test jig	85
5.5 Discussion and future work.....	87
6. Summary of articles	91
7. Conclusions and future work	95
References	99
Errata	115
Publications	117

List of Publications

This thesis consists of an overview and the following publications which are referred in the text by their Roman numerals.

- [I] K. Silvonen, K. Dahlberg, and T. Kiuru, "16-term error model in reciprocal systems," *IEEE Transactions on Microwave Theory and Techniques*, vol. 60, no. 11, pp. 3551-3558, Nov. 2012.
- [II] K. Dahlberg and K. Silvonen, "A method to determine LRRM calibration standards in measurement configurations affected by leakage," *IEEE Transactions on Microwave Theory and Techniques*, accepted for publication, 2014.
- [III] K. Dahlberg, K. Silvonen, and T. Kiuru, "A method for testing accuracy of the calibration standards based on reciprocity conditions of the error network," *Microwave and Optical Technology Letters*, vol. 56, no. 5, pp. 1036-1040, May 2014.
- [IV] K. Dahlberg, K. Silvonen, and T. Kiuru, "On-wafer characterisation of test-fixtures in the presence of cross-talk," in *Microwave Technologies and Techniques Workshop*, ESA/ESTEC, Noordwijk, The Netherlands, May 21-23, 2012.
- [V] K. Dahlberg, T. Kiuru, J. Mallat, A. V. Räisänen, and T. Närhi, "Simple waveguide-to-suspended microstrip transition with low-pass filter," in *Proceedings of 40th European Microwave Conference*, Paris, France, Sept. 28-30, 2010, pp. 671-674.
- [VI] K. Dahlberg, T. Kiuru, J. Mallat, A. V. Räisänen, and T. Närhi, "Generic jig for testing mixing performance of millimeter wave Schottky diodes," in *Proceedings of 41st European Microwave Conference*, Manchester, UK, Oct. 10-13, 2011, pp. 922-925.
- [VII] K. Dahlberg, T. Kiuru, J. Mallat, T. Närhi, and A. V. Räisänen, "Mixer-based characterisation of millimeter wave and terahertz single-anode and antiparallel Schottky diodes," *IEEE Transactions on Terahertz Science and Technology*, accepted for publication, 2014.

Author's Contribution

- [I] This is a result of collaborative work. The idea of the 16-term calibration method based on the reciprocity conditions was proposed by Dr. Kimmo Silvonen and he was responsible for derivation of the equations and writing the publication. The author carried out the simulations and measurements, processed the measured data, and was responsible for writing the measurement part of the publication. Dr. Tero Kiuru helped with the simulations and measurements.
- [II] This is a result of collaborative work. The idea of the method to determine the LRRM calibration standards in measurement configuration with leakage was proposed by Dr. Kimmo Silvonen and he was responsible for derivation of the equations. The simulations, measurements and processing of the measured data were done by the author. The author was responsible for writing the publication.
- [III] The work was mainly done by the author. The idea of the method for testing the accuracy of the calibration standards using the reciprocity conditions of the error network was proposed by the author. The simulations, measurements and data processing were done by the author. The author was responsible for writing the publication. Dr. Kimmo Silvonen and Dr. Tero Kiuru instructed the work.
- [IV] The work was mainly done by the author. The idea of the publication was proposed by the author. The author was responsible for the simulation approach to find out the possible combinations of the calibration standards for the 16-term calibration method based on reciprocity conditions of the error network. The author carried out the measurements and was responsible for writing of the publication. Dr. Kimmo Silvonen and Dr. Tero Kiuru instructed the work.

- [V] The work was mainly done by the author. The author designed the waveguide-to-suspended microstrip transition, carried out the simulations and measurements, and was responsible for writing the publication. Dr. Tero Kiuru helped with the simulations and measurements. Dr. Juha Mallat and Dr. Tapani Närhi instructed the work.
- [VI] This is a result of collaborative work. The idea was formulated by the author, Dr. Tero Kiuru, and Dr. Tapani Närhi. The author, Dr. Tero Kiuru, and Dr. Juha Mallat designed the generic test jig for characterisation of single-anode Schottky diodes. The author carried out the simulations and the measurements, and assembled the device. The mechanical structure of the device was designed by the author, Dr. Tero Kiuru, and Mr. Eino Kahra. The author was responsible for writing the publication.
- [VII] The work was mainly done by the author. The idea was formulated by the author and Dr. Tero Kiuru. The author, Dr. Tero Kiuru, and Dr. Juha Mallat designed the subharmonic test jig for characterisation of antiparallel Schottky diodes. The author carried out the simulations and measurements, and assembled the devices. The mechanical structure of the subharmonic mixer test was designed by the author and Mr. Eino Kahra. The author was responsible for writing the publication. Dr. Tapani Närhi instructed the work

List of symbols

a	Auxiliary variable
a_i, a_i'	Voltage wave at port i
A, B, C, D	Actual S-parameters of the standards
A	Attenuation
A_f	1/f noise coefficient
A^{**}	Modified Richardson constant
b	Auxiliary variable
b_i, b_i'	Voltage wave at port i
c	Auxiliary variable
C_{g1}, C_{g2}	Pad edge-to-ground capacitance
C_j	Junction capacitance
C_{j0}	Zero-bias junction capacitance
C_p	Parasitic pad-to-pad capacitance
C_T	Total capacitance
$e_{00}\dots e_{33}$	S-parameters of the error network
E	S-parameter error network matrix
$E_1\dots E_4$	Submatrices of S-parameter error network
E_{DF}, E_{DR}	Directivity (F = forward direction, R = reverse direction)
E_{LF}, E_{LR}	Load match
E_{RF}, E_{RR}	Reflection tracking
E_{SF}, E_{SR}	Source match
E_{TF}, E_{TR}	Transmission tracking
E_{XF}, E_{XR}	Transmission leakage
f_c	Cutoff frequency
f_{IF}	Intermediate frequency
f_{LO}	Local oscillator frequency
f_{RF}	Radio frequency
F	Auxiliary matrix
F_{fe}	1/f noise coefficient
I	Current
I_{sat}	Saturation current
k	Scaling factor
k_B	Boltzmann's constant

List of symbols

K_f	1/f noise coefficient
l	Length of the line
L_C	Mixer conversion loss
L_{DSB}	DSB conversion loss
L_f	Finger inductance
L_i	Conversion loss at the image frequency
L_{match}	Inductance of the Match standard
L_{RF}	Attenuation of the RF chain
L_s	Conversion loss at the signal frequency
m_i	Auxiliary variable
M	Reflection coefficient of the Match standard
\mathbf{M}	Auxiliary matrix
$\mathbf{M}_A, \mathbf{M}_B, \mathbf{M}_C, \mathbf{M}_D$	Measured raw S-parameters of the standards
n_i	Auxiliary variable
\mathbf{N}	Auxiliary matrix
N_{freq}	Number of frequency points
P_C	Noise power with cold load
P_H	Noise power with hot load
P_{IF}	Output power at the intermediate frequency
P_{RF}	Input power at the signal frequency
q	Electron charge
R	Reflection coefficient of the Open standard
r_j	Junction resistance
R_M	Resistance of the Match standard
R_S	Series resistance
S	Reflection coefficient of the Short standard
S	Area of the junction
\mathbf{S}_a	Actual S-parameters of the DUT or standards
S_{ij}	S-parameters
\mathbf{S}_m	Measured raw S-parameters of the DUT or standards
$t_0 \dots t_{15}$	T-parameters of the error network
T	Transmission coefficient of the Thru standard
\mathbf{T}	T-parameter error network matrix
$\mathbf{T}_1 \dots \mathbf{T}_4$	Submatrices of T-parameter error network
T_a	Ambient temperature
T_C	Noise temperature of the cold load
T_C^r	Corrected noise temperature of the cold load
T_e	Noise temperature of the receiver in the measurement setup
T_H	Noise temperature of the hot load
T_H^r	Corrected noise temperature of the hot load

T_{IF}	Noise temperature of the IF chain
T_J	Junction temperature
T_M	Mixer noise temperature
u	Auxiliary variable
\mathbf{U}	Auxiliary matrix
V	Voltage
\mathbf{V}	Auxiliary matrix
w	Auxiliary variable
\mathbf{W}	Auxiliary matrix
x	Auxiliary variable
X	Unknown reactance of the Match standard
y	Arbitrary scaling factor
Y	Y-factor
Z_o	Characteristic impedance
Z_{L_o}	Reverse load impedance
Z_{L_3}	Forward load impedance
Z_{S_o}	Forward source impedance
Z_{S_3}	Reverse source impedance
α	Attenuation constant
β	Phase constant
γ	Doping profile parameter of the epitaxial layer
δS	Similarity index
Δt	Delay
η	Ideality factor
Φ_B	Schottky barrier voltage
Φ_{bi}	Built-in potential
ω	Angular frequency

List of abbreviations

ACST	Advanced Compound Semiconductor Technologies GmbH
ADS	Advanced Design System
AM	Amplitude modulation
BWO	Backward wave oscillator
CPW	Coplanar waveguide
C-V	Capacitance-voltage
DC	Direct current
DSB	Double sideband
DUT	Device under test
GaAs	Gallium arsenide
HEB	Hot electron bolometer
HEMT	High electron mobility transistor
HFSS	High Frequency Structural Simulator
IF	Intermediate frequency
ISS	Impedance standard substrate
I-V	Current-voltage
LNA	Low-noise amplifier
LO	Local oscillator
LRL	Line-Reflect-Line
LRM	Line-Reflect-Match
LRRM	Line-Reflect-Reflect-Match
LSF	Least-squares-fit
LSM	Line-Short-Match
LSO	Line-Short-Open
LZZ	Line-offset offset-Open offset-Short
MIC	Microwave integrated circuit
MMIC	Monolithic microwave integrated circuit
MSO	Match-Short-Open
NIST	U.S. National Institute on Standards and Technology
RAL	Rutherford Appleton Laboratory
RF	Radio frequency
SiO ₂	Silicon dioxide
SIS	Superconductor-insulator-superconductor

List of abbreviations

SOLR	Short-Open-Load-Reciprocal
SOLT	Short-Open-Load-Thru
SSB	Single sideband
TCX	Thru-Circuit-Unknown
TMSO	Thru-Match-Short-Open
TRL	Thru-Reflect-Line
TRM	Thru-Reflect-Match
TRRM	Thru-Reflect-Reflect-Match
TSD	Thru-Short-Delay
UMS	United Monolithic Semiconductors
UVa	University of Virginia
VDI	Virginia Diodes Inc.
VNA	Vector network analyzer

1. Introduction

The terahertz region covers the frequency range between 0.3 – 3 THz of the electromagnetic spectrum corresponding to the wavelengths from 1 mm to 100 μm [1], whereas millimeter waves define the frequencies between 30 – 300 GHz that correspond wavelengths from 10 mm to 1 mm [2]. The terahertz region was earlier known as submillimeter waves. In the frequency scale below the millimeter waves are the microwaves (1 – 30 GHz) and above the terahertz region is the infrared region (3 – 430 THz).

The millimeter wave and terahertz regions are to a great extent unoccupied by commercial applications. The available bandwidth is much wider than at microwave frequencies enabling considerably higher data rates. At higher frequencies circuits with small size and weight can be realized, because the dimensions are proportional to the wavelength. However, the drawback is that the fabrication becomes more challenging and more expensive. Also the interfaces between devices are a challenge at high frequencies. The high atmospheric losses limit significantly the transmission range of the systems, but then again the strong effect of the atmosphere enables the atmospheric research at millimeter wave and terahertz frequencies. Many of the strong resonances of different gas molecules are located in the millimeter wave and terahertz region, e.g., oxygen and water vapor.

Millimeter wave and terahertz technologies are quickly developing fields and the earliest applications are from the 1960's. Important application areas at millimeter wave and terahertz frequencies are: radar [3], communications [4], [5], space science [6], Earth observation [7], [8], radio astronomy [9], [10], imaging [11], [12], plasma diagnostics [13], [14], and biology and medicine [15]. The majority of the applications are scientific, but also commercial applications become gradually available.

1.1 Motivation and scope of the thesis

The fast development of monolithic microwave integrated circuits (MMICs) has contributed also to the development of the on-wafer measurements [16]. MMIC is a circuit where the passive and active components are

fabricated on a same substrate wafer [17], [18]. The difference between MMICs and microwave integrated circuits (MICs) is that in MICs discrete active and passive components are integrated on a common substrate, e.g., by soldering. The on-wafer S-parameter measurements performed with a vector network analyzer (VNA) are used to obtain the radio frequency (RF) characteristics of the components and devices at the wafer level. That makes the on-wafer measurements significant part of the development process of the devices. There are two different directions in the development of the on-wafer measurements: to go higher frequencies and to reduce the costs at low-frequencies [16]. At low frequencies the main target is to lower the price of the probes, which are needed to make the contact to the wafer. At higher frequencies the development of the probes as well as the calibration methods are the primary objectives. Today there are probes already up to 900 GHz [19].

To get accurate S-parameter measurements an accurate calibration is also required. The high frequency and on-wafer environment introduce challenges for the calibration and the measurements. In the coaxial and waveguide environments as well as in the low frequency on-wafer measurements (< 110 GHz) traditional calibration methods based on 8 or 12 error terms are accurate enough. However, in high frequency on-wafer S-parameter measurements the leakage paths, e.g., probe-to-probe cross-talk, may be significant, and thus calibration methods based on 16-term error models can be advantageous, although the cross-talk can be reduced slightly with a proper probe design, e.g., small contact area [16].

Schottky diodes are essential components in applications at millimeter wave and terahertz frequencies, e.g., in Earth observation and space science [6], [20]. Therefore the development of the Schottky diodes is crucial. The characterisation of the Schottky diodes is a significant part of the diode development process and thus also the characterisation methods need to be improved to model the diodes accurately. Traditionally the Schottky diodes are characterized by current-voltage (I-V), capacitance-voltage (C-V), and S-parameter measurements. From the characterisation measurement results the diode parameters are extracted and an equivalent circuit is created to find out the behavior and the quality of the diodes. Accurate on-wafer S-parameter measurements are an important part of the characterisation and modelling as well as designing of the devices. However, the diode operation in the actual device, e.g. mixer, cannot be seen directly from the traditional Schottky diode characterisation results. To obtain comprehensive characterisation of Schottky diodes, e.g., mixer-based characterisation could be profitable in addition to the traditional characterisation.

This thesis discusses the development of on-wafer S-parameter calibration methods and mixer-based characterisation of Schottky diodes at millimeter wave and terahertz frequencies. A novel calibration method based on reciprocity conditions of the error network is presented to calibrate the full 16-term error network and a mixer-based characterisation method is designed for characterisation of discrete single-anode and antiparallel Schottky diodes at 183 GHz. This frequency is significant, because one of the resonance frequencies of water vapor is located at that frequency. The mixer test jigs are useful tools for diode manufacturers who can test or compare their diodes without designing and fabricating a fixed tuned mixer for every diode.

The thesis is organized as follows. In Chapter 2 the vector network analyzer, different error models, and different calibration methods are introduced. Chapter 3 presents the novel 16-term calibration method based on reciprocity conditions of the error network and the novel method to determine Line-Reflect-Reflect-Match (LRRM) calibration standards reported in publications [I] – [IV]. In Chapter 4 the principles of Schottky diodes and millimeter wave Schottky diode mixers are discussed. Chapter 5 presents the mixer-based Schottky diode characterisation method reported in publications [V] – [VII]. Chapter 6 summarizes the publications related to the thesis and Chapter 7 concludes the work done in this thesis.

1.2 Scientific contribution of the thesis

The scientific contributions in this thesis are:

1. A novel 16-term calibration method for reciprocal error networks. The use of the reciprocity conditions to reduce the number of unknown error terms allows the calibration of the full 16-term error network using only four calibration standards. [I]
2. A novel method to determine calibration standards for LRRM calibration in measurement configurations affected by leakage. The reactances of the Match, Open and Short standards are calculated from measured raw S-parameter data of the standards. The line standard and the resistance of the Match standard need to be exactly known. [II]
3. A method for testing the accuracy of the actual known S-parameters or self-calibration results of the calibration standards. The method is based on the reciprocity conditions of the 16-term error network and

it is a by-product of the 16-term calibration method presented in [I]. [III]

4. A mixer-based characterisation method for discrete single-anode and antiparallel Schottky diodes at millimeter wave and terahertz frequencies. The fundamental and subharmonic mixer test jigs can be used for characterisation and comparison of different diodes in a uniform mixer environment. It is a supplementary characterisation method in addition to the traditional characterisation methods of Schottky diodes. The diode manufacturers can use the mixer test jigs to test the mixer operation of their diode without the need to design and fabricate a fixed tuned mixer for every diode. [VI], [VII]

2. Calibration of on-wafer S-parameter measurements

On-wafer measurements have a significant role in millimeter wave and terahertz device testing. Modelling of devices rely heavily on accurate wideband S-parameter measurements performed using a vector network analyzer (VNA) [21], [22]. Therefore accurate measurement results are very important and to achieve accurate measurement results, good calibration accuracy is required especially at higher frequencies.

In this chapter basics of the vector network analyzer and different error models as well as different methods for calibration of the vector network analyzer are presented.

2.1 Two-port (four-receiver) vector network analyzer

A vector network analyzer is used to measure the scattering parameters, i.e., S-parameters of high frequency circuits. The S-parameters represent the frequency response of the circuit and describe completely the electrical behavior of a linear circuit [23]. At low frequencies circuits are mainly represented using impedance and admittance parameters, i.e., Z- and Y-parameters, respectively. For high frequency circuits the S-parameter representation is the most suitable, because a straight measurement of total currents and voltages is challenging. The S-parameters are obtained measuring the incident, reflected and transmitted waves separately for every frequency point. The measurement is done using a low level sinusoidal signal, so that the device under test (DUT) is working linearly. When too high a signal level is used especially active circuits start to work nonlinearly, whereas with too a low signal level the noise may disturb the signal [24]. Z- and Y-parameters can be derived from S-parameters using transformation formulas.

A block diagram of a two-port VNA is presented in Figure 2.1. The switches connect the signal source and load in turn to the measurement ports 1 and 2. With four single directional couplers part of the signal is coupled to the measurement channels a_0 , b_0 , a_3 , and b_3 [25]. In Figure 2.1

the switch is in forward position, thus a_0 measures the signal coming to port 1, b_0 measures the signal reflected from port 1, b_3 measures the signal passing through the DUT, and a_3 measures the signal reflected from the load. The term ‘four-receiver vector network analyzer’ comes from the number of the measurement channels. Only two-port devices can be measured, but the VNA has four measurement channels, which allows removing of the non-ideality of the switches while simultaneously modelling the measurement channel. VNAs with three measurement channels are also available. Although the three-receiver VNA has simpler structure and it is less expensive, the error correction is more advanced with the four-receiver VNA [26].

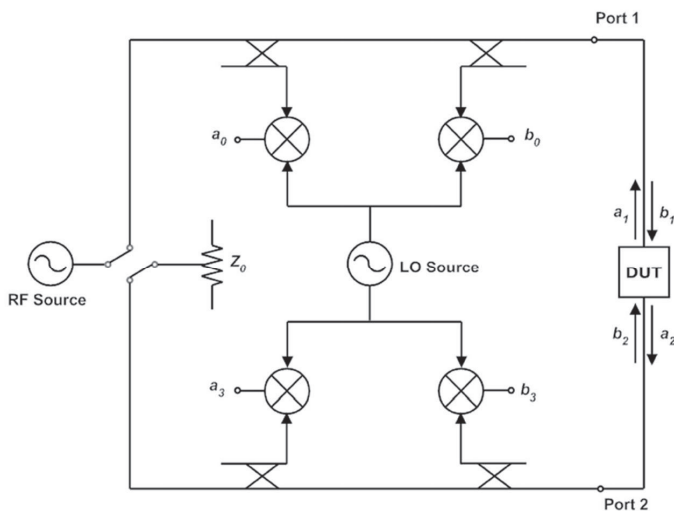


Figure 2.1.Block diagram of a two-port vector network analyzer.

The S-parameters measured with a VNA are in complex format, thus both magnitude and phase can be measured. With a scalar network analyzer only the magnitude can be measured. The measurement of both magnitude and phase components is required for several reasons: fully characterisation of linear circuits, time-domain characterisation, effective error correction, accurate circuit simulation models, and designing of matching networks [23]. The S-parameters of the DUT are determined using the measured complex voltage waves

$$S_{m11} = \frac{b_0}{a_0}, \tag{2.1}$$

$$S_{m12} = \frac{b_0'}{a_3}, \tag{2.2}$$

$$S_{m21} = \frac{b_3}{a_0}, \quad (2.3)$$

$$S_{m22} = \frac{b'_3}{a'_3}, \quad (2.4)$$

where the prime indicates the reverse position of the switches. Because the measurement of the complex voltage is challenging at high frequencies the measured signals from couplers are mixed to lower frequencies, where the measurements are easier.

2.1.1 Switching error correction

The internal switches of the VNA change the network configuration between forward and reverse measurement and non-ideality of the switches causes errors. Either the forward source impedance (Z_{S0}) is not equal to the reverse load impedance (Z_{L0}) or the forward load impedance (Z_{L3}) is not equal to the reverse source impedance (Z_{S3}). This is demonstrated in Figure 2.2 according to [27]. The switching error correction can be used only with an analyzer with four measurement channels [27], [28]. The equations for switching error correction can be found in [27].

In one-tier calibration the calibration is done at once for the whole measurement system and the switching errors need to be corrected. In two-tier calibration the network analyzer is first calibrated at the coaxial or waveguide ports and the test-fixture or the probe part is then calibrated separately with own calibration standards. The switching error correction is not needed when the second-tier calibration is used with a pre-calibrated VNA [27].

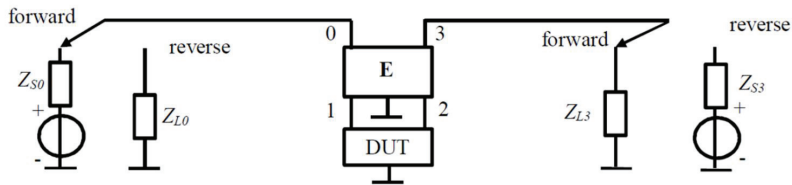


Figure 2.2. Source and load impedances in forward and reverse measurements.

2.1.2 Measurement configuration

The idea of the S-parameter measurements can be presented with the block diagrams shown in Figure 2.3 according to [29]. The block diagram a) presents the measurement and calibration situation in practice from the user's point of view, where the DUT (or standard) with S-parameters S_a is

connected to a non-ideal VNA. The block diagram b) shows the theoretical measurement situation, where the ideal network analyzer is connected to the DUT through a four-port error network E . The block diagram c) shows the actual measurement situation, where the measured raw (not calibrated) S-parameters of the DUT (or standard) S_m including the error network E and the actual S-parameters of the DUT S_a are measured by an ideal network analyzer.

The actual S-parameters of the DUT (or standard) S_a and the measured raw S-parameters S_m can be defined using the voltage waves:

$$\begin{bmatrix} a_1 \\ a_2 \end{bmatrix} = S_a \begin{bmatrix} b_1 \\ b_2 \end{bmatrix} = \begin{bmatrix} S_{a11} & S_{a12} \\ S_{a21} & S_{a22} \end{bmatrix} \begin{bmatrix} b_1 \\ b_2 \end{bmatrix}, \quad (2.5)$$

$$\begin{bmatrix} b_0 \\ b_3 \end{bmatrix} = S_m \begin{bmatrix} a_0 \\ a_3 \end{bmatrix} = \begin{bmatrix} S_{m11} & S_{m12} \\ S_{m21} & S_{m22} \end{bmatrix} \begin{bmatrix} a_0 \\ a_3 \end{bmatrix}. \quad (2.6)$$

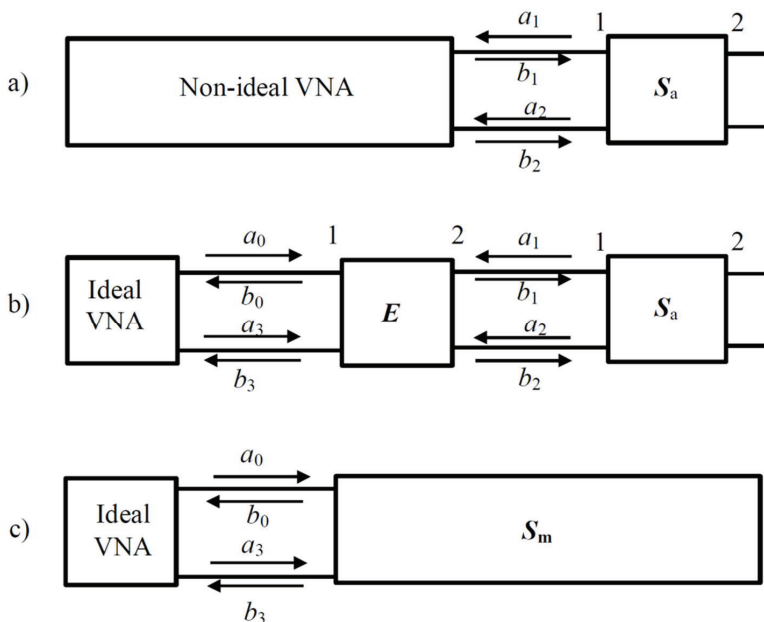


Figure 2.3. Block diagrams of the measurement configuration. a) Practical measurement situation, b) theoretical measurement situation, c) actual measurement situation.

2.2 Error correction and calibration standards

The measured S-parameters S_m include systematic errors, which are represented with the error network E . Calibration means removal of these systematic errors during or after the measurements. The typical error sources causing systematic errors can be, e.g., imperfection of directional

couplers, cables, adapters, and on-wafer probes [30]-[32]. The calibration does not correct for random errors that are not predictable, e.g., noise, dynamic range, and repeatability of the cables [31], [32]. The random errors caused by noise can be reduced by increasing source power, narrowing intermediate frequency (IF) bandwidth, or using averaging [32]. The change in the performance of the VNA after the calibration is called drift error, which is caused mainly by temperature variations. The speed of the drift defines how often an additional calibration is needed and the errors can be minimized by using a controlled temperature [32]. In practice calibration means that the parameters of the error network need to be determined to get the actual S-parameters of the DUT. This is done by measuring known calibration standards.

Usually the calibration standards are passive, well known components, but when the self-calibration is used, some of the S-parameters of the calibration standards can be unknown and solved during the calibration. The following calibration standards are typically used in the calibration:

- **Thru, T:** transmission line (typically $50\ \Omega$ and zero-length). For on-wafer measurements a true Thru standard does not exist, because the probes cannot be connected directly to each other and thus a short transmission line is used as a Thru standard.
- **Line, L:** short transmission line (typically $50\ \Omega$), which defines the normalization impedance.
- **Delay, D:** the same as Line, typically the length of the Delay is $20^\circ - 160^\circ$ different than Thru.
- **Reflect, R:** an unknown reflective termination; the reflection coefficient does not need to be known, but needs to be the same in both measurement ports. Usually used in self-calibration methods. Typically Short or Open termination.
- **Open, O:** Open circuit; the reflection coefficient needs to be known.
- **Short, S:** Short circuit; the reflection coefficient needs to be known.
- **Match, M:** matched load, which defines the normalization impedance.
- **Load, L:** resistive termination (typically $50\ \Omega$). Thus the same as Match.

2.3 Error models and calibration methods

The calibration of VNAs is based on error models that include error terms determined by complex S-parameters. Different error models and calibration methods to define the error network are studied and developed a lot, and a short summary of those is presented in this section.

2.3.1 16-term error model

In the 16-term error model all linear error terms are included in the calibration, which means that in addition to the reflection and transmission terms also the leakage paths can be taken into account. Thus with a 16-term calibration method the full 16-term error network can be determined. High frequency on-wafer measurements are one of the applications where the 16-term calibration method may be advantageous, because the probe heads are very close to each other, which can cause unwanted probe-to-probe or wafer level coupling.

The error terms of the 16-term error model are shown in Figure 2.4. The DUT is connected to terminals a_1, b_1, a_2, b_2 and terminals a_0, b_0, a_3, b_3 are the ports of the non-ideal (real) network analyzer, when two-tier calibration is used as in Figure 2.4 (VNA is calibrated first at the waveguide ports). If one-tier calibration is used a hypothetical ideal network analyzer is connected to ports 0 and 3.

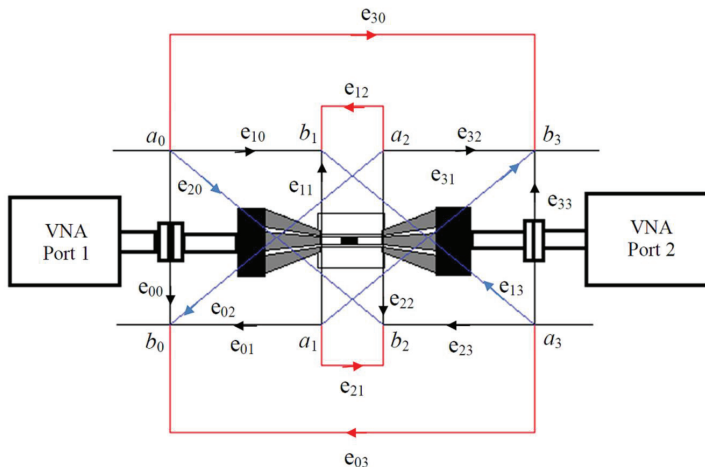


Figure 2.4. The error terms of the 16-term error model.

The S-parameters E and the scattering transfer parameters, i.e., T-parameters T of the 16-term error network are determined using the voltage waves in (2.7) and (2.8) [27], [33]

$$\begin{bmatrix} b_0 \\ b_3 \\ b_1 \\ b_2 \end{bmatrix} = \mathbf{E} \begin{bmatrix} a_0 \\ a_3 \\ a_1 \\ a_2 \end{bmatrix} = \begin{bmatrix} \mathbf{E}_1 & \mathbf{E}_2 \\ \mathbf{E}_3 & \mathbf{E}_4 \end{bmatrix} \begin{bmatrix} a_0 \\ a_3 \\ a_1 \\ a_2 \end{bmatrix}, \mathbf{E} = \begin{bmatrix} e_{00} & e_{03} & e_{01} & e_{02} \\ e_{30} & e_{33} & e_{31} & e_{32} \\ e_{10} & e_{13} & e_{11} & e_{12} \\ e_{20} & e_{23} & e_{21} & e_{22} \end{bmatrix}, \quad (2.7)$$

$$\begin{bmatrix} b_0 \\ b_3 \\ a_0 \\ a_3 \end{bmatrix} = \mathbf{T} \begin{bmatrix} a_1 \\ a_2 \\ b_1 \\ b_2 \end{bmatrix} = \begin{bmatrix} \mathbf{T}_1 & \mathbf{T}_2 \\ \mathbf{T}_3 & \mathbf{T}_4 \end{bmatrix} \begin{bmatrix} a_1 \\ a_2 \\ b_1 \\ b_2 \end{bmatrix}, \mathbf{T} = \begin{bmatrix} t_0 & t_1 & t_4 & t_5 \\ t_2 & t_3 & t_6 & t_7 \\ t_8 & t_9 & t_{12} & t_{13} \\ t_{10} & t_{11} & t_{14} & t_{15} \end{bmatrix}, \quad (2.8)$$

where e_{ij} are the parameters of the \mathbf{E} matrix and t_{ij} are the parameters of the \mathbf{T} matrix. The calibration and the de-embedding are based on (2.9) or (2.10) [27], [33]. Either of the equations can be used, but the T-parameter equation (2.9) is used throughout this work, because it produces linear equations in respect to error terms.

$$\mathbf{S}_m(\mathbf{T}_3\mathbf{S}_a + \mathbf{T}_4) = (\mathbf{T}_1\mathbf{S}_a + \mathbf{T}_2), \quad (2.9)$$

$$(\mathbf{S}_m - \mathbf{E}_1)\mathbf{E}_3^{-1}(\mathbf{S}_a^{-1} - \mathbf{E}_4) = \mathbf{E}_2. \quad (2.10)$$

Each calibration standard forms from (2.9) a set of four linear equations in terms of the 16 error parameters. The error parameters can be solved using calibration standard measurements. When the error network is solved, the actual S-parameters \mathbf{S}_a of the DUT can be solved using equation (2.9).

Usually five two-port calibration standards are needed for calibration of the full 16-term error network. At least one of the standards needs to be non-symmetrical (e.g. Match-Short) [27]. With four standards the solution is non-unique, because the system of equations is underdetermined. Only 15 error parameters need to be solved, if one of the error parameters is considered as a common scaling factor. Still one of the remaining error parameters needs to be known to find a unique solution with four standards. The possibilities for that are: the use of symmetry or reciprocity conditions [34], [35], or neglecting one or more of the weak leakage paths [36]. In [37], [38] the reciprocity conditions are not used to reduce the number of calibration standards, but the reciprocity is used to solve the scaling factor.

Several papers about the 16-term calibration methods have been published [27], [28], [33], [39] – [43], but rarely used in commercial calibration software or on-wafer measurements. The methods in [27], [39] – [42] are based on closed-form equations resulting in a smaller computational effort, while methods in [28], [33], [43] are based on

numerical iteration. In [I] a novel 16-term calibration method based on reciprocity conditions of the error network and in [II] a novel method to determine LRRM calibration standards in presence of leakage are presented.

2.3.2 12-term error model

The 12-term calibration model is one of the most used calibration models. In vector network analyzers with three measurement channels, where the third channel measures a_0 in forward direction and a'_3 in reverse direction, the 12-term error model is the only choice to remove the switching errors. A 12-term error correction is also used for four channel vector network analyzers, and also then additional switching error correction is not needed. The error terms of the 12-term error model are shown in Figure 2.5.

The error terms in forward (F) and reverse (R) directions are: directivity (E_{DF}, E_{DR}), source match (E_{SF}, E_{SR}), reflection tracking (E_{RF}, E_{RR}), load match (E_{LF}, E_{LR}), transmission tracking (E_{TF}, E_{TR}), and transmission leakage (isolation, crosstalk) (E_{XF}, E_{XR}). The mathematical formulas of the 12-term calibration method can be found in [44].

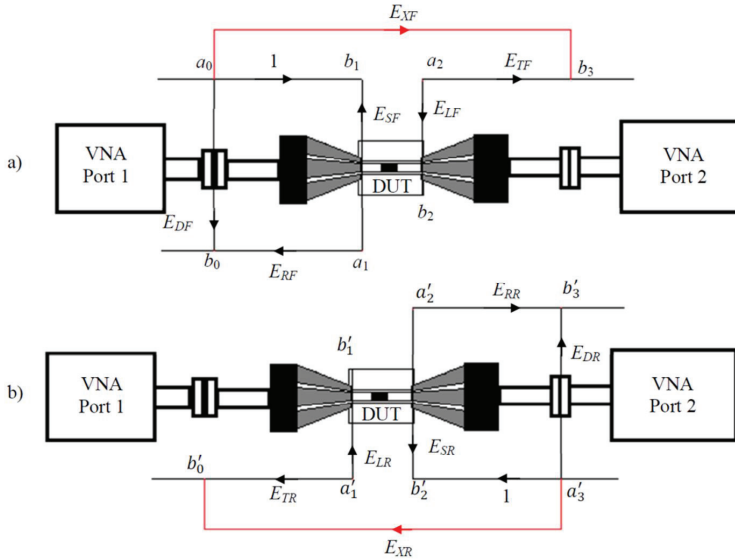


Figure 2.5. The error terms of the 12-term error model. a) Forward direction, b) reverse direction.

Short-Open-Load-Thru (SOLT) calibration method is typically used to determine the 12-term error model and it is available for every commercial vector network analyzer. The disadvantage of the SOLT procedure is that all four calibration standards must be known and the self-calibration is not

possible. It is also sensitive to the probe location. SOLT is commonly used in coaxial calibration, but it is not recommended for an on-wafer calibration method. Short-Open-Load-Reciprocal (SOLR) and Thru-Match-Short-Open (TMSO) are variations of SOLT. In SOLR the Thru standard is replaced with an unknown but reciprocal two-port standard [45]. SOLR can be used also with orthogonal probe positions, where the Thru standard is hard to realize [46]. In TMSO all the standards except the Thru are connected to only one port, which reduces the number of connections [47].

2.3.3 10- and 8-term error models

The 10-term and 8-term calibration methods are simplifications of the 16- and 12-term calibration methods. The error terms of the 10- and 8-term error model are shown in Figure 2.6. In 10-term calibration method two leakage (crosstalk) terms e_{30} , and e_{03} are taken into account in calibration using transmission measurement with matched loads at the measurement ports. With the 10-term error model only the inner crosstalk of the analyzer can be taken into account, but not the crosstalk over the test-fixture. The S-parameters \mathbf{E} and the T-parameters \mathbf{T} of the 10- and 8-term error networks are determined in (2.11) and (2.12)

$$\mathbf{E}_{10-term} = \begin{bmatrix} e_{00} & e_{03} & e_{01} & 0 \\ e_{30} & e_{33} & 0 & e_{32} \\ e_{10} & 0 & e_{11} & 0 \\ 0 & e_{23} & 0 & e_{22} \end{bmatrix}, \mathbf{E}_{8-term} = \begin{bmatrix} e_{00} & 0 & e_{01} & 0 \\ 0 & e_{33} & 0 & e_{32} \\ e_{10} & 0 & e_{11} & 0 \\ 0 & e_{23} & 0 & e_{22} \end{bmatrix}, \quad (2.11)$$

$$\mathbf{T}_{10-term} = \begin{bmatrix} t_0 & t_1 & t_4 & t_5 \\ t_2 & t_3 & t_6 & t_7 \\ t_8 & 0 & t_{12} & 0 \\ 0 & t_{11} & 0 & t_{15} \end{bmatrix}, \mathbf{T}_{8-term} = \begin{bmatrix} t_0 & 0 & t_4 & 0 \\ 0 & t_3 & 0 & t_7 \\ t_8 & 0 & t_{12} & 0 \\ 0 & t_{11} & 0 & t_{15} \end{bmatrix}. \quad (2.12)$$

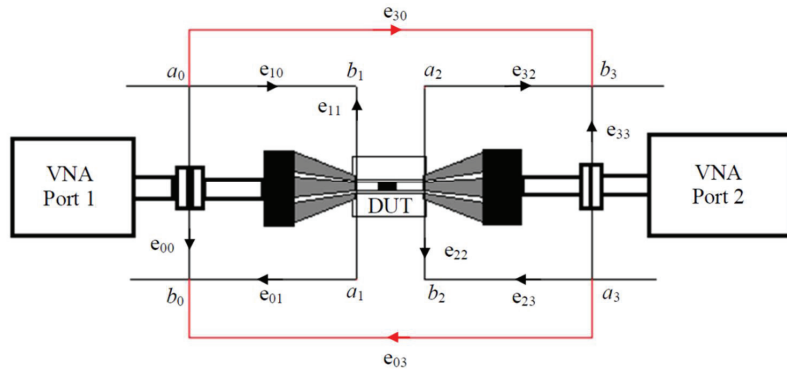


Figure 2.6. The error terms of the 10- and 8-term error models. The error terms e_{30} and e_{03} (red lines) are included only in the 10-term error model.

In the 10- and 8-term calibration methods usually three two-port calibration measurements are needed. The ports can be measured separately and full two-port measurements for reflection type standards are not needed. If the test-fixture is symmetrical, two calibration standards are enough [48]. The equations of the 16-term calibration method can be applied directly for the 10- and 8-term calibration methods assuming the leakage terms to be zero.

An important advantage of the 10- and 8-term calibration methods is the possibility to use self-calibration, because of the redundant data. Typically used calibration methods for the 10- and 8-term error models using three two-port calibration standards are (the methods in parentheses are working similarly but with different standards):

- **Thru-Reflect-Line, TRL (Line-Reflect-Line, LRL):** Thru must be fully known, when the reference plane is moved to the probe tips from the center of the Thru. The line length difference should not be near multiple of 180° (in practice 20° - 160° is suitable). Reflect is a pair of unknown Shorts or Opens. For wider bandwidths multiple line lengths are required to get suitable phase differences over a wide bandwidth. The method is not suitable for fixed probe spacing. [49] – [56]
- **Multi-line TRL:** Developed by U.S. National Institute on Standards and Technology (NIST). The conventional TRL method uses multiple lines for different frequency ranges, but does not use them simultaneously. In the NIST multi-line TRL calibration method the additional continuously varying optimally weighted average data from the redundant standards are used to minimize the total random error (e.g. connector repeatability). With multi-line TRL, improvements in accuracy and bandwidth can be achieved. The propagation constants of the standards at every frequency are estimated accurately and used for S-parameter correction. It is possibly the most accurate calibration method if done correctly. NIST multi-line TRL is used as a benchmark when the accuracy of the calibration method is verified. The method is not suitable for fixed probe spacing. [57] – [62]
- **Line-Reflect-Match, LRM (Thru-Reflect-Match, TRM):** Thru must be fully known and a broadband Match with a known resistance value is used to set the system impedance level. Reflect is an unknown Short or Open. The one-port standards are used as identical pairs or at least each

standard connected once to both ports. The method is suitable for fixed probe spacing. [31], [56], [63] – [71]

- **Line-Reflect-Reflect-Match, LRRM (Thru-Reflect-Reflect-Match, TRRM):** Thru must be fully known and a broadband Match with a known resistance value in one port is needed to be measured. Two unknown reflection standard pairs are needed (usually Short and Open). The redundant information is used to calculate the inductance of the Match. The reference plane is in the probe tips. The method provides calibration accuracy comparable to the NIST multi-line TRL method. The method is suitable for broadband calibrations and fixed probe spacing. [31], [72] – [75]
- **Thru-Short-Delay, TSD:** The first self-calibration method. The length of Thru and Delay are unknown and Short standard (also Open can be used) needs to be known. The line length difference should not be near multiple of 180° (in practice 20° - 160° is suitable). The method is not suitable for fixed probe spacing. [76], [77]

Other possible, but less frequently used calibration methods are: Match-Short-Open (MSO, suitable only for 1-port calibration), Line-Short-Open (LSO), and Line-Short-Match (LSM). Most of the 8-term calibration methods can be handled with Thru-Circuit-Unknown (TCX) algorithm [78]. The first standard needs to be fully known with a transmission path, the second standard is a partly known two- or one-port, and the third standard is an unknown symmetrical standard, which can be solved using self-calibration. The mathematical formulation is presented in [78]. When Line-offset offset-Open offset-Short (LZZ) method, which uses known transmission line and two highly reflecting but unknown offset loads, is used, the 8-term error model can be calibrated without the characterisation of a match standard [79]. However the transmission line needs to be characterised accurately.

2.4 Selection of a suitable calibration method

The used calibration method and the error model determine mainly the accuracy of the calibration, but also the accuracy of the calibration standards and the repeatability of the measurements have an influence on the calibration accuracy [25], [80]. The calibration standards need to be of high quality and known accurately or self-calibration can be used to achieve accurate calibration and measurements [31], [81]. It is also very important

in on-wafer calibration and measurement that the probe contacts to the standards and DUT are done always as similarly as possible. Offsets in the probe positioning will affect the accuracy of the calibration and the measurements [82] – [84].

Usually in VNAs and in commercial calibration software (e.g. WinCal XE 4.2 by Cascade Microtech) SOLT, TRL, multi-line TRL, LRM, and LRRM calibration methods are implemented [85]. All the methods (except SOLT) are based on the 8-term error model, which means that the leakage terms cannot be determined. Several factors affect the selection of a suitable calibration method and error model for the measurement: accuracy requirement, available calibration standards, frequency range, device under test, fixed probe spacing or not, leakage and crosstalk included or not, etc. Different on-wafer calibration methods are widely compared in [82], [86] – [91].

The 8-term calibration methods are very accurate in the situations where the leakage and crosstalk terms are almost negligible. It means that in those cases the 16-term error model calibration is not expected to be more accurate than the 8-term error model calibrations. When the leakage and crosstalk terms become significant, calibration with the 16-term error model can be more accurate. For high frequency (above 110 GHz) on-wafer measurements it is plausible that the leakage and cross talk terms are already significant and need to be taken into account in the calibration. In this kind of situations a 16-term error model should be chosen for the calibration method, and a fixed probe spacing is required to model the leakage paths correctly, which means that Delay or Line standards cannot be used.

One challenge in the 16-term calibration methods is that the leakage terms are assumed to be constant. Thus the probe distance should be the same both in calibration and measurement. In addition the environment around the probes may have an effect on the leakage terms. For instance, when commercial calibration standards are used, the DUT is fabricated on a different substrate than the calibration standards, which causes different environments for calibration and measurement of the DUT. The best option would be to fabricate the calibration standards on the same wafer with the DUT to keep the leakage terms as constant as possible.

3. Calibration of the reciprocal 16-term error network

Usually five calibration standards are needed to solve the full 16-term error network, but if the reciprocity conditions are used to reduce the number of unknown error terms, a unique solution can be found for the calibration equation, and the full 16-term error model can be solved using only four calibration standards. Also symmetry conditions could be used to reduce the number of unknowns, but it is very questionable in practice. Significant non-symmetry can be caused easily, e.g., by minor changes in probe positioning. As a general rule, reciprocity can be considered as a good foundation for accurate calibration, because networks consisting only linear passive structures, e.g., resistors, capacitors, and inductors, are always reciprocal.

The DUT may be non-reciprocal, but the error network needs to be reciprocal, which is typical in on-wafer S-parameter measurements. This means also that the reciprocal calibration method can be used only as a second-tier calibration for on-wafer part of measurement system (including the possible cables or waveguides) with a pre-calibrated network analyzer. If the whole measurement system with the vector network analyzer was calibrated, the error network would not be reciprocal because of the switching errors and differences in the receivers of the four measurement channels. The use of two-tier calibration is a common practice, e.g., in the measurements of integrated circuits. The use of commercial calibration standards such as Cascade Microtech impedance standard substrate (ISS) is allowed, because a non-symmetrical custom-made standard is not needed. Besides, the calibration accuracy may be improved by leaving out the fifth, possibly less accurate, standard.

This chapter presents a 16-term calibration method based on reciprocity conditions and a method to determine LRRM calibration standards in measurement configurations affected by leakage. The complete equations for the definition of the calibration standards are presented in [II] and the reciprocal calibration procedure is described in [I]. In this chapter only the key equations and results are presented.

3.1 Definition of the LRRM calibration standards

The Thru standard needs to be fully known as also the resistance of the Match standard. The reactances of the two unknown lossless reflect standards (Open and Short) and the Match standard are calculated using their measured raw (not calibrated) S-parameters. The standards are defined as follows (the two latter standards can be interchanged and offset Short and Open standards are applicable, too):

A: T Thru

B: M-M Symmetrical double Match with parasitic reactance

C: S-S Lossless symmetrical double Short

D: R-R Lossless symmetrical double Open

$$\mathbf{A} = \begin{bmatrix} 0 & T \\ T & 0 \end{bmatrix}, \quad (3.1)$$

$$\mathbf{B} = \begin{bmatrix} M & 0 \\ 0 & M \end{bmatrix}, \quad (3.2)$$

$$\mathbf{C} = \begin{bmatrix} S & 0 \\ 0 & S \end{bmatrix}, \quad (3.3)$$

$$\mathbf{D} = \begin{bmatrix} R & 0 \\ 0 & R \end{bmatrix}. \quad (3.4)$$

The Thru standard can be non-ideal with attenuation α and delay Δt . The transmission coefficient for the Thru standard can be calculated from equation

$$T = e^{-\alpha l} \cdot e^{-\beta l}, \quad (3.5)$$

$$\alpha l = \frac{A/(dB)}{20} \ln 10, \quad (3.6)$$

$$\beta l = \omega \Delta t, \quad (3.7)$$

where l is the length of the line, ω is the angular frequency. The reflection coefficient M of the Match standard is allowed to include positive or negative reactance, which can vary as a function of frequency. The reflection coefficient of the Match standards is

$$M = \frac{R_M - Z_0 + \overbrace{j\omega L_{match}}^X}{R_M + Z_0 + \underbrace{j\omega L_{match}}_X}, \quad (3.8)$$

where R_M is the resistance value of Match standard, Z_0 is the characteristic impedance of the line that determines the S-parameter reference (typically 50 Ω), L_{match} is the inductance of the Match standard, and reactance X is unknown, which can be found from the second order equation that is

derived in [II]. Also equations (3.9) and (3.10) for R and S are derived in [II].

$$R = \frac{M + uT}{I + \frac{uM}{T}}, \quad (3.9)$$

$$S = \frac{R - wT}{I - \frac{wR}{T}}, \quad (3.10)$$

where

$$u^2 = I - 4 \times \frac{\det(\mathbf{F}_1)}{\text{trace}^2(\mathbf{F}_1)}, \quad (3.11)$$

$$\mathbf{F}_1 = (\mathbf{M}_A - \mathbf{M}_D)^{-1}(\mathbf{M}_C - \mathbf{M}_D)(\mathbf{M}_B - \mathbf{M}_C)^{-1}(\mathbf{M}_A - \mathbf{M}_B), \quad (3.12)$$

$$w^2 = I - 4 \times \frac{\det(\mathbf{F}_2)}{\text{trace}^2(\mathbf{F}_2)}, \quad (3.13)$$

$$\mathbf{F}_2 = (\mathbf{M}_A - \mathbf{M}_D)^{-1}(\mathbf{M}_B - \mathbf{M}_D)(\mathbf{M}_B - \mathbf{M}_C)^{-1}(\mathbf{M}_A - \mathbf{M}_C), \quad (3.14)$$

where $\mathbf{M}_A \dots \mathbf{M}_D$ are the measured raw S-parameters with standards **A...D**, respectively. The equations do not assume anything about the parameter values of the standards, but in the LRRM method it is a common practice to define Short and Open lossless. After solving X , the reflection coefficients M, S, and R can be found from equations (3.8) – (3.10) separately at each frequency.

The feasibility of the method is demonstrated by a simulation approach and practical on-wafer S-parameter measurements in [II]. Here only the measurement results are presented. Structures of the commercial Cascade Microtech ISS are used as calibration standards. Figure 3.1 shows micrographs of the used calibration standards. The measurements are performed using a measurements system including a Cascade Microtech probe station, Agilent E8361C PNA Vector Network Analyzer (10 MHz – 67 GHz) and Agilent N5260A Millimeter Head Controller with Agilent extension units for the frequency band of 67 – 110 GHz. Figure 3.2 shows a block diagram and a photograph of the measurement setup. The VNA is first calibrated at the coaxial ports before the probe heads using a SOLT and the offset Short standards of the Agilent 85059A calibration kit. Figure 3.3 presents the defined S-parameters of the calibration standards calculated from LRRM standard definition equations (3.5), (3.8) – (3.10) using the measured raw S-parameter data of the standards in addition to the preliminary information about the Thru and Match standards. For a comparison, measured and calculated S-parameters are presented.

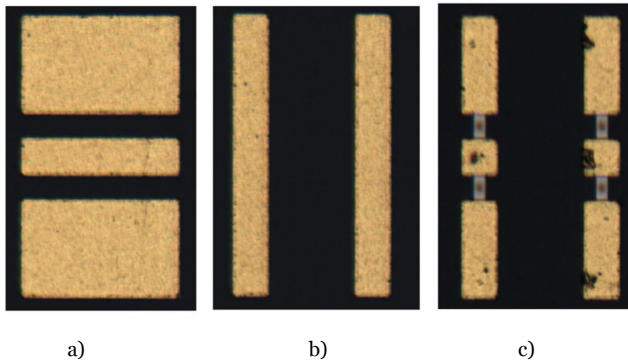


Figure 3.1. Micrographs of the calibration standards from Cascade Microtech ISS used in the measurements. The length of the standards is $200\ \mu\text{m}$ and the material of the substrate is alumina. a) Thru, b) Short, c) Match. Open standard is synthesized by lifting the probes in air.

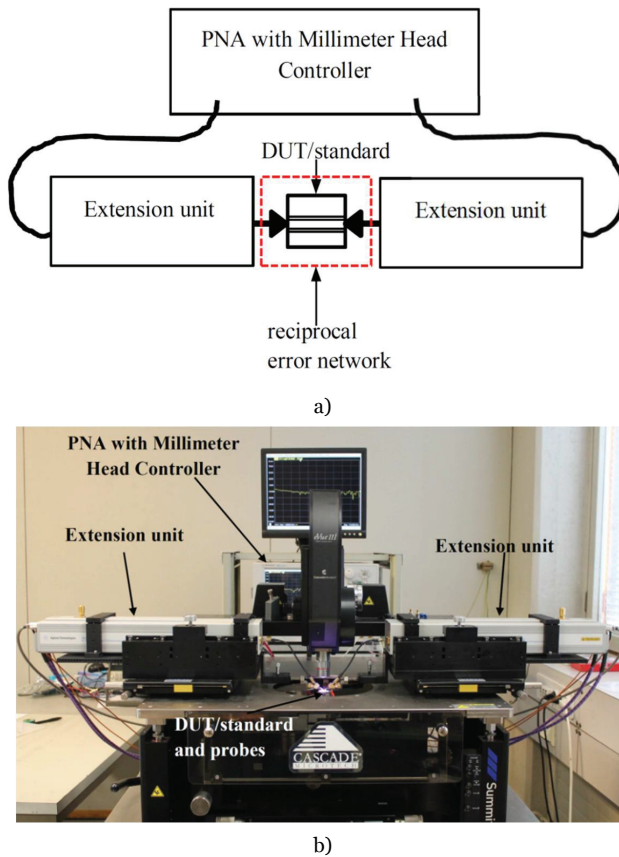


Figure 3.2. a) Block diagram of the measurement system. The method is implemented as a second-tier calibration to the on-wafer part, shown inside the dashed rectangle. b) Photograph of the measurement system.

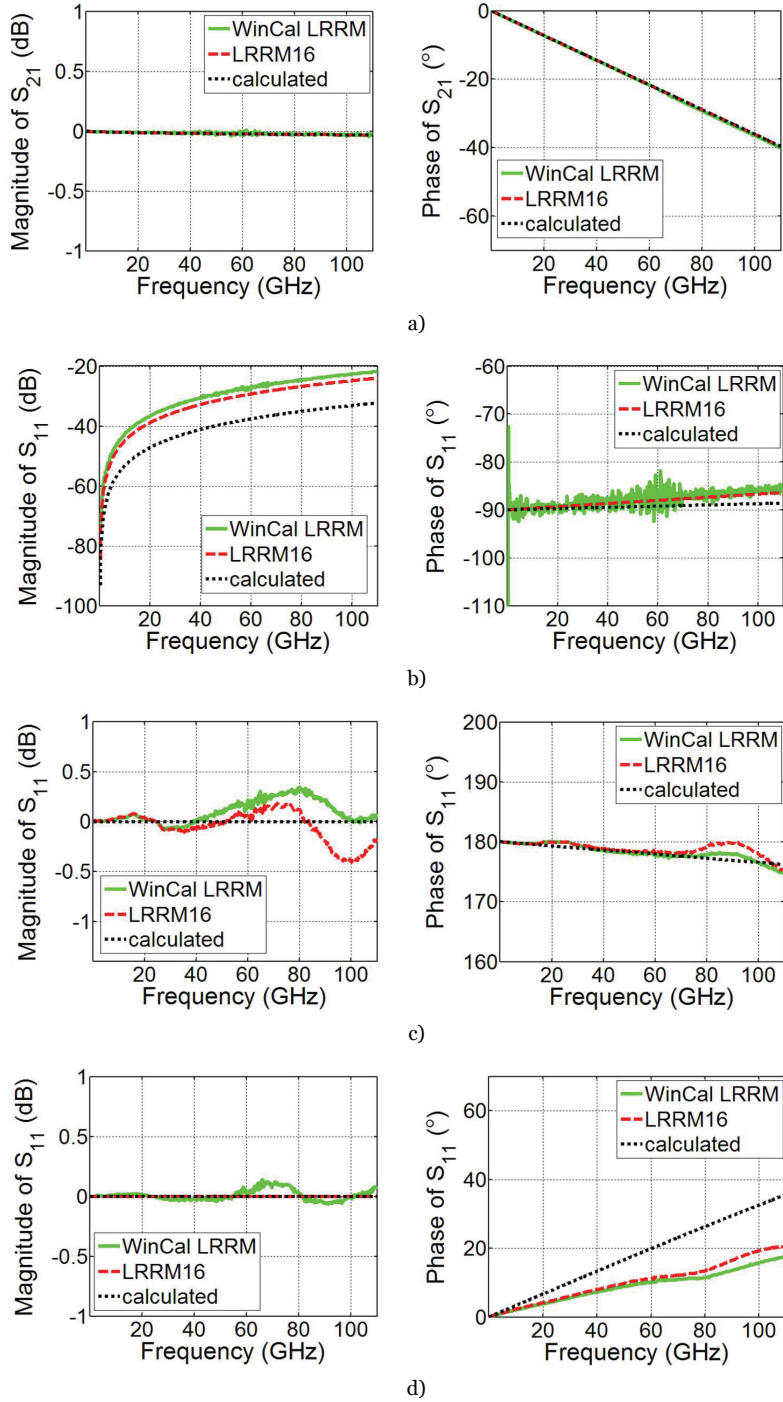


Figure 3.3. S-parameters of the calibration standards from the following methods: 8-term WinCal LRRM (solid green line), 16-term LRRM (dashed red line), parameter-based calculation (dotted black line). a) Magnitude and phase of S_{21} for Thru, b) magnitude and phase of S_{11} for Match, c) magnitude and phase of S_{11} for Short, d) magnitude and phase of S_{11} for Open.

The WinCal 8-term LRRM calibration method is used in the comparison measurements and the parameter values given by Cascade Microtech are used to find the calculated S-parameters of the standards. With all three methods, very similar results are obtained. The calculated values are achieved using constant values at all frequencies, while the LRRM standard determination method solves the reactances separately at every frequency. In addition, in the LRRM standard determination method the true value of the inductance of the Match standard is extracted from the redundant data from the calibration measurements, but in the calculations the initial value for the inductance is used. For the defined inductance of the Match standard a constant (an average of the inductance values at different frequencies) value is used to reduce the computational error due to the very small numerical values used in calculating the inductance, especially at low frequencies (< 20 GHz).

Ideally the measured magnitudes of the reflection coefficients of Short and Open standards should be 0 dB. In practice it will never be perfect, because LRRM is a self-consistent calibration method and errors will be seen in the magnitude of the reflection coefficients. This can be seen in Figure 3.3 where the magnitude of S_{11} of Short standard is greater than 0 dB at some frequencies. The phase of the Open standard (probes in the air) is positive because of the negative capacitance caused by the faster propagation of waves in the air than in the substrate.

3.2 16-term calibration based on reciprocity conditions

The actual calibration procedure of the 16-term calibration method is fully based on the reciprocity conditions of the error network [1]. The calibration procedure is an accurate closed-form solution; it does not involve any approximations or restrictions concerning the DUT. The reciprocity conditions of the S-parameters of the error matrix are very simple:

$$e_{30} = e_{03}, \quad (3.15)$$

$$e_{10} = e_{01}, \quad (3.16)$$

$$e_{20} = e_{02}, \quad (3.17)$$

$$e_{31} = e_{13}, \quad (3.18)$$

$$e_{32} = e_{23}, \quad (3.19)$$

$$e_{12} = e_{21}. \quad (3.20)$$

The drawback of the S-parameter reciprocity conditions is the non-linear equation (2.10). The T-parameters can be calculated from the S-parameters and vice versa using the conversion equations shown in [27]. The complexity of the conversion equations causes complicated reciprocity conditions for T-parameters, but because of the linear calibration equation (2.9), T-parameters are used in this method:

$$t_6 t_{15} - t_7 t_{14} = t_5 t_{12} - t_4 t_{13}, \quad (3.21)$$

$$t_{15} = (t_{12} t_{15} - t_{13} t_{14}) t_0 - (t_4 t_{15} - t_5 t_{14}) t_8 - (t_5 t_{12} - t_4 t_{13}) t_{10}, \quad (3.22)$$

$$t_{14} = (t_4 t_{15} - t_5 t_{14}) t_9 + (t_5 t_{12} - t_4 t_{13}) t_{11} - (t_{12} t_{15} - t_{13} t_{14}) t_1, \quad (3.23)$$

$$t_{13} = (t_6 t_{15} - t_7 t_{14}) t_8 + (t_7 t_{12} - t_6 t_{13}) t_{10} - (t_{12} t_{15} - t_{13} t_{14}) t_2, \quad (3.24)$$

$$t_{12} = (t_{12} t_{15} - t_{13} t_{14}) t_3 - (t_6 t_{15} - t_7 t_{14}) t_9 - (t_7 t_{12} - t_6 t_{13}) t_{11}, \quad (3.25)$$

$$t_8 t_{14} - t_{10} t_{12} = t_{13} t_{11} - t_9 t_{15}. \quad (3.26)$$

Every two-port calibration standard measurement gives four linear equations in terms of the 16 error parameters from (2.9) [28]:

$$\begin{bmatrix} S_{a11} & S_{a21} & 0 & 0 & 1 & 0 & 0 & 0, \\ S_{a12} & S_{a22} & 0 & 0 & 0 & 1 & 0 & 0, \\ 0 & 0 & S_{a11} & S_{a21} & 0 & 0 & 1 & 0, \\ 0 & 0 & S_{a12} & S_{a22} & 0 & 0 & 0 & 1, \end{bmatrix}$$

$$\begin{aligned} & -S_{m11} S_{a11} & -S_{m11} S_{a21} & -S_{m12} S_{a11} & -S_{m12} S_{a21}, \\ & -S_{m11} S_{a12} & -S_{m11} S_{a22} & -S_{m12} S_{a12} & -S_{m12} S_{a22}, \\ & -S_{m21} S_{a11} & -S_{m21} S_{a21} & -S_{m22} S_{a11} & -S_{m22} S_{a21}, \\ & -S_{m21} S_{a12} & -S_{m21} S_{a22} & -S_{m22} S_{a12} & -S_{m22} S_{a21}, \end{aligned}$$

$$\begin{aligned} & -S_{m11} & 0 \\ & 0 & -S_{m11} \\ & -S_{m21} & 0 \\ & 0 & -S_{m21} \end{bmatrix} \begin{bmatrix} t_0 \\ t_1 \\ \dots \\ t_{12} \\ t_{13} \end{bmatrix} = \begin{bmatrix} S_{m12} \\ 0 \\ S_{m22} \\ 0 \end{bmatrix} \underbrace{t_{14}}_x + \begin{bmatrix} 0 \\ S_{m12} \\ 0 \\ S_{m22} \end{bmatrix} \underbrace{t_{15}}_y. \quad (3.27a)-(3.27d)$$

The 14 unknowns on the left side are first solved as a function of t_{14} and t_{15} using 14 equations that are achieved by leaving out two equations. Which two equations are left out, depends on the order of the calibration standards. All four equations should be used for our two first standards and at least equations (3.27a) and (3.27d) should be used for the other two standards. Here (3.27b) of the third standard and (3.27c) of the fourth standard are left out. Because of the redundant calibration equations, data reduction, e.g., least-squares-fit (LSF) algorithm could be used to improve accuracy and reduce error sensitivity [38], [78]. The set of 14 equations can be written in matrix form:

$$\mathbf{U}[t_0, \dots, t_{11}, t_{12}, t_{13}]^T = \mathbf{V}t_{14} + \mathbf{W}t_{15}, \quad (3.28)$$

$$[t_0, \dots, t_{11}, t_{12}, t_{13}]^T = \underbrace{\mathbf{U}^{-1}\mathbf{V}}_{\mathbf{M}}t_{14} + \underbrace{\mathbf{U}^{-1}\mathbf{W}}_{\mathbf{N}}t_{15}. \quad (3.29)$$

The arbitrary scaling factor is $t_{15} = y$, so the equation (3.29) gives the error terms as follows

$$[t_0, \dots, t_{11}, t_{12}, t_{13}]^T = \mathbf{M}x + \mathbf{N}y, \quad (3.30)$$

where the auxiliary matrices are

$$\mathbf{M} = [m_0, \dots, m_{11}, m_{12}, m_{13}]^T, \quad (3.31)$$

$$\mathbf{N} = [n, \dots, n_{11}, n_{12}, n_{13}]^T. \quad (3.32)$$

Usually a fifth calibration standard measurement is needed to determine the value of $x = t_{14}$. Now the reciprocity conditions are used to get the additional second order equation for unknown x (the steps are shown in [I]), when $t_{15} = y = 1$ is defined for a preliminary scaling factor:

$$ax^2 + bx + c = 0, \quad (3.33)$$

where

$$a = m_4m_{10} + m_5m_{11} - m_0, \quad (3.34)$$

$$b = (n_4m_{10} + m_4n_{10} + n_5m_{11} + m_5n_{11} - n_0)y - m_1, \quad (3.35)$$

$$c = (n_4n_{10} + n_5n_{11})y^2 - n_1y. \quad (3.36)$$

The correct root for parameter x from equation (3.33) needs to be chosen and it is sufficient to choose the root that has smaller magnitude, because $x = t_{14}$ should be very small in practice. It appears that with the wrong choice of the root the values of the error parameters would interchange as follows:

$$\begin{aligned} e_{01} &\leftrightarrow e_{02}, & e_{10} &\leftrightarrow e_{20}, \\ e_{31} &\leftrightarrow e_{32}, & e_{13} &\leftrightarrow e_{23}, & e_{11} &\leftrightarrow e_{22}. \end{aligned}$$

One of the advantages of the reciprocal method is that the correct scaling factor can be found simultaneously with the error parameters due to the reciprocity conditions. The T-matrix can be scaled using a common scaling factor k and each T-parameter can be scaled by dividing it by k [27]. Without the re-scaling only the conditions $e_{03} = e_{30}$ and $e_{12} = e_{21}$ are fulfilled (if data is accurate), but the other results are non-reciprocal, because of the

wrong scaling. However the correct calibration would still be achieved without the re-scaling. The re-scaling of the results can be done by forcing

$$\frac{e_{10}}{e_{01}} = \frac{e_{13}}{e_{31}} = \frac{e_{20}}{e_{02}} = \frac{e_{23}}{e_{32}} = 1, \quad (3.37)$$

by adjusting the arbitrary scaling factor k :

$$e_{10} = e_{01} \Rightarrow \quad (3.38)$$

$$\frac{t_{15}}{k} = \left(\frac{t_{12}}{k} \frac{t_{15}}{k} - \frac{t_{13}}{k} \frac{t_{14}}{k} \right) \frac{t_0}{k} - \left(\frac{t_4}{k} \frac{t_{15}}{k} - \frac{t_5}{k} \frac{t_{14}}{k} \right) \frac{t_8}{k} - \left(\frac{t_5}{k} \frac{t_{12}}{k} - \frac{t_4}{k} \frac{t_{13}}{k} \right) \frac{t_{10}}{k}. \quad (3.39)$$

The optimum value for scaling factor k , which produces a completely reciprocal error network, can be solved from:

$$k = \pm \sqrt{\frac{t'_{15}}{t_{15}}}, \quad (3.40)$$

$$t'_{15} = (t_{12}t_{15} - t_{13}t_{14})t_0 - (t_4t_{15} - t_5t_{14})t_8 - (t_5t_{12} - t_4t_{13})t_{10}, \quad (3.41)$$

where $t_{14} = x$, $t_{15} = y = 1$, and otherwise $t_i = m_ix + n_iy$. The selected sign (plus or minus) affects the phase of individual error parameters if they are studied separately. The correct sign at each frequency can be determined based on the phase curves of error parameters that should change as a function of frequency between $+180^\circ$ and -180° . However, either of the signs gives the correct S-parameters of the DUT. After rescaling the final error parameters are:

$$t_0 = \frac{(m_0x + n_0y)}{k}, \quad (3.42)$$

...

$$t_{13} = \frac{(m_{13}x + n_{13}y)}{k}, \quad (3.43)$$

$$t_{14} = \frac{x}{k}, \quad (3.44)$$

$$t_{15} = \frac{y}{k} = \frac{1}{k}. \quad (3.45)$$

The actual S-parameters \mathbf{S}_a of the DUT can now be solved from equation (2.9).

The feasibility of the 16-term reciprocal calibration method is demonstrated by a simulation approach and practical on-wafer S-parameter measurements in [I] and [II]. The measurement results from [II] are summarized here. The measurement system (see Figure 3.2) and determined calibration standards are the same as presented in Section 3.1. The VNA is first calibrated at the coaxial ports before the probe heads using a SOLT and the offset Short standards of the Agilent 85059A calibration kit. The 16-term reciprocal calibration is then used as a second-tier calibration. Figure 3.4 shows the flow chart of the calibration procedure including the standard determination method presented in Section 3.1. The S-parameters of open coplanar waveguide (CPW) structure shown in Figure 3.5 are measured at the frequency range of 0.1 – 110 GHz and the calibration is performed using the reciprocal 16-term calibration equations (3.15) – (3.45).

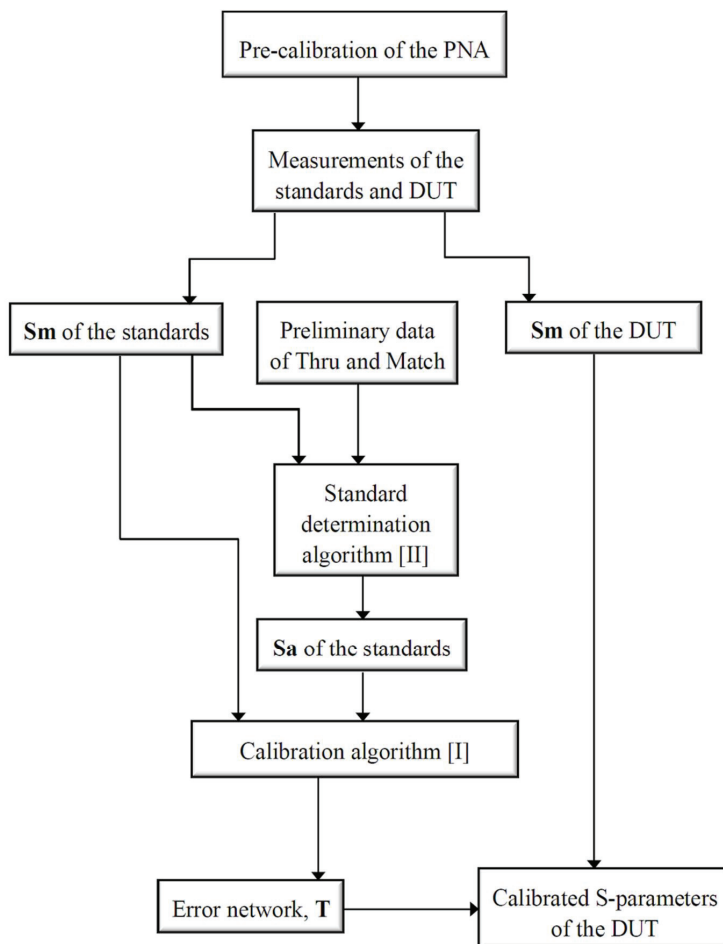


Figure 3.4. Flow chart of the calibration procedure.

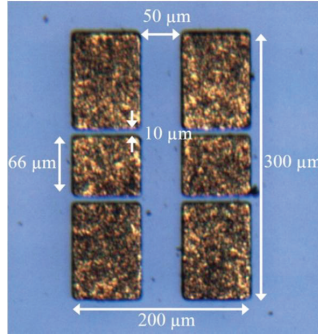


Figure 3.5. Micrograph of the measured open CPW structure. The material of the substrate is quartz.

Figure 3.6 shows the measured S-parameters of the DUT. The 16-term calibration based on reciprocity conditions is compared with the WinCal 8-term LRRM and TRL calibration methods. The calibrated S-parameters of using these three calibration methods are very similar. There are no significant leakage paths present as seen in Figure 3.7, but these small leakage parameters explain the differences in the S-parameters between the 8-term methods and the reciprocal 16-term method. To demonstrate this, the leakage parameters of the 16-term error network are set to zero, when the calibrated S_{21} of the DUT agrees well with the calibrated S_{21} using WinCal 8-term LRRM calibration method as seen in Figure 3.6 b).

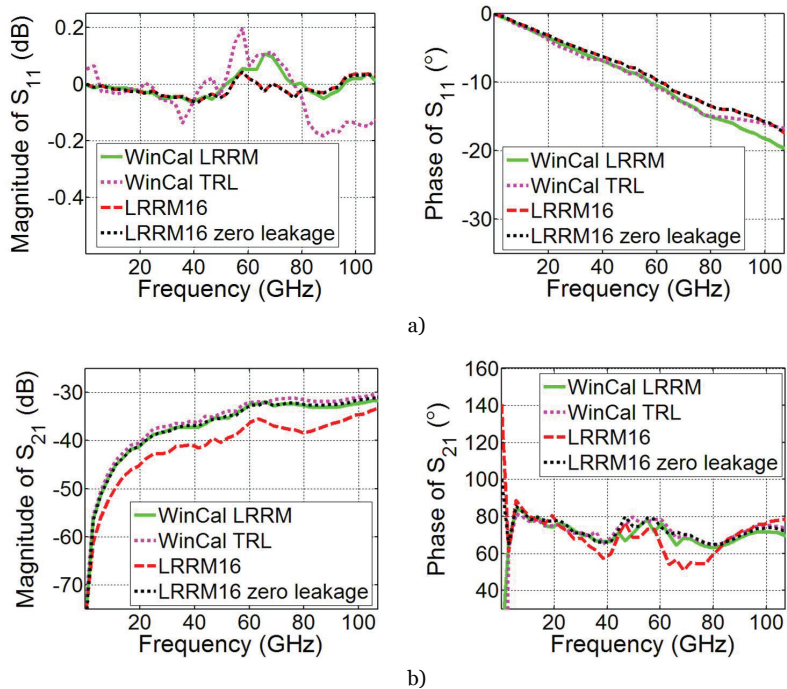


Figure 3.6. Measured S-parameters of an open CPW structure from the following methods: 8-term WinCal TRL (dotted magenta line), 8-term WinCal LRRM (solid green line), 16-term LRRM (dashed red line), and 16-term LRRM with zero leakage (dotted black line). a) Magnitude and phase of S_{11} , b) magnitude and phase of S_{21} .

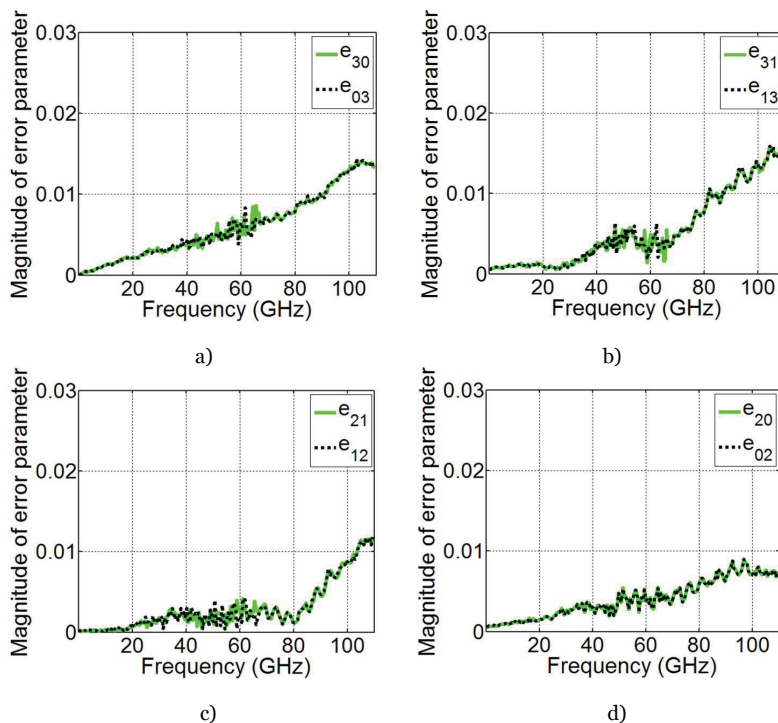


Figure 3.7. Measured magnitudes of the leakage parameters of the error network with the 16-term LRRM method. a) e_{30} (solid green line) and e_{03} (dotted black line), b) e_{31} (solid green line) and e_{13} (dotted black line), c) e_{21} (solid green line) and e_{12} (dotted black line), d) e_{20} (solid green line) and e_{02} (dotted black line).

Due to the very small leakage in the measurements the capability of the 16-term reciprocal calibration method based on reciprocity conditions to handle significant leakage is demonstrated using simulation approaches in [I] and [II]. In [I] the error matrix from the measurements is combined with an additional leakage path to increase the leakage over the DUT. The measured amplitudes of the leakage parameters are below -20 dB and with the additional simulated leakage path the amplitudes of the leakage parameters are increased even up to -6 dB. The 16-term reciprocal calibration is repeated using the calculated S-parameters of the combined error network and it is proved that the 16-term reciprocal calibration method is capable of calibrating measurements with these higher leakage levels. In [II] the whole 16-term calibration and calibration standard definition are performed using purely simulated data with significant leakage paths, and it is demonstrated that the 16-term reciprocal calibration method can be used to calibrate the full 16-term error network that includes high leakage levels. The amplitudes of the leakage parameters are even up to -3.5 dB in the simulations.

3.3 Accuracy of the calibration standards

As it is shown in calibration equation in (2.9), the calibration is based on the raw S-parameter measurement data of the standards, but also on some preliminary known data of the standards. To get accurate calibration the calibration standards need to be well-defined. Especially at millimeter wave and terahertz frequencies the determination of the standards is extremely critical, but at the same time very challenging. The determination can be based on, e.g., self-calibration, direct measurements or electromagnetic or circuit simulations.

The 16-term reciprocal calibration method can be used to test the accuracy of the actual known S-parameters or self-calibration results of the calibration standards [III]. The reciprocity conditions of the error network can be used to check if the calibration standards are well-defined. When an inaccurate definition of calibration standards is used the final error parameters are not reciprocal even though the 16-term reciprocal calibration method assumes that. With well-defined standards the reciprocity conditions of the error parameters are exactly fulfilled. No extra calculations or measurements are needed, because the accuracy of the standards can be verified from the solved error parameters as a by-product of the calibration.

The feasibility of the method to test the accuracy of the calibration standards is demonstrated by simulations and practical on-wafer measurements in [III]. Here only the measurement results are presented. The measurement setup shown in Figure 3.8 consists of a Cascade Microtech probe station with Infinity probes, and Agilent N5250C PNA Network analyzer with Oleson Microwave frequency extension modules for frequency range of 110 – 170 GHz. Structures of the Cascade Microtech ISS are used as calibration standards (Thru, Match, Short, and Open). Figure 3.9 shows the micrographs of the used standards. The vector network analyzer needs to be calibrated first at the waveguide ports, because the error network needs to be reciprocal, and the 16-term calibration method is used as a second-tier calibration.

Two different methods are used to define the calibration standards:

1. The method to determine LRRM calibration standards presented in Section 3.1 and [II].
2. Direct calculation based solely on manufacturer data.

The calibration method, the calibration standards, and the raw S-parameter measurements are the same for both standards definition methods. The calibration procedure presented in Figure 3.4 is exactly the

same for the method 1. For the method 2 the standard definition algorithm is different, but otherwise the calibration procedure is the same.

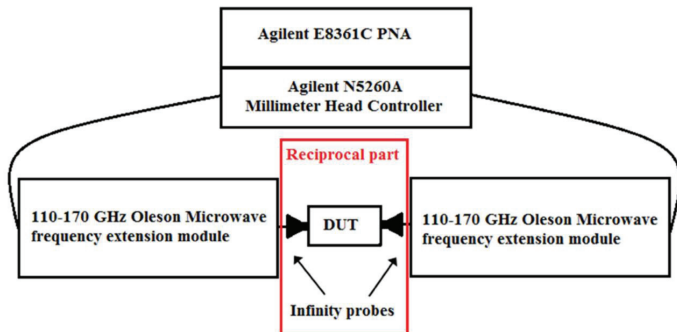


Figure 3.8. Block diagram of the measurement setup. The VNA is pre-calibrated and the 16-term calibration method is used as a second-tier calibration for reciprocal error network inside the red rectangle.

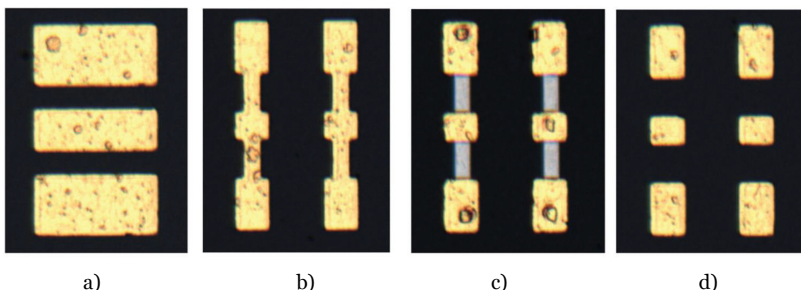
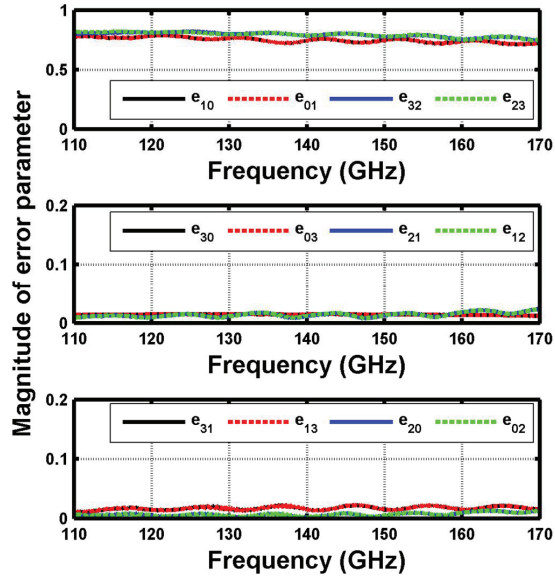


Figure 3.9. Micrographs of the calibration standards from Cascade Microtech ISS used in the measurements. The length of the standards is 135 μm and the material of the substrate is alumina. a) Thru, b) Short, c) Match, d) Open.

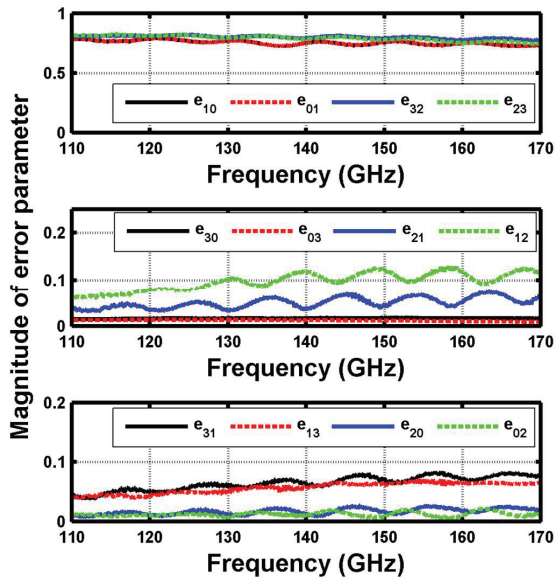
Figure 3.10 presents the error parameters from the calibration when the two methods to define the calibration standards are used. When method 1 is used, all reciprocity conditions of the error parameters are fulfilled, but using method 2 the error parameters are not reciprocal. The reciprocity condition $e_{01} = e_{10}$ is always fulfilled, because it is used to find the correct scaling factor in the reciprocal calibration method in (3.38). In method 1 the inductances of the Match and Short standards, and capacitance of the Open standard are defined separately for all frequency points, but in method 2 constant values are used for all frequency points. Based on the reciprocity conditions fulfillment, method 1 is a better and more accurate method to define the calibration standards.

The accuracy of the calibration standard definition has naturally an effect on the calibrated S-parameters of the DUT, which is now a CPW line shown in Figure 3.11. Figure 3.12 shows the final calibrated S-parameters of the DUT. Slightly different results are obtained with the two definition methods

of the calibration standards. This demonstrates that it is extremely important to define the calibration standards well to achieve accurate measurement results.



a)



b)

Figure 3.10. Error parameters of the calibration. a) Method 1: self-calibration, b) method 2: calculated from manufacturer data.

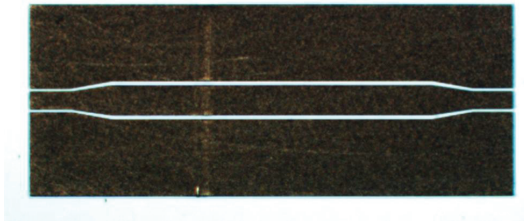


Figure 3.11. Micrograph of the DUT used in the measurement. The length of the DUT is 1500 μm , the center conductor width at the center is 110 μm and 66 μm at the ends, the center conductor to ground gap is 15 μm at the center and 10 μm at the ends, and the material of the substrate is quartz.

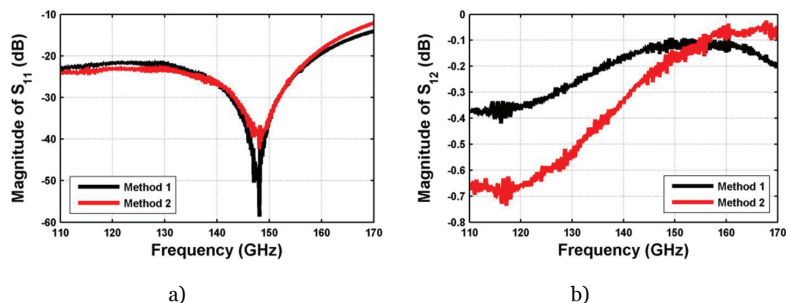


Figure 3.12. Measured S-parameters of the DUT with both standard definition methods. a) S_{11} , b) S_{12} .

3.4 Combinations of calibration standards

LRRM is just one of the combinations of the calibration standards that can be used in the 16-term calibration method based on reciprocity conditions. All the possible different combinations of four two-port calibration standards for the 16-term reciprocal calibration method are tested with the S-parameters simulated in Agilent Advanced Design System (ADS) circuit simulators and the calibration is done in MATLAB [IV]. Figure 3.13 shows the ADS circuit schematic for simulation of the actual S-parameters \mathbf{S}_a and the raw S-parameters \mathbf{S}_m of Thru standard. The same circuits can be used for the other standards. The simulated error network includes RLC networks in both ports representing the connection discontinuities and a resistor representing the leakage path from port to port. Figure 3.14 shows the flow chart illustrating the interaction between ADS and MATLAB. The calibration in MATLAB is performed separately for every combination of four two-port calibration standards.

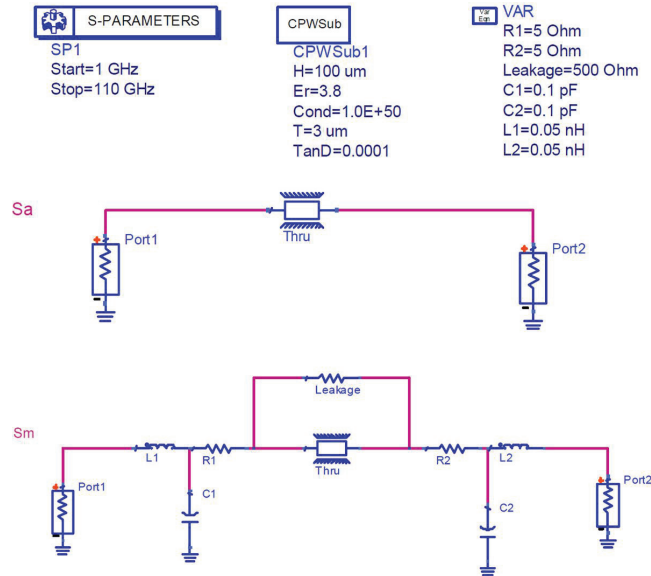


Figure 3.13. ADS circuit schematic for simulation of S_a and S_m of Thru standard.

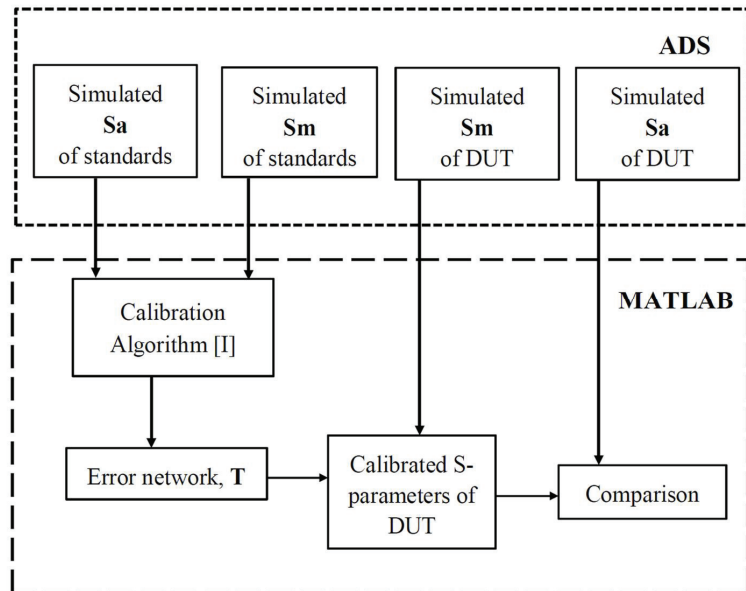


Figure 3.14. Flow chart illustrating the interaction between ADS and MATLAB.

The used standards are Thru (T), Delay (D) and different combinations of Match (M), Short (S), and Open (O). For example M-S means Match standard in port 1 and Short standard in port 2 simultaneously. S and O can be interchanged and M-M can always be replaced with D.

A Thru standard is always used as a first standard and when Delay is used as a second standard all combinations can be used for the two last standards. When one of the other standard pairs is used as a second standard it defines the non-singular combinations that allow the solution of the calibration equation. All the other combinations can be used, except the combinations, where the first port of the third standard is the same as the first port of the second standard (e.g. combination T, O-O, O-S, and S-S) or the second port of the fourth standard is the same as the second port of the second standard (e.g. combination T, O-M, S-S, and S-M). These singular combinations do not allow the solution of the calibration equation. In Table 3.1 the 32 possible non-singular combinations of four two-port calibration standard pairs are presented for S-S and M-S as a second standard. Similar tables can be done for the rest of the standard pairs. These combinations work only for this selection of the 14 linear equations from (3.27a)-(3.27d) presented in Section 3.2, but if the equations were selected some other way the list of the combinations would be different. However, these different combinations can be considered dual cases of the corresponding original combinations.

A similarity index δS is used to compare the accuracy of the different possible combinations [48]

$$\delta S = \sqrt{\frac{\sum_{freq} (|\delta S_{11}|^2 + |\delta S_{12}|^2 + |\delta S_{21}|^2 + |\delta S_{22}|^2)}{4N_{freq}}}, \quad (3.46)$$

where δS_{ij} is the difference between the actual S-parameter and the calibrated S-parameter values and N_{freq} is the number of frequency points. The similarity index is the mean error of each S-parameter. Evenly distributed random noise is added at every frequency for all simulated raw S-parameters S_m of the standards to simulate some of the different errors occurring in practical measurements. Without the added random noise all these possible combinations give equally accurate solution. The similarity indexes of different combinations are shown in Table 3.1. Based on the similarity indexes there are clear differences between the accuracy of different combinations and some of the combinations work better than the others. However, with some other selection of the linear equations also the less accurate combinations may work better, but in this work only one selection of linear equations is used.

Table 3.1. Combinations of four two-port calibration standard pairs for the 16-term reciprocal calibration method, when S-S and M-S are used as a second standard.

St.1	St.2	St.3	St.4	$\delta S \cdot 10^3$	St.1	St.2	St.3	St.4	$\delta S \cdot 10^3$
T	S-S	O-O	M-M	1	T	M-S	S-S	M-M	88
T	S-S	O-O	S-M	290	T	M-S	S-S	O-O	446
T	S-S	O-O	S-O	6	T	M-S	S-S	S-M	19
T	S-S	O-O	M-O	8	T	M-S	S-S	S-O	15
T	S-S	O-O	O-M	7	T	M-S	S-S	M-O	19
T	S-S	M-M	O-O	1	T	M-S	S-S	O-M	423
T	S-S	M-M	S-M	7	T	M-S	O-O	M-M	471
T	S-S	M-M	S-O	33	T	M-S	O-O	S-M	1
T	S-S	M-M	M-O	9	T	M-S	O-O	S-O	6
T	S-S	M-M	O-M	8	T	M-S	O-O	M-O	10
T	S-S	M-S	M-M	9	T	M-S	O-O	O-M	10
T	S-S	M-S	O-O	346	T	M-S	S-M	M-M	11
T	S-S	M-S	S-M	6	T	M-S	S-M	O-O	1
T	S-S	M-S	S-O	4	T	M-S	S-M	S-O	6
T	S-S	M-S	M-O	6	T	M-S	S-M	M-O	84
T	S-S	M-S	O-M	663	T	M-S	S-M	O-M	5
T	S-S	O-S	M-M	71	T	M-S	S-O	M-M	735
T	S-S	O-S	O-O	6	T	M-S	S-O	O-O	8
T	S-S	O-S	S-M	4	T	M-S	S-O	S-M	7
T	S-S	O-S	S-O	3	T	M-S	S-O	M-O	11
T	S-S	O-S	M-O	35	T	M-S	S-O	O-M	1
T	S-S	O-S	O-M	9	T	M-S	O-S	M-M	93
T	S-S	M-O	M-M	7	T	M-S	O-S	O-O	6
T	S-S	M-O	O-O	6	T	M-S	O-S	S-M	221
T	S-S	M-O	S-M	658	T	M-S	O-S	S-O	158
T	S-S	M-O	S-O	9	T	M-S	O-S	M-O	5
T	S-S	M-O	O-M	1	T	M-S	O-S	O-M	10
T	S-S	O-M	M-M	11	T	M-S	O-M	M-M	10
T	S-S	O-M	O-O	7	T	M-S	O-M	O-O	10
T	S-S	O-M	S-M	5	T	M-S	O-M	S-M	5
T	S-S	O-M	S-O	28	T	M-S	O-M	S-O	1
T	S-S	O-M	M-O	1	T	M-S	O-M	M-O	103

3.5 Discussion and future work

As MMIC devices have become more common, the importance of the on-wafer S-parameter measurements is significantly increasing in millimeter wave and terahertz device modelling and design. To measure the S-parameters accurately the calibration of the VNA should be performed using an error model that takes into account all of the possible error sources. At the lower frequencies (< 110 GHz) an accurate calibration can be achieved by using 8-term calibration methods, but at millimeter wave and terahertz frequencies, where the leakage paths may become more significant, the 16-term calibration can be advantageous.

The 16-term calibration based on reciprocity conditions presented in this chapter can calibrate the full 16-term error network. The novel 16-term calibration method based on reciprocity conditions of the error network enables the calibration of full 16-term error network using only four calibration standards. In addition the novel method to determine LRRM

calibration standards in measurement configurations affected by leakage is presented.

In [I] – [IV] the feasibility of the 16-term reciprocal calibration method and LRRM calibration standard definition method are demonstrated with practical measurements. In the example measurements the leakage paths are almost negligible (below -20 dB), thus the difference between 8-term and 16-term calibration methods is minor, but even that minor difference can be explained with the leakage terms. The capability of the 16-term reciprocal calibration method to calibrate the full 16-term error network in the presence of significant leakage paths (even up to -3.5 dB) is demonstrated with simulations in [I] and [II].

To get accurate measurement results it is extremely important to define the calibration standards accurately. The reciprocal 16-term calibration method can be used to test the accuracy of the defined calibration standards. If the calibration standards are accurately defined the reciprocity conditions of the error network are fulfilled. Whereas, error in the definition increases the non-reciprocity in the error network.

The reciprocal 16-term calibration method is compared with the WinCal 8-term LRRM and TRL calibrations. Based on the measurement results presented in this work it is difficult to quantify the accuracies of the different calibration methods. In the future one possibility could be to use the verification technique developed by NIST, which determinates the error bounds for the calibration method by a comparison with the NIST TRL benchmark calibration [86].

The future work is to perform measurements, where the leakage paths are significant, e.g., by using higher frequencies. So far commercial calibration standards are used in the calibration, but in the future the calibration standards should be fabricated on the same wafer with the DUT to keep the leakage terms constant during the calibration and measurement of the DUT. One great advantage of the LRRM calibration method compared to TRL is that in LRRM the calibration standards are much shorter and thus take less space on the wafer. Whereas the fabrication of the Match standard becomes challenging for high frequencies, because usually the resistance is not anymore 50 Ω as it is assumed in the LRRM calibration method.

4. Millimeter wave planar Schottky diodes and mixers

The Schottky diode is based on an interface between a semiconductor and a metal that is called the Schottky junction. The rectifying effect of a metal-semiconductor junction was found out by Braun as early as in 1874 [92], but the name for the diode comes after Walter Schottky (1886-1976), who was one of the earliest developers of the metal-semiconductor junction [93].

This chapter presents briefly the fundamentals of the Schottky diode and the traditional measurement and characterisation methods of the Schottky diodes. Detailed and comprehensive theory and physics behind the Schottky diode can be found, e.g., in [94], [95]. In this chapter also basic theory behind Schottky diode mixers and the most commonly used mixers at millimeter wave and terahertz frequencies are presented.

4.1 Schottky diode structure and characteristics

Previously in millimeter and submillimeter wave mixers, whisker-contacted Schottky diodes have been used as a mixing element. The structure of a whisker-contacted diode is very simple and it enables low parasitic capacitance values, but the assembly and reliability of the contact bring considerable drawbacks. Since late 1980's whisker-contacted Schottky diodes are replaced by planar Schottky diodes [96] – [98]. A planar Schottky diode has a robust structure and the fabrication process enables integration of multiple diodes and integration of the diode with the rest of the circuit. The drawback of the planar diode is the increase of the parasitic capacitance.

Figure 4.1 shows the structure of a planar Schottky diode [96]. On a heavily doped n^+ gallium arsenide (GaAs) substrate there is a thin slightly doped n -type GaAs layer (epitaxial layer) and on top of that there is a metal contact (anode contact pad and finger) forming the Schottky junction. At the other end there is an ohmic contact, which forms the cathode. Under the anode finger there is a surface channel that reduces the parasitic

capacitances close to the anode. The semi-insulating GaAs substrate makes the diode robust and silicon dioxide (SiO_2) layer is used to insulate the anode.

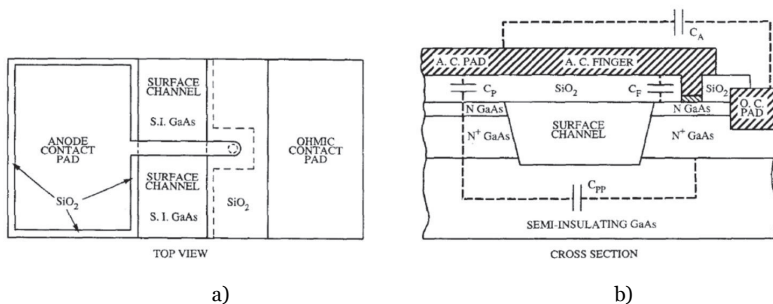


Figure 4.1. A planar Schottky diode. a) Top view, b) cross sectional view [96].

In the following the Schottky diode theory is presented according to text books, e.g. [94], [95]. Figure 4.2 shows the energy band diagram for a metal-semiconductor interface in four different conditions: not in contact, in contact, in contact with forward-bias, and in contact with reverse-bias. If metal and semiconductor are not in contact (Figure 4.2 a), the Fermi level in semiconductor is higher than the Fermi level in metal. When the metal and semiconductor are brought together (Figure 4.2 b), electrons flow from semiconductor to metal forming a positively charged depletion region to the semiconductor side. The electron flow stops when the created potential compensates the difference between the Fermi energies before the contact. The electrons collected on the metal create a potential barrier for the electrons in the semiconductor. The height of this barrier is called the built-in potential of the junction Φ_{bi} . The potential barrier seen by the electrons in the metal is called the Schottky barrier Φ_B .

There are two main current transport mechanisms in the Schottky diodes: thermionic emission of majority carriers (i.e. electrons) over the barrier and the quantum tunneling of electrons through the barrier. The Schottky diode is a majority carrier device, which causes its high speed performance, because the switching speed is not limited by minority carrier effects. When a positive forward voltage is applied over the diode (Figure 4.2 d), the barrier height seen by the electrons in semiconductor is lowered and the potential energy of the electrons increased allowing electrons to transfer easier from semiconductor to the metal via thermionic emission. The diode current I depends exponentially on the voltage over the junction

$$I = I_{sat} \left[\exp \left(\frac{q(V - IR_S)}{\eta k_B T_J} \right) - 1 \right], \quad (4.1)$$

where V is the applied voltage, q is the electron charge, η is the ideality factor, k_B is Boltzmann's constant, T_J is the junction temperature, R_S is the series resistance and I_{sat} is the reverse saturation current, which can be described by equation

$$I_{sat} = SA^{**} T_J^2 \exp\left(-\frac{q\Phi_B}{k_B T_J}\right), \quad (4.2)$$

where S is the area of the junction, A^{**} is the modified Richardson constant, and Φ_B is the Schottky barrier voltage. The tunneling of the electrons increases when the barrier thickness is decreasing, thus the tunneling is not significant at forward voltage [99]. Also at low temperatures and high doping densities tunneling might have significant effect, but in most of the cases tunneling current is insignificant.

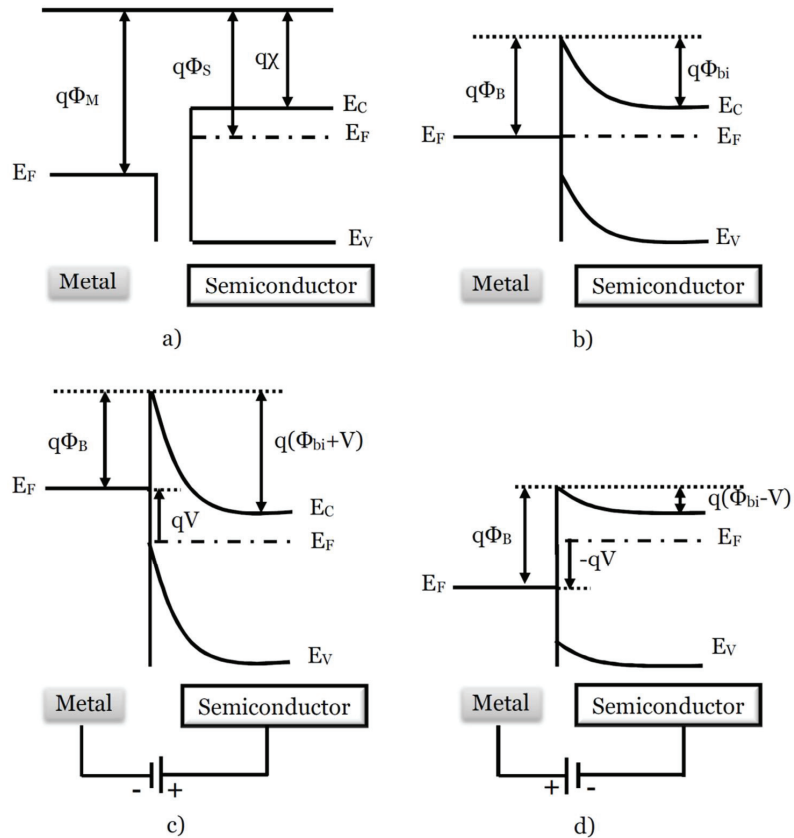


Figure 4.2. Energy band diagram of a metal-semiconductor junction. a) Not in contact, b) in contact, c) in contact with reverse-bias condition, d) in contact with forward-bias condition.

Figure 4.3 presents a typical equivalent circuit for a Schottky diode, which consists of a series resistance R_s , junction resistance r_j , and junction capacitance C_j . There are two types of operating mode in Schottky diodes: resistive (varistor) and capacitive (varactor). The operation of detectors and mixers are based on nonlinear junction resistance of resistive diodes, and the junction resistance can be calculated from the I-V characteristic, with equation (4.3). The operation of frequency multipliers is based mainly on nonlinear junction capacitance of varactor diodes, which can be described by equation (4.4). Resistive diodes can be used also in multipliers achieving wide frequency range, but the efficiency is not as good as in varactor multipliers. The diodes used in this thesis and the publications [VI] and [VII] are resistive diodes.

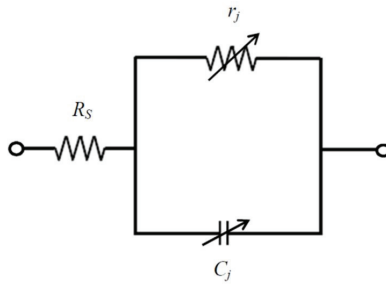


Figure 4.3. Simple equivalent circuit of a Schottky diode.

$$r_j = \left(\frac{dI}{dV} \right)^{-1} = \frac{\eta k_B T_J}{q(I + I_{sat})}, \quad (4.3)$$

$$C_j = \frac{C_{j0}}{\left(1 - \frac{V}{\Phi_{bi}} \right)^\gamma}, \quad (4.4)$$

where C_{j0} is the zero-bias junction capacitance, Φ_{bi} is the built-in voltage, and γ is the doping profile parameter of the epitaxial layer. Typically for an abrupt junction γ is 0.5. The total capacitance of the diode can be obtained from equation

$$C_T = \frac{C_{j0}}{\left(1 - \frac{V}{\Phi_{bi}} \right)^\gamma} + C_p, \quad (4.5)$$

where parasitic pad-to-pad capacitance C_p is mainly caused by the diode pads and the circuit, where the diode is attached. The cutoff frequency can

be considered as a quality criterion of the Schottky diode and can be calculated as

$$f_c = \frac{I}{2\pi R_S C_{j0}}. \quad (4.6)$$

The cutoff frequency should be at least 10 times higher than the operating frequency of the diode [100]. The series resistance R_S is caused mainly by the resistance of the undepleted epitaxial layer, the spreading resistance of the highly doped contact layer, and the resistance of the ohmic contact [100].

4.2 Traditional Schottky diode measurements

The characterisation of Schottky diodes is usually done by traditional current-voltage (I-V), capacitance-voltage (C-V), and S-parameter measurements. Parameter extraction and equivalent circuits are performed based on the measurements results to find out the behavior and the quality of the diodes.

Current-voltage measurement is the most general measurement for the Schottky diodes. The I-V measurement is performed using, e.g., semiconductor parameter analyzer. From the measurement results the I-V diode parameters, such as series resistance, ideality factor, and saturation current are extracted by fitting the theoretical I-V equation (4.1) to the measured results [101] – [106]. Figure 4.4 shows an example of I-V measurement result with the fitted I-V curve and the ideal I-V curve without effect of series resistance for a single-anode Schottky diode.

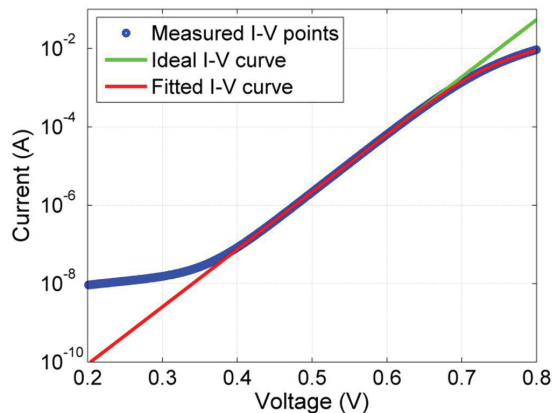


Figure 4.4. I-V extraction of a single-anode Schottky diode. Measured I-V points (blue circles), fitted I-V curve (red line), and ideal I-V curve without the effect of series resistance (green line).

In [107], [108] the series resistance extraction is done using a method that takes into account the temperature dependence of the saturation current and ideality factor. Because the bias current heats up the junction, the saturation current and ideality factor are not constant. This is a significant effect for small diodes that are optimized for high millimeter wave and terahertz frequencies. If the self-heating effect is not taken into account, the extracted series resistance is too small. The self-heating can be minimized by using pulsed I-V measurements [109] – [111]. In the pulsed I-V measurement the I-V curve is measured using very fast pulses so that the diode junction does not have time to heat up. The pulses should be faster than the thermal time constant of the diode to avoid self-heating. In [111] it is shown that when the I-V measurement is performed using fast pulses, the series resistance of the diode is higher than the series resistance obtained from the direct current (DC) I-V measurements.

The total capacitance of the Schottky diode can be measured as a function of voltage using, e.g., LCR meter [102], [112] – [114] or the total capacitance can be extracted from low-frequency (3-10 GHz) S-parameter measurements [109], [114]. The magnitude of the transmission coefficient is dependent only on the value of the total capacitance of the diode at low microwave frequencies and in bias voltages where the diode is not yet conducting. Thus the total capacitance can be extracted by fitting the measured transmission coefficient to a calculated value. C-V parameters such as zero bias junction capacitance, parasitic capacitance and built-in voltage are extracted by fitting the nonlinear capacitance equation (4.5) to the measured total capacitances. Figure 4.5 presents an example of C-V measurement results with the fitted C-V curve for a single-anode Schottky diode using extracted total capacitances from S-parameter measurements.

The comparison between capacitance measurements using an LCR meter and extraction from S-parameter measurements in [114] showed that for discrete diodes both methods give similar results, but for monolithically integrated diodes the extraction from the S-parameters should be used to get more accurate results. In LCR meter measurements the capacitance of the test structure cannot be totally separated from the parasitic capacitance of the diode, thus the measured total capacitance is too high. Also the trapping effects can make the LCR meter measurements challenging or even impossible [114]. The capacitance values can be determined also from theoretical calculations [115], physical simulations [116], and full-wave simulations [22], [117], [118]. The C-V extraction of the antiparallel Schottky diodes is not possible, because antiparallel diodes cannot be reverse-biased.

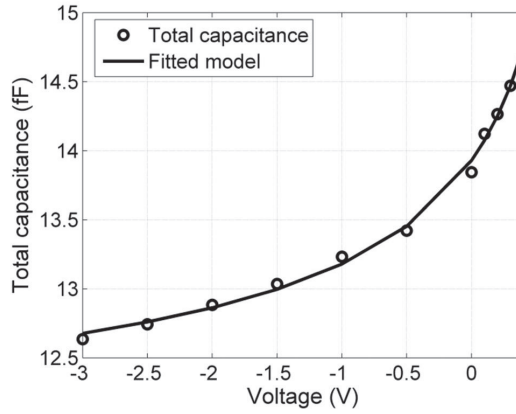


Figure 4.5. C-V extraction of a single-anode Schottky diode. Measured C-V points (circles) and fitted C-V curve (solid line).

The S-parameter measurements can be used to verify the results from I-V and C-V extraction methods, to perform the equivalent circuit of the diode, and to extract the anode finger inductance of the diode [22]. Also series resistance and total capacitance of a Schottky diode can be extracted from the equivalent circuit that is fitted to the measured S-parameters. The equivalent circuit procedure is an important part of the diode design and optimization. To model higher order effects (e.g. skin effect and eddy currents) at higher frequencies more complicated equivalent circuits are needed [119].

A simple equivalent circuit of a single-anode Schottky diode on a CPW test mount is presented in Figure 4.6. The parameters of the Schottky junction are presented inside the rectangle and in addition to those the equivalent circuit includes the finger inductance of the diode L_f , parasitic capacitance C_p , capacitances from the ends of the CPW pads to the ground C_{g1} and C_{g2} , and small pieces of CPW line of the test mount. Figure 4.7 shows the measured and simulated S-parameters from the equivalent circuit of a single-anode Schottky diode up to 110 GHz. There is a small difference between measurements and simulations in S_{11} with 0 V bias voltage at the frequencies above 90 GHz, otherwise the simulated S-parameters agree well with the measured S-parameters. Table 4.1 presents the extracted diode parameters from I-V and C-V measurements and equivalent circuit. Different extraction methods give slightly different values for the extracted parameters.

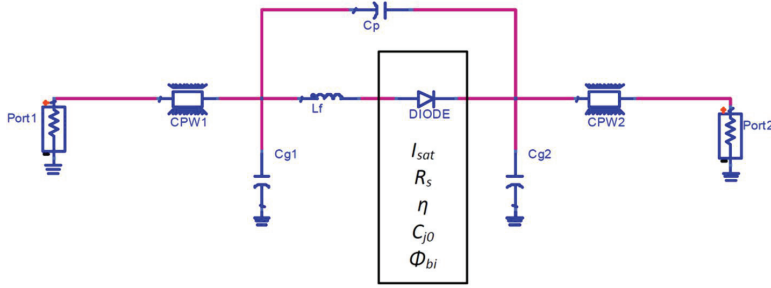


Figure 4.6. The equivalent circuit for a single-anode Schottky diode on a CPW test mount.

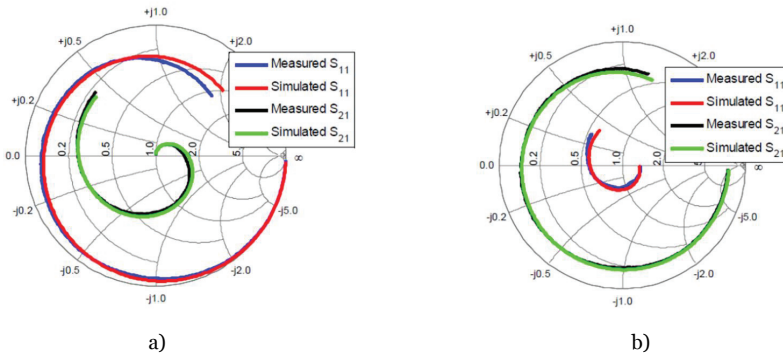


Figure 4.7. Measured and simulated reflection and transmission coefficients for a single-anode Schottky diode. a) 0 V bias point, b) 5 mA bias point.

Table 4.1. Extracted diode parameters from traditional Schottky diode characterisation for a single-anode Schottky diode.

I-V extraction		C-V extraction from LCR meter				C-V extraction from S-parameters			Extraction from equivalent circuit		
R_s (Ω)	η	I_{sat} (fA)	C_{j0} (fF)	C_p (fF)	C_T (fF)	C_{j0} (fF)	C_p (fF)	C_T (fF)	R_s (Ω)	C_T (fF)	L_f (pH)
4.58	1.12	7.9	3.61	10.88	14.49	2.41	11.52	13.93	9.47	13.13	50.6

4.3 Millimeter wave Schottky diode mixers

A mixer converts the frequency of a signal so that the information of the signal remains. The operation of a mixer is based on the properties of a nonlinear circuit, where the output signal includes signal at the input frequency f_i , but also at additional frequencies such as DC component, harmonic frequencies of the input signal mf_i , and when two signals at

frequencies f_1 and f_2 are fed to the circuit also the sum and difference frequencies of the input frequencies $mf_1 \pm nf_2$ ($m, n = 0, 1, 2, \dots$). In transmitters the mixing is done upwards and in receivers downwards. The principle of downward mixing is presented in Figure 4.8, where the local oscillator (LO) power is fed into the LO port at frequency f_{LO} and the radio frequency (RF) signal is fed into RF port at frequency f_{RF} . At the output port a signal at a low intermediate frequency (IF) is obtained

$$f_{IF} = |f_{RF} - f_{LO}|. \quad (4.7)$$

The signal is also mixed to the IF frequency from the image frequency $f_i = 2f_{LO} - f_{RF}$ that is one of the most important sidebands of the mixer. In a single sideband (SSB) mixer the signal band is either the upper sideband ($f_{LO} + f_{IF}$) or the lower sideband ($f_{LO} - f_{IF}$). In a double sideband (DSB) mixer both sidebands are signal bands.

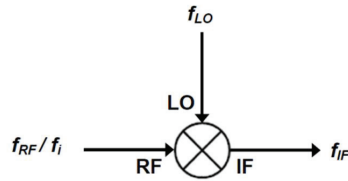


Figure 4.8. Principle of downward mixing.

The high speed switching capability of the Schottky diode makes it the most common mixing element at millimeter wave and terahertz frequencies. The Schottky diode mixers cover the whole millimeter and terahertz frequency range [120]. At millimeter wave and terahertz frequencies mixers can also be based on superconductor-insulator-superconductor (SIS) junctions up to 1.4 THz [121], hot electron bolometers (HEBs) up to 4.7 THz [122], and high electron mobility transistors (HEMTs) up to 100 GHz [123]. SIS and HEB mixers are very sensitive, but also very complicated to use and are therefore used only in scientific applications. Schottky diode and HEMT mixers are appropriate for commercial applications.

Nowadays low-noise amplifiers (LNAs) are beginning to be available also at millimeter wave frequencies up to 670 GHz [124], but usually when LNAs are not available, mixer is the first stage in a receiver. It means that the mixer should be very sensitive as the conversion loss and the noise temperature of the mixer determine the sensitivity of the whole receiver.

Mixer conversion loss defines the efficiency of the mixing and it is determined as

$$L_C = \frac{P_{RF}}{P_{IF}}, \quad (4.8)$$

where P_{RF} is the available input power at the signal frequency and P_{IF} is the output power coupled to the load at IF. The noise temperature of a mixer describes how much noise the mixer generates.

A comprehensive discussion of the noise in Schottky diodes and mixers can be found in [125], [126]. The shot noise in the diode junction is the main noise contributor in the diode mixers. Also the thermal noise from the series resistance and circuit losses causes noise in the diode mixers. The series resistance of the diode increases the conversion loss of the mixer, and this has a bigger effect to the noise temperature than the thermal noise caused by the series resistance. Diodes also produce low-frequency $1/f$ noise, but it is significant only when IF is very low [125].

The series resistance needs to be minimized in order to achieve high cut-off frequency and low mixer conversion loss [127]. At high frequencies also the junction capacitance should be as low as possible as it can be seen in (4.6). The capacitance can be decreased by smaller anode area or by lower doping concentration, but both will increase the series resistance [99]. The high ideality factor and parasitic capacitance increase also the conversion loss. The design and the optimization of the millimeter wave and terahertz Schottky diodes is a trade-off between the diode parameters to get the best operation. It is also very important to have good RF, IF, and LO matching to get low conversion loss for the mixer.

4.3.1 Single-diode mixers

In a single-diode mixer the RF and LO signals are fed into the same waveguide and a diplexer or a coupler is needed to combine the signals. The diplexer is needed to filter the LO noise at the signal and image frequencies. In single-diode mixers the signal is mixed with the fundamental frequency of the local oscillator thus single-diode mixers are also called as fundamental mixers. Single-diode mixers have very simple structure and require low LO power, but at higher frequencies the producing of sufficient LO power becomes challenging. Conversion loss and LO power requirement of a fundamental mixer can be reduced by applying DC bias to the diode [125]. Figure 4.9 shows an example of a single-diode mixer structure for millimeter wave frequencies [128]. The design procedure of single-diode mixers is presented comprehensively in [126], [127].

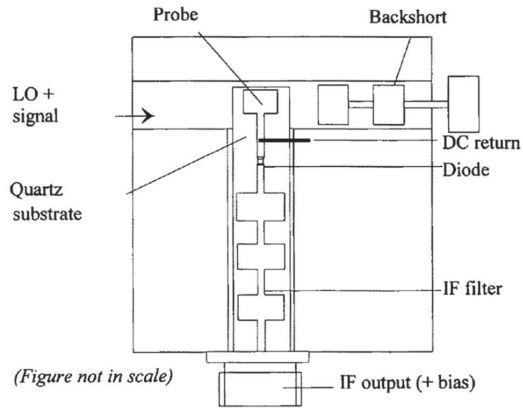


Figure 4.9. Structure of a single-diode mixer [128].

4.3.2 Subharmonic mixers

The mixers, where the signal is mixed with the harmonic frequencies of the local oscillator nf_{LO} , where $n = 2, 3, 4, \dots$, are called harmonic mixers. A harmonic mixer, where $n = 2$ is called subharmonic mixer. The LO frequency is smaller than in the single-diode mixers, because the second harmonic of the LO is used in the mixing. The structure of a subharmonic mixer is more complicated than that of the single-diode mixers. LO reject filtering is needed and RF and LO signals are fed into different waveguides since the RF frequency is much higher than the LO frequency and the dimensions of the waveguide are determined by the used frequency. Additionally an antiparallel diode is used as a mixing element instead of a single-anode diode. When an antiparallel diode with identical diode junction characteristics is pumped by a LO signal only even harmonics of the LO will be produced whereas fundamental frequency component and fundamental frequency mixing products are suppressed [129]. An example of a subharmonic mixer structure is shown in Figure 4.10 [130].

Nowadays Schottky diode mixers operating above 100 GHz are almost always realized as subharmonic mixers. The performance at millimeter wave and terahertz wavelengths is improved much and the conversion loss and the noise temperature are as good as in a case of single-diode mixers [120]. The amplitude modulation (AM) noise of the LO is strongly attenuated in subharmonic mixers and thus subharmonic mixers might have better noise properties [131]. Another great advantage, especially at higher millimeter wave and terahertz frequencies, where the LO power is scarce, is that the subharmonic mixers are pumped at the LO frequency, which is about half of the RF frequency. However, the antiparallel diodes

cannot be biased and therefore one optimization possibility is lost and more LO power is required.

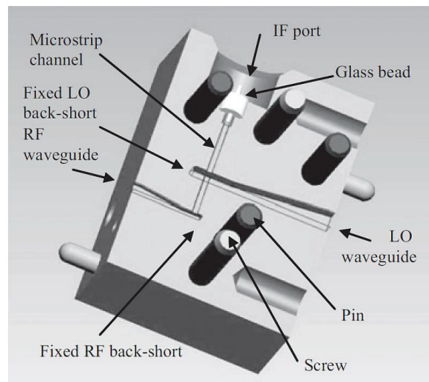


Figure 4.10. Structure of a subharmonic mixer [130].

4.4 Waveguide-to-planar transmission line transitions

At millimeter wave frequencies often a transition between a rectangular waveguide and a planar transmission line is required; for example in mixers, frequency multipliers, and LNAs. There are several ways to realize a transition between a waveguide and a planar transmission line. Perhaps the simplest and the most used transition is a transition based on a probe [132-141]. The probe is formed by the end of a transmission line that enters into the waveguide through an aperture in the broad wall of the waveguide. Figure 4.11 shows a transition based on a probe. The probe is usually placed in the maximum of the E-field ($\lambda/4$ from the waveguide backshort), so that the coupling from the waveguide to the transmission line is at highest. The transition transforms the TE_{10} waveguide mode to the quasi-TEM mode of the transmission line. In order to get better match between the waveguide and the planar transmission line, a reduced height waveguide may be used. The probe shown in Figure 4.11 is placed so that the surface of the substrate is along the direction of wave propagation in the waveguide (longitudinally mounted case). The other option is to place the surface of the substrate perpendicular to the direction of wave propagation in the waveguide (broadside mounted case) [132]. The probe may also have a radial shape instead of the rectangular shape. With a radial probe a wider bandwidth can be achieved [134].

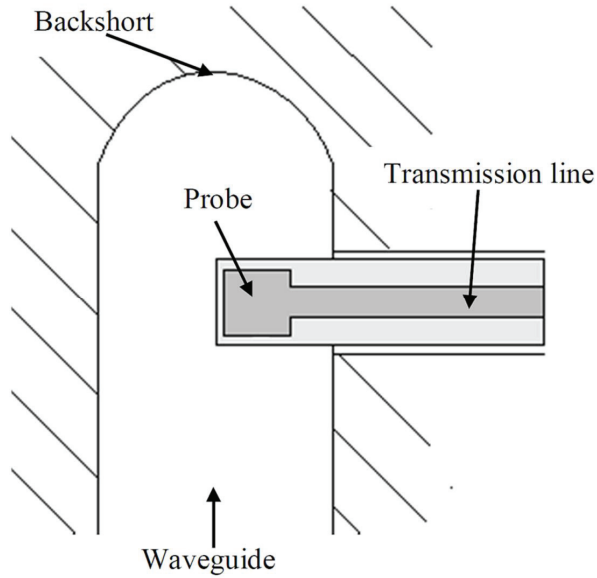


Figure 4.11. Waveguide-to-microstrip transition based on a probe.

The transition from a rectangular waveguide to a planar transmission line could also be based on aperture coupling [142], [143], a ridged waveguide [144] – [146], a quasi-Yagi or a dipole antenna [147] – [149], or an antipodal fin-line [150], [151]. In millimeter wave mixers, the most used transmission line is the microstrip line, however when using a suspended microstrip line, the dielectric losses are smaller than in the microstrip line, because a bigger part of the field is in air.

5. Mixer-based characterisation of Schottky diodes

The characterisation of Schottky diodes is usually done by the traditional I-V, C-V, and S-parameter measurements that are presented in Section 4.2. Based on the measurement results a parameter extraction is performed and an equivalent circuit is created to find out the behavior and the quality of the diodes. However, these extracted parameters do not necessarily tell about the operation of the diodes in the actual environment of the final application, e.g., in mixers and frequency multipliers. It is also possible that the traditional I-V and C-V extraction become challenging because of thermal or trapping effects. For antiparallel diodes the C-V extraction is not even possible because the diodes cannot be reverse-biased. The combination of the traditional and mixer-based Schottky diode characterisation allows a comprehensive comparison of different Schottky diodes. To characterize and compare the mixer operation (conversion loss and noise temperature) of different discrete single-anode and antiparallel Schottky diodes a fundamental and a subharmonic mixer test jigs have been designed and fabricated in [VI] and [VII].

The mixer test jig is a waveguide block that is the same for all diodes and includes a substrate with filtering elements but no impedance matching. The impedance matching conditions of the different diodes are realized with an integrated adjustable waveguide tuner. This allows testing and comparison of different diodes under conditions optimized for each diode, but using the same waveguide block and identical substrates. The mixer-based characterisation is a useful tool for diode manufacturers to test the mixer operation of their diodes without designing and fabricating a fixed tuned mixer for each diode and to reveal possible problems during the development process of the diodes.

The designs of the mixer test jigs are very simple and the DC/IF connections are designed in a way that the substrate with the diode can be easily changed and the contacts can be repeated several times. A miniature SMA connector is used to realize the DC/IF contact and the DC/IF ground contact is made with a copper plate pressed down with a screw through the upper waveguide block. An integrated EH-tuner is used for RF impedance

matching and in the fundamental mixer test jig also for LO impedance matching. The LO matching in the subharmonic mixer test jig can be done using external double E-tuner [152]. The IF impedance matching for both mixer test jigs can be done with an external coaxial tuner. Easy changing of the diodes, flexible embedding impedance matching, and repeatable DC/IF connections enable the comparison of different Schottky diodes under comparable conditions in their actual operating environment.

This chapter presents the mixer-based characterisation results of single-anode and antiparallel Schottky diodes using the mixer test jigs. The nominal RF frequency of the mixer test jigs is 183 GHz. In this chapter also the waveguide-to-suspended microstrip line transition used in the mixer test jigs is presented.

5.1 Waveguide-to-suspended microstrip line transition

To couple the RF and LO signals from the waveguide to the suspended microstrip line a transition is needed in the mixer test jigs. The waveguide-to-suspended microstrip transition is based on a simple probe that extends through the full-height WR-5 waveguide in the E-plane. The probe transition is here chosen to keep the structure as simple as possible. Figure 5.1 shows the cross section views of the transition and Table 5.1 presents the dimensions of the transition. Between the probe and the DC/IF filter there is a narrow line to improve the operation of the transition. The width of the center conductor of the suspended microstrip line is determined by the average width of the Schottky diodes used in the mixer test jigs. The dimensions of the suspended microstrip line channel are designed so that only the fundamental mode is propagating and the waveguide modes are at cut-off.

Table 5.1. Dimensions of the waveguide-to-suspended microstrip line transition (see Figure 5.1).

Parameter	Value	Parameter	Value
w_1	400 μm	l_3	250 μm
w_2	80 μm	w_c	460 μm
w_3	50 μm	h_c	250 μm
w_4	320 μm	w_s	400 μm
w_5	10 μm	h_s	100 μm
d	540 μm	w_g	300 μm
b	650 μm	g	50 μm
l_1	120 μm	s	30 μm
l_2	250 μm	t	3 μm

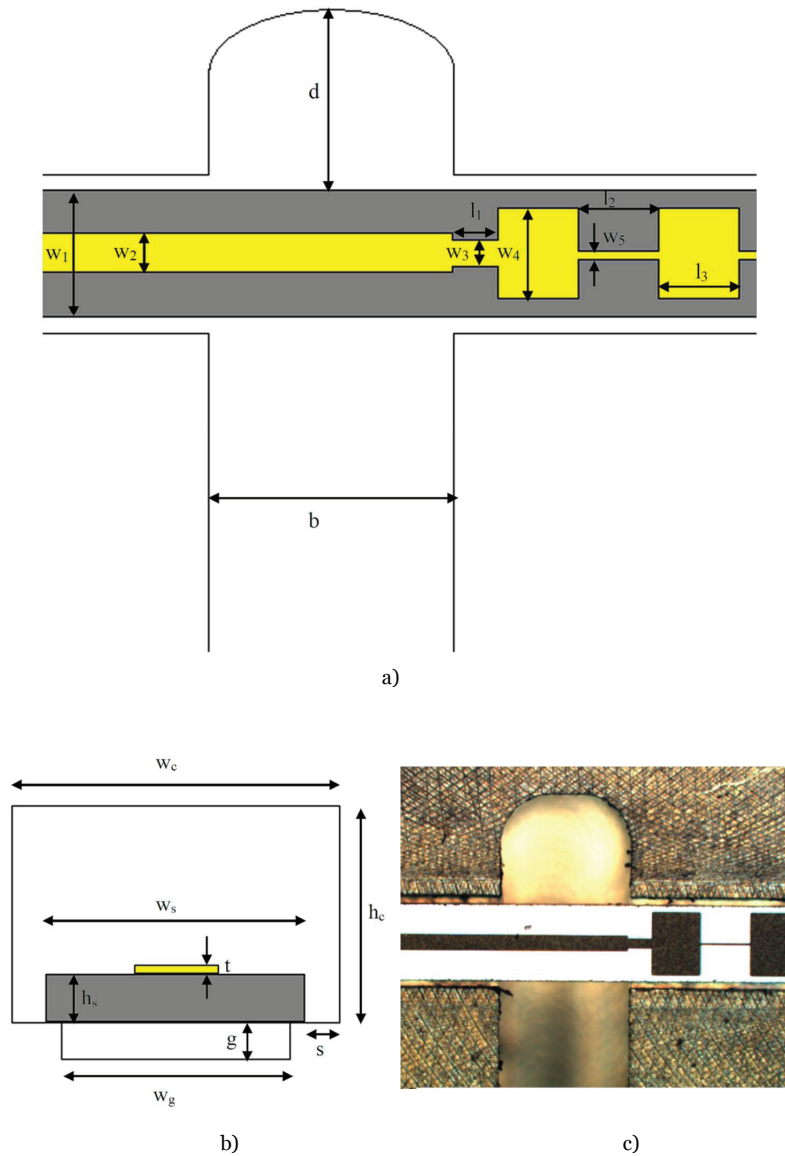


Figure 5.1. Cross section views of the waveguide-to-suspended microstrip transition. a) Top view, b) view from the suspended microstrip channel, c) micrograph of the transition.

Figure 5.2 presents the simulated and measured transmission and reflection coefficients of the back-to-back transition test structure. The simulated transition with the designed dimensions has a wider bandwidth than the measured transitions because of inaccuracies with the fabricated dimensions. The simulated transition with the measured dimensions agrees better with the measurements. The measured transmission loss per single transition (including 10 mm input waveguide losses) is 0.45 dB at 183 GHz based on the measured 0.9 dB loss of the back-to-back transition. The

design and the operation of the waveguide-to-suspended microstrip line transition are presented in [V]. In fundamental mixer test jig one transition can be used to couple RF and LO signals, but in subharmonic mixer test jig separate transitions are needed. The transition presented in [V] is used for RF and LO signals in fundamental mixer test jig and for RF signal in subharmonic mixer test jig. The LO transition in subharmonic mixer test jig has similar design, but for lower frequencies.

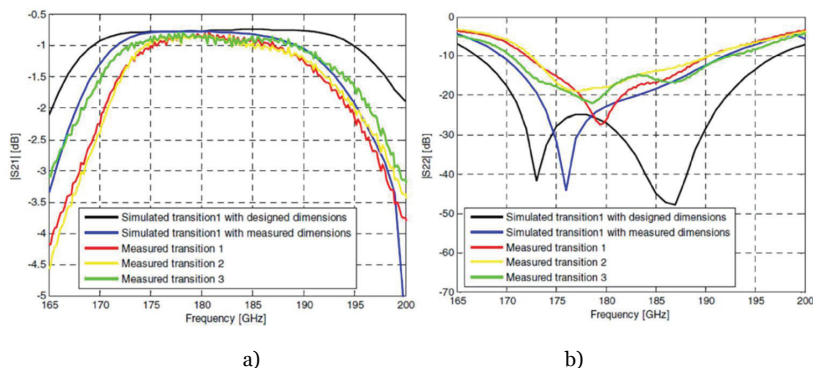


Figure 5.2. Simulated and measured transmission and reflection coefficients of the back-to-back waveguide-to-suspended microstrip line transition. a) Transmission coefficient and b) reflection coefficient.

5.2 Fundamental mixer test jig

Figure 5.3 shows a photograph of the fundamental mixer test jig. A 3D-illustration of the lower waveguide block and a micrograph of the transition part of the fundamental mixer test jig are presented in Figure 5.4. The EH-tuner, RF/LO input waveguide, substrate channel and IF structures are milled in the same split-waveguide block made of brass. The RF/LO input waveguide and the EH-tuner arms are WR-5 waveguides. The design and test measurements of the EH-tuner and dielectric based backshorts for the tuner are presented in [153], [154]. The 100 μm thick quartz substrate ($\epsilon_r = 3.8$) includes a waveguide-to-suspended microstrip transition for the RF and LO signals, a gap for the diode, an RF and LO ground filter, and a DC/IF low-pass filter.

The feasibility of the fundamental mixer test jig is first tested with a commercial VDI-SC2T6 single-anode Schottky diode [VI] and after that the fundamental test jig is used for comparison of different single-anode Schottky diodes from various diode manufacturers with an improved measurement setup [VII]. The results of the comparison measurement [VII] are summarized in this section.

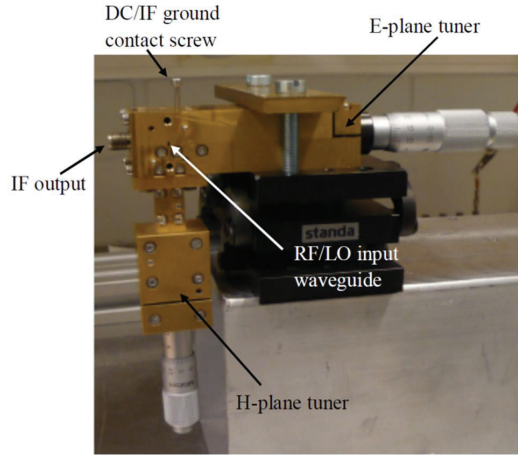
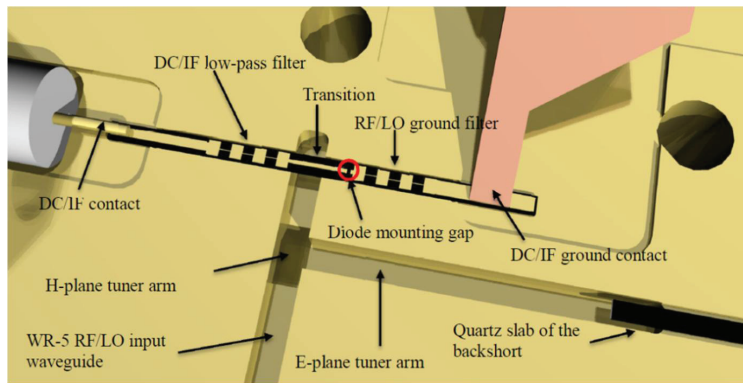
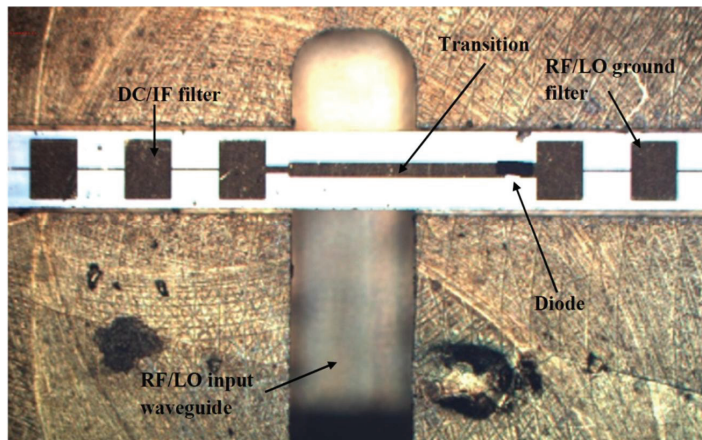


Figure 5.3. Photograph of the fundamental mixer test jig on a supporting device.



a)



b)

Figure 5.4. Lower waveguide block of the fundamental mixer test jig. a) 3D-illustration, b) micrograph of the transition part.

The instability and the noise of the LO source introduced challenges in the feasibility tests in [VI], because the measurement setup was based on a backward wave oscillator (BWO) as a LO source. A quasi-optical diplexer was used to filter the disturbing noise from the BWO that was mixed to the IF frequency. In [VII] the measurement setup is enhanced by replacing the noisy BWO with a Gunn oscillator and 180 GHz frequency doubler. The stability and the repeatability of the measurement setup are improved by using the Gunn oscillator with the frequency doubler as a LO source. The improved measurement setup allows comparison of different single-anode Schottky diodes, because it is possible to get rid of the problems caused by the noise that is mixed to the IF frequency from the noisy LO source.

Figure 5.5 presents the measurement setup used for noise-based determination of DSB conversion loss and mixer noise temperature of the fundamental mixer test jig. A hot/cold load with a horn antenna and a waveguide combination are used as an RF source. Room temperature (295 K) is used for the hot load and liquid nitrogen (77 K) for the cold load. A directional coupler is used to combine RF and LO signals. The IF chain including an isolator, a variable attenuator and two LNAs, is used to amplify the weak IF signal. The IF chain is packaged to avoid mechanical and RF interference.

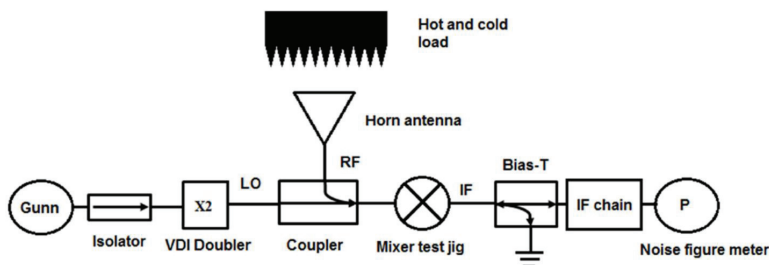


Figure 5.5. Measurement setup for noise-based measurements of fundamental mixer test jig.

The measurement of the conversion loss and noise temperature of the mixer is based on the so-called Y-factor method [155] and the method presented in [156]. First the noise temperature of the IF chain T_{IF} is measured at four attenuation points of the variable IF attenuator. The noise power of the whole measurement setup is then measured with the same adjustments of the variable IF attenuator as above using the Y-factor method

$$Y = \frac{P_H}{P_C} = \frac{T_H + T_e}{T_C + T_e}, \quad (5.1)$$

where P_H is the noise power with hot load, P_C is the noise power with cold load, T_H is the noise temperature of the hot load, and T_C is the noise temperature of the cold load. The noise temperature of the whole setup T_e (mixer and IF chain) can be calculated with equation

$$T_e = \frac{T'_H - YT'_C}{Y - I}, \quad (5.2)$$

where T'_H and T'_C are the corrected hot and cold noise temperatures. These must be used because the loads are not connected directly to the mixer. Thus the attenuation of the RF chain including horn antenna and waveguide combination and directional coupler needs to be taken into account with equation

$$T'_{H,C} = \frac{T_{H,C}}{L_{RF}} + \left(1 - \frac{I}{L_{RF}}\right) T_a, \quad (5.3)$$

where L_{RF} is the attenuation of the RF chain and T_a is the ambient temperature. The DSB mixer noise temperature T_M and DSB conversion loss L_{DSB} can be solved from the equation (5.4) by plotting the noise temperature of the whole setup against the noise temperature of the IF chain at the four attenuation points of the variable IF attenuator. This is demonstrated in Figure 5.6, where a straight line is fitted to the measurement results. The DSB noise temperature of the mixer is the intersection point of the y-axis and the slope of the line is the DSB conversion loss.

$$T_e = T_M + L_{DSB} T_{IF}. \quad (5.4)$$

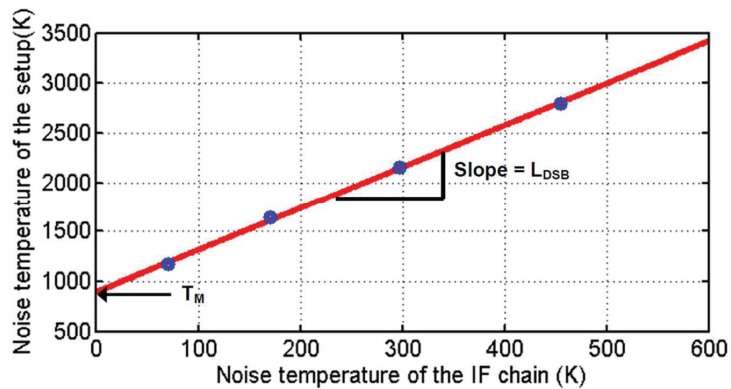


Figure 5.6. Measured noise temperature of the measurement setup as a function of measured noise temperature of the IF chain at the attenuation points of the variable IF attenuator (dots) and the fitted line (solid line).

Figure 5.7 shows the measured DSB conversion losses and noise temperatures as a function of the IF frequency for three single-anode Schottky diodes, when the nominal LO frequency (182 GHz) is used. The available LO power is 1.4 mW and that is used in all fundamental mixer test jig measurements. The bias current and EH-tuner are optimized for the minimum conversion loss at the nominal IF frequency (1 GHz). The tuning and optimizing is done when Agilent PNA 5250A Vector network analyzer is used as a coherent RF source. It is also used to measure the conversion loss to verify the conversion loss measurement results using the noise-based measurement.

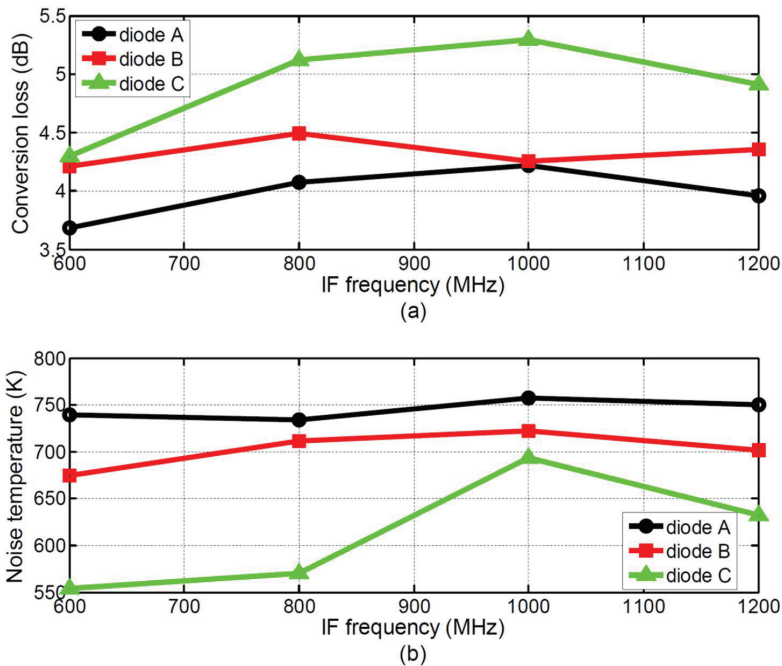


Figure 5.7. Measurements of the single-anode diodes in fundamental mixer test jig as a function of IF frequency. a) DSB conversion loss, b) DSB noise temperature

An external coaxial Microlab S2-05N stub tuner is used to match the IF impedance to improve the conversion loss. Table 5.2 presents the measured conversion losses and noise temperatures of the single-anode diodes in fundamental mixer test jig with and without the IF tuner. The measurements are done at the nominal IF frequency (1 GHz) using optimum bias current. The conversion losses are measured also using the coherent RF signal for a comparison and the conversion loss results from both measurements agree very well. The DSB conversion loss from SSB conversion loss measurements using coherent RF signal can be calculated using equation [155]

$$L_{DSB} = \frac{L_S L_i}{L_S + L_i}, \quad (5.5)$$

where L_S is SSB conversion loss at the signal frequency and L_i is SSB conversion loss at the image frequency.

The uncertainties of the fundamental mixer test jig measurements are calculated using Monte Carlo simulation. The values of the parameters are changed with random values within the limits given for the simulation. The simulation is repeated 10000 times and the standard deviation of the simulated conversion losses or mixer noise temperatures is the uncertainty of the measurement. The uncertainties of the IF output power, the RF input power, the attenuation of bias-T, and the attenuation of the RF chain are included in the uncertainty analysis for SSB conversion loss for which ± 0.2 dB uncertainty limit is obtained. In the uncertainty analysis for noise-based measurements the uncertainties of the noise powers of hot and cold loads, noise temperature of the IF chain, and attenuation of the RF chain are taken into account. The uncertainty limits are for DSB conversion loss ± 0.9 dB and for DSB noise temperature ± 180 K. The uncertainties are quite large because of the high attenuation of the RF chain (10 dB) that is mainly caused by the directional coupler, which leads to a small Y-factor that is more sensitive to uncertainties in the measured noise powers of the hot and cold loads.

Table 5.2. Measurement results of the single-anode diodes in fundamental mixer test jig with and without the IF tuner.

	diode A		diode B		diode C	
	No IF tuner	IF tuner	No IF tuner	IF tuner	No IF tuner	IF tuner
$L_S^{(1)}$ (dB)	7.0	6.1	7.4	6.5	8.0	7.6
$L_i^{(1)}$ (dB)	7.0	6.1	7.3	6.8	8.2	7.8
$L_{DSB}^{(1)}$ (dB)	4.0	3.1	4.4	3.6	5.1	4.7
$L_{DSB}^{(2)}$ (dB)	4.2	3.0	4.3	3.5	5.3	4.8
$T_M^{(2)}$ (K)	760	540	720	510	690	590

⁽¹⁾ From coherent RF signal measurements. L_{DSB} is calculated from measured L_S and L_i

⁽²⁾ From noise-based measurements

5.3 Subharmonic mixer test jig

Figure 5.8 presents a photograph of the subharmonic mixer test jig and Figure 5.9 shows a 3D-illustration of the lower waveguide block of the subharmonic mixer test jig. The structure of the subharmonic mixer test jig is similar to the structure of the fundamental mixer test jig, but there are separate waveguides for RF and LO signals. The RF waveguide is WR-5 waveguide and the LO waveguide is WR-10 waveguide. Thus also two separate waveguide-to-suspended microstrip transitions and reject filters for RF and LO signals are needed. The subharmonic mixer test jig is used to compare four different millimeter wave antiparallel Schottky diodes in [VII].

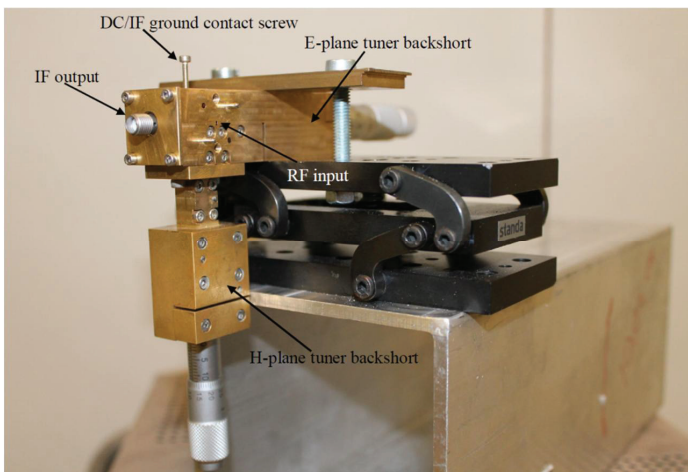


Figure 5.8. Photograph of the subharmonic mixer test jig on a supporting device.

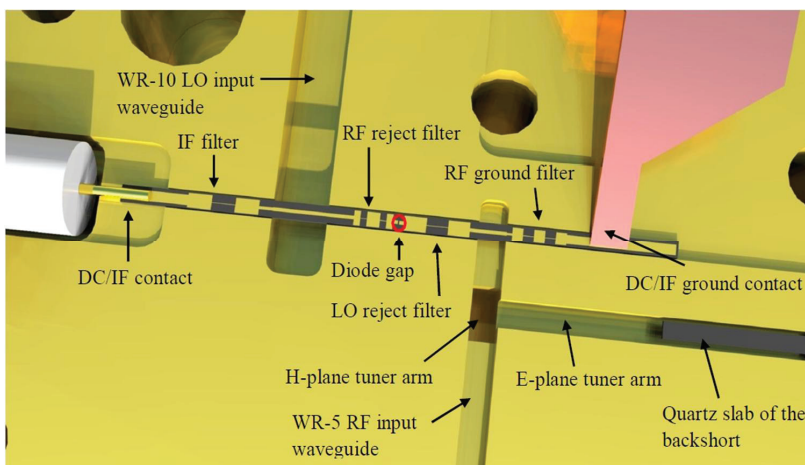


Figure 5.9. 3D-illustration of the lower waveguide block of the subharmonic mixer test jig.

The measurement setup for noise-based determination of DSB conversion loss and noise temperature of the subharmonic mixer test jig is presented in Figure 5.10. A Gunn oscillator is used as the LO source and the LO power can be adjusted with a variable attenuator and monitored with a reference power meter and spectrum analyzer. A hot/cold load with a horn antenna and a waveguide combination are used as an RF source. A packaged IF chain including a variable attenuator and two LNAs is used to amplify the IF signal. The measurement procedure is the same as that used in the fundamental mixer test jig measurements.

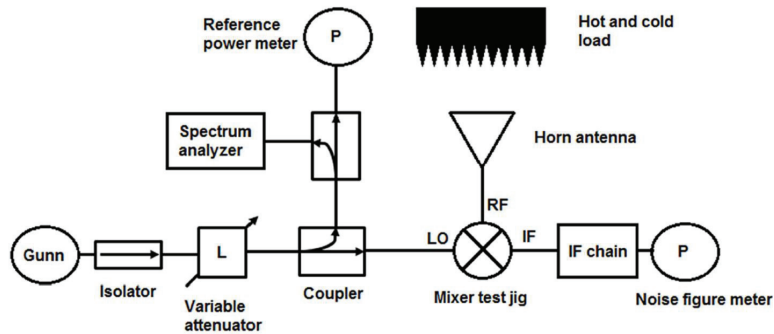


Figure 5.10. Measurement setup for noise-based measurement of subharmonic mixer test jig.

Figure 5.11 presents the measured DSB conversion losses and noise temperatures of the subharmonic mixer test jig with four different antiparallel Schottky diodes as a function of LO power, when the nominal LO frequency (91.5 GHz) and IF frequency (200 MHz) are used. The EH-tuner is optimized for minimum conversion loss at the optimum LO power level. The IF tuner is used to demonstrate the improvement in conversion loss and noise temperature when the IF impedance is matched for diode 2 and diode 4. A 600 MHz IF frequency is used in the measurement, because a coaxial tuner for the nominal IF frequency was not available at the time of these measurements. Table 5.3 shows the measured conversion losses and noise temperatures of the subharmonic mixer test jig with and without the IF tuner.

The uncertainty limits of the subharmonic mixer test jig measurements are calculated using similar Monte Carlo simulation as for fundamental mixer test jig measurements. For measured SSB conversion loss the uncertainty limit is ± 0.2 dB. For noise-based measurements the uncertainty limits are for DSB conversion loss ± 0.6 dB and for DSB noise temperature ± 120 K.

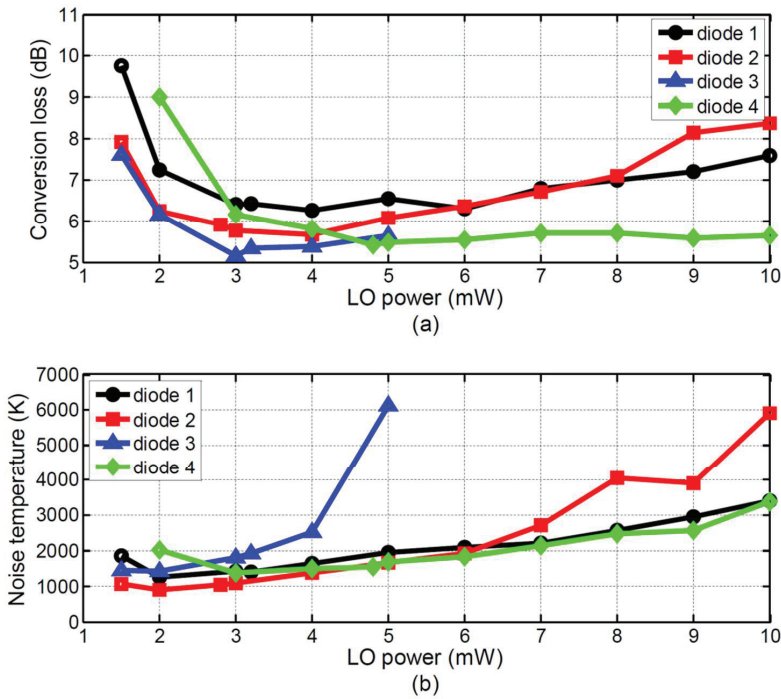


Figure 5.11. Measurements of the antiparallel diodes in subharmonic mixer test jig as a function of LO power. a) DSB conversion loss, b) DSB noise temperature.

Table 5.3. Measurement results of the antiparallel diodes in subharmonic mixer test jig with and without the IF tuner.

	diode 2		diode 4	
	No IF tuner	IF tuner	No IF tuner	IF tuner
$L_s^{(1)}$ (dB)	8.7	7.5	8.7	7.5
$L_i^{(1)}$ (dB)	8.8	7.7	8.8	7.7
$L_{DSB}^{(1)}$ (dB)	5.7	4.6	5.7	4.6
$L_{DSB}^{(2)}$ (dB)	6.0	4.8	5.9	4.9
$T_M^{(2)}$ (K)	1170	990	1730	1590

⁽¹⁾ From coherent RF signal measurements. L_{DSB} is calculated from measured L_s and L_i

⁽²⁾ From noise-based measurements

5.4 Comparison of traditional Schottky diode characterisation and mixer-based characterisation

The measured results of the mixer test jigs can be compared to a simulation-based approach that uses the diode parameters extracted from the traditional I-V, C-V, and S-parameter measurements as input parameters. A full 3D-model of the whole mixer and the diode is built in Ansys High Frequency Structural Simulator (HFSS), where a small coaxial port is connected in place of the diode junction. The HFSS model of the subharmonic mixer test jig is presented in Figure 5.12. The simulated S-parameters of the mixer are exported to ADS circuit simulator, where the physical model for the junction is connected to the coaxial port. The measured diode parameter values from traditional Schottky diode measurements are given for the diode model in ADS. A harmonic balance analysis is then performed to obtain the mixer operation of the circuit to get the simulated DSB conversion losses and noise temperatures.

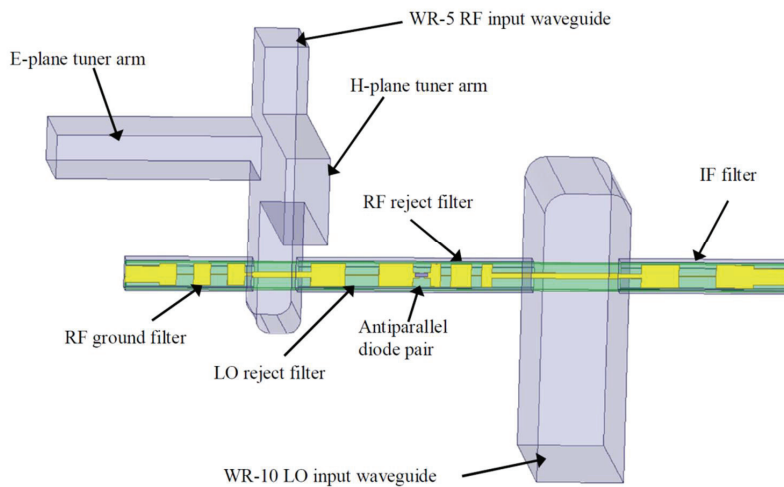


Figure 5.12. HFSS model of the subharmonic mixer test jig.

5.4.1 Fundamental mixer test jig

By using the traditional Schottky diode measurements all diode parameters can be extracted for single-anode diodes. The 3D-diode model from the manufacturer of the diode A is used for all diodes. The parasitic capacitances of the diodes are taken into account in the HFSS simulation. For diodes B and C, whose parasitic capacitances are higher than the

parasitic capacitance of diode A, an additional capacitance is added in the ADS diode model. The S-parameters are simulated in HFSS from 0.1 GHz to 400 GHz and the losses of the waveguide structures (material: brass), substrate (material: quartz), and metal conductor (material: gold) are included in the simulation.

Figure 5.13 presents the ADS circuit schematic for the fundamental mixer test jig and Table 5.4 shows the extracted diode parameters from traditional Schottky diode characterisation in addition to the simulated and measured DSB conversion losses and noise temperatures of the fundamental mixer test jig for different diodes. The simulated DSB conversion losses agree well with the measured conversion losses, but to get more realistic results, individual 3D-diode models from diode manufacturers for all diodes should be used. Unfortunately those are not usually available, e.g., for commercial diodes.

The simulated noise temperatures are much lower than the measured noise temperatures, but the simulated values are underestimated, because all noise mechanisms are not taken into account in the simulation. If, e.g., $1/f$ noise coefficients or leakage conductance of the diodes were known and included in the simulation, the simulated noise temperatures would be closer to the measured values. Furthermore an additional noise source could be added to simulate also the hot electron noise [157]. For diode A the $1/f$ noise coefficients are measured by a partner in cooperation, but for the other diodes the $1/f$ noise coefficients are not known and thus cannot be included in the simulations. In ADS simulation the values of the $1/f$ noise coefficients can be given for the diode model and the $1/f$ noise is characterized by spectral density

$$S(f) = K_f \frac{I^{A_f}}{f^{F_{Fe}}}, \quad (5.6)$$

where K_f , A_f , and F_{Fe} are the $1/f$ noise coefficients. By including the measured $1/f$ noise coefficients in the simulation for diode A, the simulated noise temperature agrees well with the measured noise temperature. The $1/f$ noise needs to be studied more, to find out the actual contribution to the mixer noise temperature. It means that the $1/f$ noise coefficients of all diodes should be measured and included in the simulations. Unfortunately the $1/f$ noise measurement of the diodes was not possible at the time of this work.

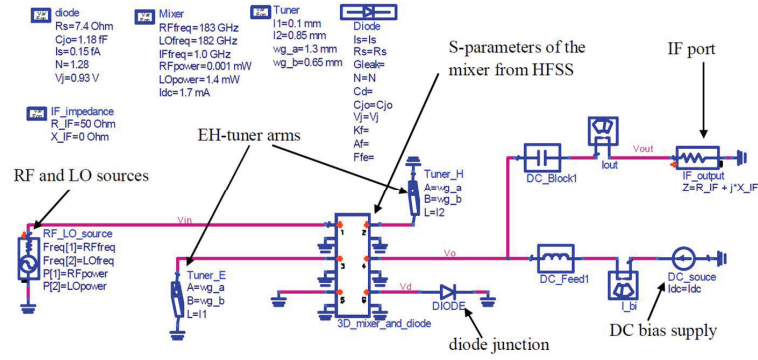


Figure 5.13. ADS circuit schematic of the fundamental mixer test jig simulation.

Table 5.4. Extracted diode parameters from traditional Schottky diode characterisation and simulated and measured DSB conversion loss and noise temperature of fundamental mixer test jig.

	diode A	diode B	diode C
C_{j0} (fF)	1.18	1.73	2.49
C_p (fF)	5.57	8.45	11.52
Φ_{bi} (V)	0.93	0.78	0.92
η	1.28	1.25	1.21
I_{sat} (fA)	0.15	0.12	7.9
R_s (Ω)	7.3	4.9	4.9
$L_{DSB}^{(1)}$ (dB)	3.9	4.0	4.9
$L_{DSB}^{(2)}$ (dB)	4.2	4.3	5.3
$T_M^{(1)}$ (K)	310	320	430
$T_M^{(1)*}$ (K)	755	-	-
$T_M^{(2)}$ (K)	760	720	690

⁽¹⁾ Simulated mixer DSB conversion loss and noise temperature with extracted diode parameters from traditional diode measurements

^{(1)*} Simulated mixer DSB noise temperature including measured $1/f$ noise coefficients

⁽²⁾ Measured DSB mixer conversion loss and noise temperature

5.4.2 Subharmonic mixer test jig

For antiparallel Schottky diodes the traditional I-V characterisation can be performed, but the C-V characterisation is not possible, because the diodes cannot be reverse-biased. The C-V parameters can be obtained, e.g., by measuring similar single-anode diodes or using calculated estimations for zero bias capacitance. The 3D-diode model of diode 2 is used for all diodes

and additional parasitic capacitances are not included in the simulations, which means that only the parasitic capacitance included in the 3D-diode model is taken into account. Figure 5.14 shows the ADS circuit schematic for the subharmonic mixer test jig and Table 5.5 presents the extracted diode parameters from traditional Schottky diode characterisation in addition to the simulated and measured DSB conversion losses and noise temperatures of the subharmonic mixer test jig for different diodes. The $1/f$ noise coefficients of the antiparallel diodes measured in subharmonic mixer test jig are not known and thus not included in the simulations.

The measured and simulated DSB conversion loss values of the subharmonic mixer test jig do not agree as well as the conversion losses of the fundamental mixer test jig. The measured and simulated DSB conversion loss values differ from 0.4 dB to 1.8 dB. The best measured DSB conversion loss value is obtained with the diode 3 and the worst with the diode 1, but the simulated DSB conversion loss of diode 3 is the worst and diode 1 is the best. The simulated noise temperatures are again much lower than measured noise temperatures, but as in the fundamental mixer test jig simulations the simulated noise temperatures are too optimistic. Based on the comparison between simulated and measured DSB conversion loss, mixer-based Schottky characterisation is needed to see the operation of the diodes in the actual mixer environment especially for antiparallel Schottky diodes that cannot be characterised by using traditional C-V measurements.

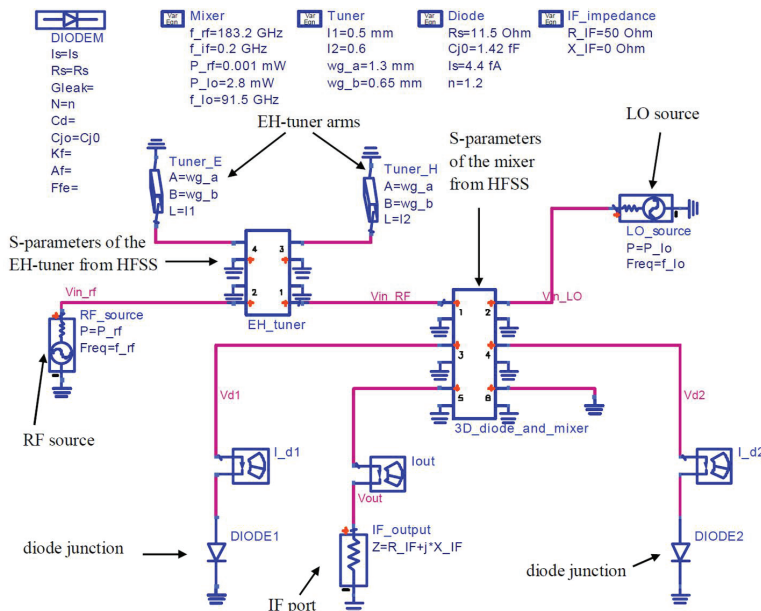


Figure 5.14. ADS circuit schematic of the subharmonic mixer test jig simulation.

Table 5.5. Extracted diode parameters from traditional Schottky diode characterisation and simulated and measured DSB conversion loss and noises temperature of subharmonic mixer test jig.

	diode 1	diode 2	diode 3	diode 4
C_{jo} (fF)	2.29	1.42	2.49	3.49
η	1.16	1.20	1.28	1.25
I_{sat} (fA)	2.9	4.4	1.4	5.0
R_S (Ω)	9.6	11.5	11.8	9.0
$L_{DSB}^{(1)}$ (dB)	4.6	4.7	4.9	4.8
$L_{DSB}^{(2)}$ (dB)	6.4	5.9	5.3	5.4
$T_M^{(1)}$ (K)	420	400	470	490
$T_M^{(2)}$ (K)	1400	1040	1930	1550

⁽¹⁾ Simulated mixer DSB conversion loss and noise temperature with extracted diode parameters from traditional diode measurements

⁽²⁾ Measured DSB mixer conversion loss and noise temperature

5.5 Discussion and future work

The extracted parameters from the traditional Schottky diode characterisation measurements provide very important data from the Schottky diode design and fabrication point of view. The design process of the millimeter wave and terahertz diode mixers relies heavily on the extracted parameters. However the diode operation in the final application such as mixer cannot be completely predicted by using only the extracted diode parameters. In addition to the traditional Schottky diode characterisation method, the mixer-based Schottky diode characterisation offers useful and comprehensive knowledge about the diodes. The mixer-based characterisation offers an effective method for testing single-anode and antiparallel Schottky diodes in their actual environment in the final application. The test jig allows reliable comparison between different Schottky diodes in identical environment utilizing flexible impedance matching for the different diodes.

The test jig is a helpful tool for diode manufacturers to test the new diodes during the development process without designing and fabricating fixed tuned mixer for every diode. It can be used to reveal problems with the diode. For instance one diode that had some fabrication problems was characterised using traditional Schottky diode measurements and mixer test jig measurements. In the traditional measurements only problems with the capacitance measurements were noticed, but the mixer-based characterisation revealed remarkable problems in the measured SSB

conversion loss that was about 20 dB even with the optimized LO power level.

Table 5.6 summarizes the results of different millimeter wave fundamental and subharmonic mixers using planar Schottky diodes [128], [158] – [168], [VII]. Although, Schottky diode mixers up to 1.2 THz are published [169], Table 5.6 presents mixers operating close to the frequency used in this work. For the fundamental mixers more recent results are not found, because nowadays almost always subharmonic mixers are used. However, the fundamental mixer test jig results can be compared to the subharmonic mixer results. From Table 5.6 it can be seen that the measured DSB conversion loss values and noise temperatures of the fundamental mixer test jig are close to the state-of-the-art fixed tuned mixers. The best measured DSB conversion loss values of the subharmonic mixer test jig are as well close to the state-of-the-art, but the noise temperatures are about 400 K higher. The possible error sources in noise measurements of mixers can be [125]:

- **Test-system stability:** If the gain of the test system is not stable between the hot and cold measurements, the error in noise temperature measurement is increased. This can be avoided by measuring the hot and cold measurements quickly. The stability of the test setup in mixer test jig measurements was tested measuring the conversion loss of the mixer and the gain of the IF chain for several minutes and by repeating the measurements several times.
- **Noise from LO source:** The noise from the LO source at the RF frequency is mixed to IF frequency increasing the noise temperature of the mixer. The mixer test jig measurements were done by using two different Gunn oscillators and one frequency multiplier chain including phase locking circuit, and the results were similar (within 200 K) with all three LO sources, thus the LO noise is unlikely the reason for high noise temperatures.
- **Reflected noise:** The noise from the mixer can be reflected back from the IF chain because of imperfect output match and increase the measured noise temperature. An isolator was added in the input of the IF chain in mixer test jig measurements, but the noise temperature was not improved.
- **Spurious signals:** Spurious signal at the measurement frequencies can increase the noise temperature. The spurious signal can be coupled in the input of the mixer or within the IF chain. The IF chain in mixer test jig measurements is shielded to prevent the spurious signals and spurious signals close to the IF frequency were not observed during the measurements.

- **Uncorrected losses:** Additional losses caused by cables or waveguide in the measurement setup increase the noise temperature. In the mixer test jig measurements the losses of the cables and waveguides are removed by calculations.
- **Impedance error of the noise source:** If the hot and cold loads do not have same impedance, the error in noise temperature measurements is increased. In the mixer test jig measurement the only difference in the hot and cold measurements is the noise temperature of the load, thus the impedance of the noise sources are similar.

The measurement setup is very similar to the measurement setup used in fundamental mixer test jig measurements and many of the components of the measurement setups are the same. However, the noise temperatures of the fundamental mixer test jig are lower, thus the subharmonic mixer test jig itself might be the reason for the higher noise temperatures. The losses in the subharmonic mixer test jig are slightly higher than in the fundamental mixer test jig that can be seen in higher conversion loss values. Thus also the noise temperature should be higher, but 400 K is more than is expected. Without the IF impedance matching the noise temperature can be expected to be 200 – 250 K higher than the state-of-the-art values as in fundamental mixer test jig measurements. One possible reason can be $1/f$ noise, because the nominal IF frequency is 200 MHz that is significantly lower than in the fundamental mixer test jig. Unfortunately the measured $1/f$ noise coefficient values of only one single-anode diode were available. In the future the $1/f$ noise coefficients of the diodes should be measured and included in the simulations to find out the actual contribution of the $1/f$ noise to the noise temperatures of fundamental and subharmonic mixer test jigs. In the subharmonic mixer test jig measurements the optimization of the EH-tuner is done at the nominal IF frequency even in the measurements at higher IF frequencies, but optimizing the EH-tuner at every IF frequency lower conversion loss and noise temperatures might be achieved. In the future measurements the optimization should be done separately at every frequency point to get optimal results.

Table 5.6. Performance of millimeter wave fundamental and subharmonic mixers using planar Schottky diodes.

f (GHz)	L_{DSB} (dB)	T_M (K)	Type	diode/manufacturer	reference/year
119	7*	900*	Fundam.	disc./UVa	[128]/1996
183	3.0	540	Fundam.	disc./this work	[VII]/2014
345	9.5*	1370	Fundam.	disc./UVa	[158]/1991
183	6.6	700	Subharm.	disc./ACST (inGaAs)	[159]/2010
183	6.0	500	Subharm.	disc./ACST (GaAs)	[160]/2010
183	4.9	608	Subharm.	int./UMS	[160]/2011
183	6.9	988	Subharm.	foundry/UMS	[161]/2007
183	5.1	530	Subharm.	disc./VDI	[162]/2003
183	4.7	600	Subharm.	disc./RAL	[163]/2003
183	4.8	990	Subharm.	disc./this work	[VII]/2014
240	5.4	510	Subharm.	int./UVa	[164]/1998
330	6.3	700	Subharm.	disc./UVa	[165]/2005
340	6.0	780	Subharm.	disc./VDI	[166]/2012
366	6.9	1220	Subharm.	int./UMS	[160]/2011
380	8.5	850	Subharm.	int./VDI	[167]/2000
380	10.9	3667	Subharm.	foundry/UMS	[168]/2009

* SSB value

disc. = discrete diode

int. = integrated diode

ACST = Advanced Compound Semiconductor Technologies GmbH

RAL = Rutherford Appleton Laboratory

UMS = United Monolithic Semiconductors

UVa = University of Virginia

VDI = Virginia Diodes Inc.

6. Summary of articles

Publication I: “16-term error model in reciprocal systems”

A novel 16-term calibration method based on reciprocity conditions of the error network is presented and demonstrated by practical on-wafer measurements. The reciprocity conditions of the error network are used to reduce the number of unknown error terms. Thus the full 16-term error network can be solved using only four calibration standards. The solution is based on closed-form equations and no approximations are included. This enables also the use of commercial calibration standards, because the non-symmetrical custom-made standard is not needed anymore.

Publication II: “A method to determine LRRM calibration standards in measurement configurations affected by leakage”

A novel method to determine LRRM calibration standards in presence of leakage is introduced and demonstrated by simulation approach and practical on-wafer measurements. The procedure is based on four two-port calibration measurements. The line standard and the resistance of the Match standard need to be exactly known and the reactances of the Match and lossless Short and Open standards are found using their raw S-parameter measurement data. Simple closed-form equations for calibration standard definition are presented.

Publication III: “A method for testing accuracy of the calibration standards based on reciprocity conditions of the error network”

In this publication a novel method for testing the accuracy of the calibration standards based on reciprocity conditions of the error network is presented. To get accurate measurement results it is important to define the calibration standards accurately. The 16-term calibration method based on reciprocity conditions [I] can be used to test the accuracy of the actual known S-parameters or self-calibration results of the calibration standards. The reciprocity conditions of the error terms are exactly fulfilled, if the calibration standards are well-defined, and an error in the definition increases the non-reciprocity in the error network. The feasibility of the

method is demonstrated with a simulation based study and practical on-wafer measurements.

Publication IV: “On-wafer characterisation of test-fixtures in the presence of cross-talk”

In this publication different combinations of four two-port calibration standards for the 16-term calibration method based on reciprocity conditions of the error network [I] are presented. With a simulation based approach the non-singular combinations that allow the solution of the calibration equation are found out. Practical on-wafer measurements using one of the combinations are carried out to demonstrate the usability of one combination in practice.

Publication V: “Simple waveguide-to-suspended microstrip transition with low-pass filter”

This publication presents a simple and low-loss waveguide-to-suspended microstrip transition with low-pass filter designed for generic jig for mixer-based characterisation of Schottky diodes in [VI] and [VII]. The design process, simulations, and back-to-back transition measurement results are presented. The transition is designed for 165-200 GHz frequency band and optimized for specific frequency of 183 GHz with 0.45 dB loss per single transition.

Publication VI: “Generic jig for testing mixing performance of millimeter wave Schottky diodes”

In this publication a fundamental mixer test jig for single-anode Schottky diode mixer-based characterisation at 183 GHz is designed. The feasibility of the test jig is tested with one high quality commercial Schottky diode. The tuning of the embedding impedances and the easy changing of the diode under test allow the characterisation and comparison of different Schottky diodes in their actual operating environment. The measured DSB conversion loss is 4.6 dB and DSB noise temperature is 650K. By using the mixer-based characterisation in addition to the traditional I-V, C-V and S-parameter measurements a comprehensive characterisation of Schottky diodes can be achieved.

Publication VII: “Mixer-based characterisation of millimeter wave and terahertz single-anode and antiparallel Schottky diodes”

The mixer-based characterisation method using the fundamental mixer test jig designed in [VI] is used to compare three different single-anode

Schottky diodes with an improved measurement setup. The noisy backward wave oscillator used as the LO source in [VI] is replaced with a Gunn oscillator and a frequency doubler to get rid of the problems caused by the noise that is mixed to the IF frequency from the LO source. In this paper also a subharmonic mixer test jig for mixer-based characterisation of antiparallel Schottky diodes at 183 GHz is designed and used to compare four different diodes. With high quality Schottky diodes state-of-the-art conversion loss and noise temperature values can be obtained. The traditional characterisation measurements are compared to the mixer-based measurements using a simulation approach that uses the extracted diode parameters from traditional Schottky diode I-V, C-V, and S-parameter measurements.

7. Conclusions and future work

The research for this doctoral thesis focuses on millimeter wave and terahertz range calibration of on-wafer S-parameter measurements and Schottky diode characterisation. The results of the research work are published in publications [I] – [VII]. Chapters 1-6 summarize the background and the theory behind the topics, the research work made by the author, and a comparison of the achieved results and the state-of-the-art results as well as the scientific contribution of the work.

The first part of the thesis concentrates on the calibration of on-wafer S-parameter measurements performed with a VNA. In Chapter 2 the basics about the VNA and different error models and methods for VNA calibration are introduced. Chapter 3 presents the work done in this thesis related to the field of on-wafer calibrations. A novel 16-term calibration method based on reciprocity conditions of the error network is presented and demonstrated with practical on-wafer measurements [I]. This is the first time when the reciprocity conditions of the calibration standards are used to reduce the number of calibration standards from generally required five standards to four standards. In addition a method to determine LRRM calibration standards in measurement configurations affected by leakage is presented and demonstrated with practical on-wafer measurements [II]. The 16-term calibration method based on the reciprocity conditions allows also the use of commercial calibration standards, because no non-symmetrical standard is needed, and this is demonstrated with the practical on-wafer measurements in [I] – [IV].

Generally 8-term calibration methods are used in calibration of VNA. In coaxial and waveguide measurements and in low frequency on-wafer measurements the 8-term error model is sufficiently accurate, but in the measurement systems in the presence of leakage paths, the 16-term error model may be more profitable and more accurate. The millimeter wave and terahertz range on-wafer measurements are application areas of the 16-term calibration methods. The measurement results in [I] – [IV] show that with the 16-term reciprocal calibration method at least as good results as with the commercial 8-term calibration methods can be achieved. However, the capability of the method to truly calibrate the full 16-term error network

in the presence of significant leakage paths is demonstrated with simulation approaches in [I] and [II], because the leakage in the actual measurement setups is almost insignificant at the used frequency range.

To get accurate calibration the used calibration standards need to be well-defined, which becomes more difficult at higher frequencies. Also the fabrication of the calibration standards becomes harder at higher frequencies. The 16-term calibration method based on reciprocity conditions can be used to test the accuracy of the definition of the calibration standards [III]. The reciprocity conditions of the final solved error network will tell, if the standards are well-defined. If the reciprocity conditions are exactly fulfilled, the standards are well-defined. If there is any non-reciprocity in the error network, there is increased inaccuracy in the definition of the calibration standards. This is a useful method to check the accuracy of the calibration standard definition after the calibration. LRRM is only one possible combination of the calibration standards for the 16-term calibration method based on reciprocity conditions. In [IV] all possible combinations of four calibration standards are presented. The presented list is long, but it might be possible to make the list shorter, if some common factors can be found from the combinations.

In the calibration the error terms are assumed to be constant during the calibration and the measurements. It means that in the 16-term calibration method the probe distance and the environment should be the same during the calibration and the measurements to model the leakage paths correctly. The distance can be kept constant if the calibration standards are equally long as the measured DUT, whereas the environment can be kept equal if the calibration standards are fabricated on the same wafer with the DUT. This means that every DUT needs its own calibration standard. Also the length of the standards should be short enough to keep the standards close to ideal, which makes the calibration of the measurement for a long DUT challenging. However, at higher frequencies the length of the DUT is usually short and the probes are close to each other, which can make the leakage paths significant. So far the commercial calibration standards are used, but the future work will be to design and fabricate the standards on the same wafer with the test structures that can be, e.g., integrated diodes, transistors, or passive circuits. Also the on-wafer measurements will be extended up to 325 GHz.

The second part of the thesis focuses on the characterisation of millimeter wave and terahertz Schottky diodes. Chapter 4 presents the operating principles of the Schottky diodes and millimeter wave Schottky diode mixers. Chapter 5 shows the work done in this thesis related to the mixer-based Schottky diode characterisation. The traditional Schottky diode

characterisation measurements include I-V, C-V, and S-parameter measurements and parameter extraction. These extracted parameters are extremely important in the diode development and from the device design point of view. However, these parameters do not tell how the diodes are operating in the actual application, e.g., in mixers and frequency multipliers. A fundamental mixer test jig is designed for characterisation of single-anode Schottky diodes and a subharmonic mixer test jig for characterisation of antiparallel Schottky diodes in [VI] and [VII].

The embedding impedances of the different diodes can be matched with impedance tuners to obtain the minimum conversion loss for each diode. The substrates with the diodes can be changed easily, which allows the comparison of different diodes in the same mixer structure. The structures of the mixer test jigs are designed as simple as possible to keep the fabrication easy and to avoid considerable error in the fabrication of the waveguide blocks and the substrates. The contacts are simple and not soldered, and are thus repeatable that allows to keep the environment for different diodes as uniform as possible. A comprehensive Schottky diode characterisation can be achieved by performing the mixer-based characterisation in addition to the traditional characterisation methods. The mixer-based characterisation can be utilized in diode development and it gives helpful information for the diode manufacturers about the diode operation in the mixer applications. It can also be used for a comparison of different Schottky diodes in a mixer environment. With a high quality diode state-of-the-art conversion loss and noise temperature values can be achieved. In the future the mixer test jig will presumably be used to test new diodes from European diode manufactures as a part of the development process of the diodes.

The two topics of this thesis are essentially related to each other. As it is mentioned, the on-wafer S-parameter measurements are an important part of the Schottky diode characterisation and modelling. The 16-term calibration method developed in the first part of the thesis can be used to get accurate calibration for on-wafer S-parameter measurements of Schottky diodes at millimeter wave and terahertz frequencies, where the leakage paths might become significant.

References

- [1] P. H. Siegel, "THz technology," *IEEE Transactions on Microwave Theory and Techniques*, vol. 50, no. 3, pp. 910-928, Mar. 2002.
- [2] J. H. Wiltse, "History of millimeter and submillimeter waves," *IEEE Transactions on Microwave Theory and Techniques*, vol. 32, no. 9, pp. 1118-1126, Sept. 1984.
- [3] T. M. Goyette, A. Gatesman, T. M. Horgan, M. Coulombe, R. Giles, and J. Waldman, "THz compact range radar systems," presented at the IEEE MTT-S International Microwave Symposium, Philadelphia, PA, USA, June 13, 2003.
- [4] T. Kleine-Ostmann and T. Nagatsuma, "A review on terahertz communications research," *Journal of Infrared, Millimeter and Terahertz waves*, vol. 32, no. 2, pp. 143-171, Jan. 2011.
- [5] T. S. Rappaport, J. N. Murdock, and F. Gutierrez, "State of the art in 60-GHz integrated circuits and systems for wireless communications," *Proceeding of the IEEE*, vol. 99, no. 8, pp. 1390-1436, Aug. 2011.
- [6] P. H. Siegel, "THz instruments for space," *IEEE Transactions on Microwave Theory and Techniques*, vol. 55, no. 11, pp. 2957-2965, Nov. 2007.
- [7] J. W. Walters *et al.*, "The Earth observing system microwave limb sounder (EOS MLS) on the Aura satellite," *IEEE Transactions on Geoscience and Remote Sensing*, vol. 44, no. 5, pp. 1075-1092, May 2006.
- [8] J. R. Wang, P. Racette, J. D. Spinhime, K. F. Evans, and W. D. Hart, "Observations of cirrus clouds with airborne MIR, CLS, and MAS during SUCCES," *Geophysical Research Letters*, vol. 25, no. 8, pp. 1145-1148, Apr. 1998.
- [9] D. Doyle, G. Pilbratt, and J. Tauber, "The Herschel and Planck space telescopes," *Proceeding of the IEEE*, vol. 97, no. 8, pp. 1403-1411, Aug. 2009.
- [10] T. G. Phillips and J. Keene, "Submillimeter astronomy," *Proceeding of the IEEE*, vol. 80, no. 11, pp. 1662-1678, Nov. 1992.
- [11] J. F. Federici, B. Schulkin, F. Huangm D. Gary, R. Barat, F. Oliveira, and D. Zimdars, "THz imaging and sensing for security

- applications – explosives, weapons and drugs,” *Semiconductor Science and Technology*, vol. 20, no.7, pp. 266-280, June 2005.
- [12] R. Appleby and R. N. Anderton, “Millimeter-wave and submillimeter-wave imaging for security and surveillance,” *Proceeding of the IEEE*, vol. 95, no. 8, pp. 1683-1690, Aug. 2007.
- [13] B. H. Deng, C. W. Domier, A. J. H. Donne, K. C. Lee, N. C. Luhmann Jr., E. Mazzucato, T. Munsat, H. Park, and M. van de Pol, “THz technique in plasma diagnostics,” in *IEEE MTT-S International Microwave Symposium Digest*, Seattle, WA, USA, June 2-7, 2002, pp. 1587-1590.
- [14] C. W. Domier, N. C. Luhmann Jr., H. K. Park, Z. Xia, and P. Zhang, “Advances in millimeter wave/THz plasma diagnostics instrumentation,” in *Joint 32th International Conference on Infrared and Millimeter Waves and 15th International Conference on Terahertz Electronic*, Gardiff, UK, Sept. 2-9, 2007, pp. 8-11.
- [15] P. H. Siegel, “Terahertz technology in biology and medicine,” *IEEE Transactions on Microwave Theory and Techniques*, vol. 52, no. 10, pp. 2438- 2447, Oct. 2004.
- [16] A. Rumiantsev and R. Doerner, “RF probe technology,” *IEE Microwave Magazine*, vol. 11, no. 7, pp. 46-58, Nov. - Dec. 2013.
- [17] I. D. Robertson and S. Lucyszyn, *RFIC and MMIC Design and Technology*, The institution of Electrical Engineers, London, UK, 2001.
- [18] S. Marsh, *Practical MMIC Design*, Artech House, Norwood, MA, USA, 2006.
- [19] M. Bauwens, L. Chen, C. Zhang, A. Arsenovic, A. Lichtenberger, N. S. Barker, and R. M. Weikle, “A terahertz micromachined on-wafer probe for WR-1.2 waveguide,” in *Proceedings of 7th European Microwave Integrated Circuits Conference*, Amsterdam, The Netherlands, Oct. 29-30, 2012, pp. 88-91.
- [20] T. W. Crowe and W. L. Bishop, “Opening the terahertz window with integrated circuits,” *IEEE Journal of Solid-State Circuits*, vol. 40, no. 10, pp. 2104-2110, Oct. 2005.
- [21] L. A. Samoska, “An overview of solid-state integrated circuit amplifiers in the submillimeter-wave and THz regime,” *IEEE Transactions on Terahertz Science and Technology*, vol. 1, no. 1, pp. 9-24, Sept. 2011.
- [22] A. Y. Tang, V. Drakinskiy, K. Yhland, J. Stenarson, T. Bryllert, and J. Stake, “Analytical extraction of a Schottky diode model from broadband S-parameters,” *IEEE Transactions on Microwave Theory and Techniques*, vol. 61, no. 5, pp. 1870-1878, May 2013.

- [23] “Understanding the fundamental principles of vector network analysis,” *Agilent Technologies Application Note 1287-1*, web address: <http://cp.literature.agilent.com/litweb/pdf/5965-7707E.pdf> (28th Apr. 2014).
- [24] K. Silvonen, *Sähkötekniikka ja piiriteoria* (in Finnish), Otatiето, Helsinki, Finland, 2009.
- [25] D. K. Rytting, “Network analyzer accuracy overview,” in *58th ARFTG Conference Digest*, San Diego, CA, USA, Nov. 29-30, 2001, pp. 1-13.
- [26] “Exploring the architectures of network analyzers,” *Agilent Technologies Application Note 1287-2*, web address: <http://cp.literature.agilent.com/litweb/pdf/5965-7708E.pdf> (28th Apr. 2014).
- [27] K. Silvonen, “LMR 16 - a self-calibration procedure for a leaky network analyzer,” *IEEE Transactions on Microwave Theory and Techniques*, vol. 45, no. 7, pp. 1041-1049, July 1997.
- [28] H. van Hamme and M. Vanden Bossche, “Flexible vector network analyzer calibration with accuracy bounds using an 8-term or a 16-term error correction,” *IEEE Transactions on Microwave Theory and Techniques*, vol. 42, no. 6, pp. 976-987, June 1994.
- [29] K. Silvonen, “New algorithms for network analyzer, test fixture, and wafer prober calibration,” Doctoral thesis, Helsinki University of Technology, Espoo, Finland, 1999.
- [30] R. F. Scholz, F. Korndörfer, B. Senapati, and A. Rumiantsev, “Advanced technique for broadband on-wafer RF device characterisation,” in *63th ARFTG Conference Digest*, Ft. Worth, TX, USA, June 11, 2004, pp. 83-90.
- [31] “On-wafer vector network analyzer calibration and measurements,” *Cascade Microtech Application Note*, web address: http://www.home.agilent.com/upload/cmc_upload/All/ONWAFER.pdf (28th Apr. 2014).
- [32] “Applying error correction to network analyzer measurements,” *Agilent Technologies Application Note 1287-2*, web address: <http://cp.literature.agilent.com/litweb/pdf/5965-7709E.pdf> (28th Apr. 2014).
- [33] J. V. Butler, D. K. Rytting, M. F. Iskander, R. D. Pollard, and M. Vanden Bossche, “16-term error model and calibration procedure for on-wafer network analysis measurements,” *IEEE Transactions on Microwave Theory and Techniques*, vol. 39, no. 12, pp. 2211-2217, Dec. 1991.
- [34] J. Martens, “Reciprocity-based multiport de-embedding and an analysis of standard sensitivity,” in *72nd ARFTG Microwave*

- Measurement Symposium Digest*, Portland, OR, Dec. 9-12, 2008, pp. 151–156.
- [35] X. Wei, G. Niu, S. L. Sweeney, Q. Liang, X. Wang, and S. S. Taylor, “A general 4-port solution for 110 GHz on-wafer transistor measurements with or without impedance standard substrate (ISS) calibration,” *IEEE Transactions on Electron Devices*, vol. 54, no. 10, pp. 2706–2714, Oct. 2007.
- [36] V. Teppati and A. Ferrero, “On-wafer calibration algorithm for partially leaky multiport vector network analyzers,” *IEEE Transactions on Microwave Theory and Techniques*, vol. 53, no. 11, pp. 3665–3671, Nov. 2005.
- [37] C. R. Curry, “How to calibrate through balun transformers to accurately measure balanced systems,” *IEEE Transactions on Microwave Theory and Techniques*, vol. MTT-51, no. 3, pp. 961–965, Mar. 2003.
- [38] Y. Zhang, K. Silvonon, and N. H. Zhu, “Measurement of a reciprocal four-port transmission line structure using the 16-term error model,” *Microwave and Optical Technology Letters*, vol. 49, no. 7, pp. 1511–1515, July 2007.
- [39] K. Silvonon, “Review of the TCX-based network analyzer calibration algorithms,” *Recent Research Developments in Microwave Theory and Techniques*, vol. 1, pp. 17-24, 1999.
- [40] K. Silvonon, “Calibration of 16-term error model,” *IEE Electronics Letters*, vol. 29, no. 17, pp. 1544-1545, Aug. 1993.
- [41] H. Heuermann and B. Schiek, “Calibration of network analyzer measurements with leakage errors,” *IEE Electronics Letters*, vol. 30, no. 1, pp. 52-53, Jan. 1994.
- [42] M. Schramm, M. Hrobak, J. Schür, and L. -P. Schmidt, “A SOLR calibration procedure for the 16-term error model,” in *42nd European Microwave Conference*, Amsterdam, The Netherlands, Oct. 29- Nov. 1, 2012, pp. 589-592
- [43] A. Ferrero and F. Sanpietro, “A simplified algorithm for leaky network analyzer calibration,” *IEEE Microwave and Guided Waves Letters*, vol. 5, no. 4, pp. 119-121, April 1995.
- [44] J. Fitzpatrick, “Error models for systems measurements,” *Microwave Journal*, vol. 21, no. 5, pp. 63-66, May 1978.
- [45] A. Ferrero and U. Pisani, “Two-port network analyzer calibration using an unknown thru,” *IEEE Microwave and Guided Wave Letters*, vol. 2, no. 12, pp. 505-507, Dec. 1992.
- [46] S. Basu and L. Hayden, “An SOLR calibration for accurate measurement of orthogonal on-wafer DUTs,” in *IEEE MTT-S International Microwave Symposium Digest*, Denver, CO, USA, June 8-13, 1997, pp. 1335-1338.

- [47] H. J. Eul and B. Schiek, "Reducing the number of calibration standards for network analyzer calibration," *IEEE Transactions on Instrumentation and Measurements*, vol. 40, no. 4, pp. 732-735, Aug. 1991.
- [48] K. J. Silvonen, "Calibration of test fixtures using at least two standards," *IEEE Transactions on Microwave Theory and Techniques*, vol. 39, no. 4, pp. 624-630, Apr. 1991.
- [49] G. F. Engen and C. A. Hoer, "Thru-Reflect-Line: an improved technique for calibrating the dual six-port automatic network analyzer," *IEEE Transactions on Microwave Theory and Techniques*, vol. MTT-27, no. 12, pp. 987-993, Apr. 1979.
- [50] "Network analysis, applying the HP 8510B TRL calibration for non-coaxial measurements," *Agilent Technologies Product Note 8510-8A*, web address: http://www.icmicrowave.com/pdf/Non_Coax_Meas_5091-3645E.pdf (28th Apr. 2014).
- [51] C. A. Hoer, "Choosing line lengths for calibrating network analyzers," *IEEE Transactions on Microwave Theory and Techniques*, vol. 31, no. 1, pp. 76-78, Jan. 1983.
- [52] D. Hollmann, G. Baumann, and R. Hierl, "Applying full two-port capabilities to a standard mm-wave system for TRL calibration," *Microwave Journal*, pp. 103-111, Mar. 1991.
- [53] J. S. Kasten, M. B. Steer, and R. Pomerleau, "Enhanced through-reflect-line characterisation of two-port measuring systems using free-space capacitance calculation," *IEEE Transactions on Microwave Theory and Techniques*, vol. 38, no. 2, pp. 215-217, Feb. 1990.
- [54] D. Rubin, "De-embedding mm-wave MICs with TRL," *Microwave Journal*, pp. 141-150, June 1990.
- [55] P. Jeroma and G. Martin, "Moving reference planes for on-wafer measurements using the TRL calibration technique," in *32nd ARFTG Conference Digest*, Tempe, AZ, USA, Dec. 1-2, 1988, pp. 131-140.
- [56] J. Stenarson and K. Yhland, "A reformulation and stability study of TRL and LRM using S-parameters," *IEEE Transactions on Microwave Theory and Techniques*, vol. 57, no. 11, pp. 2800-2807, Nov. 2009.
- [57] R. B. Marks, "Multi-line calibration for MMIC measurement," in *36th ARFTG Conference Digest*, Monterey, CA, USA, Nov. 29-30, 1990, pp. 47-56.
- [58] R. B. Marks, "A multiline method of network analyzer calibration," *IEEE Transactions on Microwave Theory and Techniques*, vol. 39, no. 7, pp. 1205-1215, July 1991.
- [59] J. A. Jargon and R. B. Marks, "Two-tier multiline TRL for calibration of low-cost network analyzers," in *46th ARFTG*

- Conference Digest*, Scottsdale, AZ, USA, Nov. 30 – Dec. 1, 1995, pp. 1-8.
- [60] D. C. DeGroot, J. A. Jargon, and R. B. Marks, “Multiline TRL revealed,” in *60th ARFTG Conference Digest*, Washington, DC, USA, Dec. 5-6, 2002, pp. 131-155.
- [61] D. F. Williams, C. M. Wang, and U. Arz, “An optimal multiline TRL calibration algorithm,” in *IEEE MTT-S International Microwave Symposium Digest*, June 8-13, 2003, pp. 1819-1822.
- [62] R. Marks and K. Phillips, “Wafer-level ANA calibrations at NIST,” in *34th ARFTG Conference Digest*, Ft. Lauderdale, FL, USA, Nov. 30 – Dec. 1, 1989, pp. 11-25.
- [63] H. J. Eul and B. Schiek, “Thru-Match-Reflect: One result of a rigorous theory for deembedding and network analyzer calibration,” in *Proceedings of 18th European Microwave Conference*, Stockholm, Sweden, Sept. 12-15, 1988, pp. 909-914.
- [64] S. Lautzenhiser, A. Davidson, and K. Jones, “Improve accuracy of on-wafer tests via LRM calibration,” *Microwaves & RF*, vol. 29, pp. 105-109, Jan 1990.
- [65] D. F. Williams and R. B. Marks, “LRM probe-tip calibrations with imperfect resistors and lossy lines,” in *42th ARFTG Conference Digest*, San Jose, CA, USA, Dec. 2-3, 1993, pp. 32-36.
- [66] D. F. Williams and R. B. Marks, “LRM probe-tip calibrations using nonideal standards,” *IEEE Transactions on Microwave Theory and Techniques*, vol. 43, no. 2, pp. 466-469, Feb. 1995.
- [67] D. F. Williams and J. B. Schappacher, “Line-reflect-match calibrations with nonideal microstrip standards,” in *46th ARFTG Conference Digest*, Scottsdale, AZ, USA, Nov. 30 – Dec. 1, 1995, pp. 35-38.
- [68] A. Davidson, E. Strid, and K. Jones, “Achieving greater on-wafer S-parameter accuracy with the LRM calibration technique,” in *34th ARFTG Conference Digest*, Ft. Lauderdale, FL, USA, Nov. 30 – Dec. 1, 1989, pp. 61-66.
- [69] J. T. Barr and M. J. Pervere, “A generalized vector network analyzer calibration technique,” in *34th ARFTG Conference Digest*, Ft. Lauderdale, FL, USA, Nov. 30 – Dec. 1, 1989, pp. 51-60.
- [70] J. A. Reynoso-Hernandez, “On-wafer LRM calibration technique using a non-reflecting lossy line of arbitrary length,” in *63rd ARFTG Conference Digest*, Fort Worth, TX, USA, June 11, 2004, pp. 205-210.
- [71] J. Marterns, “LRM: A quantitative look at reference impedance contradictions and other uncertainty impacts,” in *69th ARFTG Conference Digest*, Honolulu, HI, USA, June 8, 2007, pp. 1-7.

- [72] J. E. Pence, "Verification of LRRM calibrations with load inductance compensation for CPW measurements on GaAs substrates," in *42th ARFTG Conference Digest*, San Jose, CA, USA, Dec. 2-3, 1993, pp. 45-47.
- [73] A. Davitson, K. Jones, and R. Strid, "LRM and LRRM calibrations with automatic determination of load inductance," in *36th ARFTG Conference Digest*, Monterey, CA, USA, Nov. 29-30, 1990, pp. 57-63.
- [74] F. Purroy and L. Pradell, "New theoretical analysis of the LRRM calibration technique for vector network analyzers," *IEEE Transactions on Instrumentation and Measurement*, vol. 50, no. 5, pp. 1307-1314, Oct. 2001.
- [75] L. Hayden, "An enhanced line-reflect-reflect-match calibration," in *67th ARFTG Conference Digest*, San Francisco, CA, USA, June 16, 2006, pp. 146-149.
- [76] N. R. Franzen and R. A. Speciale, "A new procedure for system calibration and error removal in automated S-parameter measurements," in *Proceedings of 5th European Microwave Conference*, Hamburg, Germany, Sept. 1-4, 1975, pp. 67-73.
- [77] D. Brubaker and J. Versprecht, "Measured S-parameters with the TSD technique," *Microwaves & RF*, no. 11, pp. 97-101, 159, Nov. 1985.
- [78] K. J. Silvonen, "A general approach to network analyzer calibration," *IEEE Transactions on Microwave Theory and Techniques*, vol. 40, no. 4, pp. 754-759, Apr. 1992.
- [79] M. A. Pulido-Gaytán, J. A. Reynoso-Hernández, A. Zárate-de Landa, J. R. Loo-Yau, and M. del Carmen Maya-Sánchez, "Vector network analyzer calibration using a line and two offset reflecting loads," *IEEE Transactions on Microwave Theory and Techniques*, vol. 61, no. 9, pp. 3417-3423, Sept. 2013.
- [80] D. Blackham and K. Wong, "Latest advances in VNA accuracy enhancements," *Microwave Journal*, vol. 48, no. 7, pp. 78-82, Jul. 2005.
- [81] "Specifying calibration standards and kits for Agilent vector network analyzers," *Agilent Technologies Application Note 1287-11*, web address: <http://cp.literature.agilent.com/litweb/pdf/5989-4840EN.pdf> (28th Apr. 2014).
- [82] A. M. E. Safwat and L. Hayden, "Sensitivity analysis of calibration standards for SOLT and LRRM," in *58th ARFTG Conference Digest*, San Diego, CA, USA, Nov. 29-30, 2001, pp. 1-10.
- [83] H. I. Atasoy, M. Unlu, K. Topalli, I. Istanbuluoglu, E.U. Temocin, O. Bayraktar, S. Demir, O. Civi, S. Koc, and T. Akin,

- “Investigation of on-wafer calibration accuracy dependence on transitions and probe positioning,” in *Proceedings of 36th European Microwave Conference*, Manchester, UK, Sept. 10-15, 2006, pp. 1582-1585.
- [84] “A guide to better vector network analyzer calibrations for probe-tip measurements,” *Cascade Microtech Technical Brief*, web address: http://www.home.agilent.com/upload/cmc_upload/All/TECH BRIEF4.pdf (28th Apr. 2014).
- [85] web address: <http://www.cmicro.com/products/probes/wincal-xe> (12th Dec. 2013).
- [86] D. F. Williams and R. B. Marks, “Comparison of on-wafer calibrations,” in *38th ARFTG Conference Digest*, San Diego, CA, USA, Dec. 5-6, 1991, pp. 68-81.
- [87] M. Nishimoto and J. Laskar, “Study of millimeter-wave on-wafer calibration techniques and effect upon HEMT parameter extraction,” in *43rd ARFTG Conference Digest*, San Diego, CA, USA, May 27, 1994, pp. 19-23.
- [88] M. Nishimoto, J. Laskar, and R. Lai, “On-wafer calibration techniques and applications at V-band,” *IEEE Microwave and Guided Wave Letters*, vol. 4, no. 11, pp. 370-372, Nov. 1994.
- [89] J. Pla, M. Struble, and F. Colomb, “On-wafer calibration technique for measurement of microwave circuits and devices on thin substrates,” in *IEEE MTT-S International Microwave Symposium Digest*, Orlando, FL, USA, May 16-20, 1995, pp. 1045-1048.
- [90] “Technique verifies LRRM calibrations for GaAs measurements,” *Cascade Microtech Technical Brief*, 1994.
- [91] A. J. Lord, “Comparing the accuracy and repeatability of on-wafer calibration techniques to 110 GHz,” in *Proceedings of 29th European Microwave Conference*, Munich, Germany, Oct. 5-7, 1999, pp. 28-31.
- [92] F. Braun, “Über die Stromleitung durch Schwefelmetalle,” *Annalen der Physik und Chemie*, vol. 156, pp. 556-563, Nov. 1874.
- [93] W. Schottky, “Halbleitertheorie der Sperrschicht,” *Naturwissenschaften*, vol. 26, p. 843, Dec. 1938.
- [94] S. M. Sze and K. K. Ng, *Physics of Semiconductor Devices*, 3th ed., John Wiley & Sons Inc., Hoboken, NJ, USA, 2007.
- [95] M. Shur, *GaAs Devices and Circuits*, Plenum Press, New York, NY, USA, 1987.
- [96] W. L. Bishop, K. McKinney, R. J. Mattauch, T. W. Crowe, and G. Green, “A novel whiskerless Schottky diode for millimeter and

- submillimeter wave applications,” in *IEEE MTT-S International Microwave Symposium Digest*, June 9-11, 1987, pp. 607-610.
- [97] D. G. Garfield, R. J. Mattauch, and S. Weinreb, “RF performance of a novel planar millimeter-wave diode incorporating an etched surface channel,” *IEEE Transactions on Microwave Theory and Techniques*, vol. 39, no. 1, pp. 1-5, Jan. 1991.
- [98] J. L. Hesler, “Planar Schottky diodes in submillimeter-wavelength waveguide receivers,” Ph.D. dissertation, School of Engineering and Applied Science, University of Virginia, Charlottesville, United States, 1996.
- [99] P. Sobis, “Advanced Schottky diode receiver front-ends for terahertz applications,” Ph.D. dissertation, Department of Microtechnology and Nanoscience, Chalmers University of Technology, Gothenburg, Sweden, 2011.
- [100] A. Y. Tang, “Modelling and characterisation of terahertz planar Schottky diodes,” Ph. D. dissertation, Department of Microtechnology and Nanoscience, Chalmers University of Technology, Gothenburg, Sweden, 2013.
- [101] S. A. Maas, *Microwave Mixers*, Artech House, Nordwood, MA, USA, 2002.
- [102] V. S. Möttönen, J. Mallat, and A. V. Räisänen, “Characterisation of European millimeter-wave planar diodes,” in *Proceedings of 34th European Microwave Conference*, Amsterdam, The Netherlands, Oct. 12-14, 2004, pp. 921-924.
- [103] H. Norde, “A modified forward I-V plot for Schottky diodes with high series resistance,” *Journal of Applied Physics*, vol. 50, pp. 5052-5053, July 1979.
- [104] R. M. Cibils and R. H. Buitrago, “Forward I-V plot for Schottky diodes with high series resistance,” *Journal of Applied Physics*, vol. 58, pp. 3655-3657, Nov. 1985.
- [105] S. K. Cheung and N. W. Cheung, “Extraction of Schottky diode parameters from forward current-voltage characteristics,” *Journal of Applied Physics*, vol. 49, pp. 85-87, July 1986.
- [106] T. C. Lee, S. Fung, C. D. Beling, and H. L. Au, “A systematic approach to the measurement of ideality factor, series resistance, and barrier height for Schottky diodes,” *Journal of Applied Physics*, vol. 72, pp. 4739-4742, Nov. 1992.
- [107] T. Kiuru, J. Mallat, A. V. Räisänen, and T. Närhi, “Schottky diode series resistance and thermal resistance extraction from S-parameter and temperature controlled I-V measurements,” *IEEE Transactions on Microwave Theory and Techniques*, vol. 59, no. 8, pp. 2108-2116, Aug. 2011.
- [108] T. Kiuru, “Characterization, modeling, and design for applications of waveguide impedance tuners and Schottky

- diodes at millimeter wavelengths,” Doctoral thesis, Aalto University, School of Electrical Engineering Department of Radio Science and Engineering, Espoo, Finland, 2011.
- [109] P. B. Winson and S. D. Pritchett, “On-wafer GaAs Schottky diode characterization using an integrated pulse I-V/pulse S-parameter measurement system,” in *38th ARFTG Conference Digest*, Florida, USA, Dec. 5-6, 1991, pp. 36-43.
- [110] L. Dunleavy, W. Clausen, and T. Weller, “Pulsed IV for non-linear modeling,” *Microwave Journal*, Mar. 2003.
- [111] S. Khanal, “Pulsed and transient characterization of THz Schottky diodes,” Master’s Thesis, Aalto University, School of Electrical Engineering Department of Radio Science and Engineering, Espoo, Finland, 2012.
- [112] C. D. Wang, C. Y. Zhu, G. Y. Zhang, J. Shen, and L. Li, “Accurate electrical characterization of forward AC behavior of real semiconductor diode: giant negative capacitance and nonlinear interfacial layer,” *IEEE Transactions on Electron Devices*, vol. 50, no. 4, pp. 1145-1148, Apr. 2003.
- [113] H. Xu, G. S. Schoenthal, L. Liu, Q. Xiao, J. L. Hesler, and R. M. Weikle II, “On estimating and canceling parasitic capacitance in submillimeter-wave planar Schottky diodes,” *IEEE Microwave Wireless Components Letters*, vol. 19, no. 12, pp. 807–809, Dec. 2009.
- [114] T. Kiuru, K. Dahlberg, J. Mallat, A. V. Räisänen, and T. Närhi, “Comparison of low-frequency and microwave frequency capacitance determination techniques for mm-wave Schottky diodes,” in *Proceedings of 6th European Microwave Integrated Circuits Conference*, Manchester, UK, Oct.10-11, 2011, pp. 53-56.
- [115] J. -M. Dieudonne, B. Adelseck, K. -E. Schmegner, R. Rittmeyer, and A. Colquhoun, “Technology related design of monolithic millimeter-wave Schottky diode mixers,” *IEEE Transactions on Microwave Theory and Techniques*, vol. 40, no. 7, pp. 1466-1474, July 1992.
- [116] D. Salameh and D. Linton, “Study of the relation between doping profile and diode CV characteristics,” *IEEE Transactions on Microwave Theory and Techniques*, vol. 47, no. 4, pp. 506-509, Apr. 1999.
- [117] J. Zhang, P. V. Piironen, V. S. Möttönen, J. T. Louhi, A. O. Lehto, A. Simon, C. -I. Lin, and A. V. Räisänen, “Model of a quasi-vertical planar anti-parallel Schottky diode,” in *International Conference on Microwave and Millimeter Wave Technology*, China, Aug. 18-20, 1998, pp. 130-133.
- [118] A. Y. Tang, V. Drakinskiy, P. Sobis, J. Vukusic, and J. Stake, “Modeling of GaAs Schottky diodes for terahertz application,” in *Proceedings of 34th International Conference on Infrared*,

- Millimeter, and Terahertz Waves*, Korea, Sept. 21-25, 2009, pp. 1-2.
- [119] A. Y. Tang and J. Stake, "Impact of eddy currents and crowding effects on high-frequency losses in planar Schottky diodes," *IEEE Transactions on Electron Devices*, vol. 58, no. 10, pp. 3260-3269, Oct. 2010.
- [120] A. Maestrini, B. Thomas, H. Wang, C. Jung, J. Treuttel, Y. Jin, G. Chattopadhyay, I. Mehdi, and G. Beaudin, "Schottky diode-based terahertz frequency multipliers and mixers," *Comptes Rendus de l'Académie des Sciences, Physique*, vol. 11, no. 7-8, pp. 480-495, Aug. – Oct. 2010.
- [121] A. Karpov, D. Miller, F. Rice, J. A. Stern, B. Bumble, H. G. LeDuc, and J. Zmuidzinas, "Low noise 1 THz – 1.4 THz mixer using Nb/Al-AlN/NbTiN SIS junctions," *IEEE Transactions on Applied Superconductivity*, vol. 17, no. 2, pp. 343-346, June 2007.
- [122] P. Pütz, D. Büchel, C. E. Honingh, K. Jacobs, M. Schultz, and J. Stutzki, "Hot electron bolometer waveguide mixers up to 4.7 THz for the upGREAT focal plane array receiver on SOFIA," in *Proceedings of 38th International Conference on Infrared, Millimeter, and Terahertz Waves*, Mainz, Germany, Sept. 1-6, 2013, pp. 1.
- [123] Y. Kwon, D. Pavlidis, P. Marsh, G. -I. Ng, and T. L. Brock, "Experimental characteristics and performance analysis of monolithic InP-based HEMT mixers at W-band," *IEEE Transactions on Microwave Theory and Techniques*, vol. 41, no. 1, pp. 1-8, Jan. 1993.
- [124] W. R. Deal, K. Leong, V. Radisic, S. Sarkozy, B. Gorospe, J. Lee, P. H. Liu, W. Yoshida, J. Zhou, M. Lange, R. Lai, and X. B. Mei, "Low noise amplification at 0.67 THz using 30 nm InP HEMTs," *IEEE Microwave and Wireless Components Letters*, vol. 21, no. 7, pp. 368-370, July 2011.
- [125] S. A. Maas, *Noise in Linear and Nonlinear Circuits*, Artech House, Norwood, MA, USA, 2005.
- [126] S. A. Maas, *Microwave Mixers*, 2nd ed., Artech House, Norwood, MA, USA, 1993.
- [127] I. D. Robertson and S. Lucyszyn, *RFIC and MMIC Design and Technology*, The Institution of Electrical Engineers, London, UK, 2001.
- [128] P. Lehtinen, J. Mallat, P. Piironen, A. Lehto, J. Tuovinen, and A.V. Räisänen, "A 119 GHz planar Schottky diode mixer for a space application," *International Journal of Infrared and Millimeter Waves*, vol. 17, no. 5, pp. 807-818, May 1996.
- [129] M. Cohn, J. E. Degenford, and B. A. Newman "Harmonic mixing with and antiparallel diode pair," *IEEE Transactions on*

- Microwave Theory and Techniques*, vol. MTT-23, no. 8, pp. 667-673, Aug. 1975.
- [130] S. Marsh, B. Alderman, D. Matheson, and P. de Maagt, "CAD techniques for 183 GHz fixed tuned sub-harmonic mixer using foundry diodes," in *Proceedings of 1st European Microwave Integrated Circuits Conference*, Sept. 10-13, 2006, pp. 91-94.
- [131] P. S. Henry, B. S. Glance, and M. V. Schneider, "Local-oscillator noise cancellation in the subharmonically pumped down-converter," *IEEE Transactions on Microwave Theory and Techniques*, vol. MTT-24, no. 5, pp. 254-257, May 1976.
- [132] Y. -C. Leong and S. Weinreb, "Full band waveguide-to-microstrip probe transitions," in *IEEE MTT-S International Microwave Symposium Digest*, vol. 4, June 13-19, 1999, pp. 1435-1438.
- [133] T. Q. Ho and Y. -C. Shih, "Spectral-Domain analysis of E-plane waveguide-to-microstrip transitions," *IEEE Transactions on Microwave Theory and Techniques*, vol. 37, no. 2, pp. 388-392, Feb. 1989.
- [134] J. W. Kooi, G. Chattopadhyay, S. Withington, F. Rice, J. Zmuidzinas, C. Walker, and G. Yassin, "A full-height waveguide to thin-film microstrip transition with exceptional RF bandwidth and coupling efficiency," *International Journal Infrared Millimeter Waves*, vol. 24, no. 3, pp. 261-284, Mar. 2003.
- [135] Y. Lin, Y. Zhang, R. Xu, J. Xie, and S. Wang, "A compact transition structure integrated with DC feed filter for submillimeter wave application," *IEEE International Symposium on Microwave, Antenna, Propagation and EMC Technologies for Wireless Communications*, Aug. 16-17, 2007, pp. 297-299.
- [136] S. C. Shi and J. Inatani, "A waveguide-to-microstrip transition with a DC/IF return path and offset probe," *IEEE Transactions on Microwave Theory and Techniques*, vol. 45, no. 3, pp. 442-446, Mar. 1997.
- [137] Y. Tikhov, J. -W. Moon, and Y. -J. Kim, "Refined characterisation of E-plane waveguide to microstrip transition for millimeter-wave applications," in *2000 Asia-Pacific Microwave Conference*, Sydney, Australia, Dec. 3-6, 2000, pp. 1187-1190.
- [138] V. S. Möttönen and A. V. Räisänen, "Novel wide-band coplanar waveguide-to-rectangular waveguide transition," *IEEE Transactions on Microwave Theory and Techniques*, vol. 52, no. 8, pp. 1836-1842, Aug. 2004.
- [139] J. Schur, S. Biber, F. Gumbmann, B. Mottet, O. Cojocari, L.-P. Schmidt, and H. -L. Hartnagel, "Micromachined split-block Schottky-diode mixer for 600 GHz," in *Joint 29th International*

- Conference on Infrared and Millimeter Waves and 12th International Conference on Terahertz Electronics*, Karlsruhe, Germany, Sept. 27 – Oct. 1, 2004, pp. 325-326.
- [140] L. Samoska, W. R. Deal, G. Chattopadhyay, D. Pukala, A. Fung, T. Gaier, M. Soria, V. Radisic, X. Mei, and R. Lai, "A submillimeter-wave HEMT amplifier module with integrated waveguide transitions operating above 300 GHz," *IEEE Transactions on Microwave Theory and Techniques*, vol. 56, no. 6, pp. 1380-1388, June 2008.
- [141] A. Tessmann, A. Leuther, V. Hurm, I. Kallfass, H. Massler, M. Kuri, M. Riessle, M. Zink, R. Loesch, M. Seelmann-Eggebert, M. Schlechtweg, and O. Ambacher, "Metamorphic HEMT MMICs and modules operating between 300 and 500 GHz," *IEEE Journal of Solid-State Circuits*, vol. 46, no. 10, Oct. 2011, pp. 2193-2202.
- [142] W. Grabherr, B. Huder, and W. Menzel, "Microstrip to waveguide transition compatible with mm-wave integrated circuits," *IEEE Transactions on Microwave Theory and Techniques*, vol. 42, no. 9, pp. 1842-1843, Sept. 1994.
- [143] W. Simon, M. Werthen, and I. Wolff, "A novel coplanar transmission line to rectangular waveguide transition," in *IEEE MTT-S International Microwave Symposium Digest*, Baltimore, MD, USA, June 7-12, 1998, pp. 257-260.
- [144] J. H. C. Heuen, "A new integrated waveguide-microstrip transition," *IEEE Transactions on Microwave Theory and Techniques*, vol. 24, no. 3, pp. 144-147, Nov. 1976.
- [145] J. Hinojosa, J.F Kruck, and G. Dambrine, "Ridged waveguide to microstrip transition for electromagnetic characterisation of materials in V-band," *IEE Electronic Letters*, vol. 36, no. 17, pp. 1468-1470, Aug. 2000.
- [146] G. C. Dalman, "New waveguide-to-coplanar waveguide transition for centimetre and millimeter wave applications," *IEE Electronics Letters*, vol. 26, no. 13, pp. 830-831, June 1990.
- [147] N. Kaneda, Y. Qian, and T. Itoh, "A broad-band microstrip-to-waveguide transition using quasi-Yagi antenna," *IEEE Transactions on Microwave Theory and Techniques*, vol. 47, no. 12, pp. 2562-2567, Dec. 1999.
- [148] K. M. K. H. Leong, W. R. Deal, V. Radisic, X. Bing Mei, J. Uyeda, L. Samoska, A. Fung, T. Gaier, and R. Lai, "A 340-380 GHz integrated CB-CPW-to-waveguide transition for sub millimeter-wave MMIC packaging," *IEEE Microwave and Wireless Components Letters*, vol. 19, no. 6, pp. 413-415, June 2009.
- [149] R. -Y. Fang, C. -T. Wang, and C. -L. Wang, "A direct CPW-to-rectangular waveguide transition using a dipole slot antenna," in *Proceedings of 39th European Microwave Conference*, Rome, Italy, Sept. 29 – Oct.1, 2009, pp. 157-160.

- [150] J. V. Bellantoni, R. C. Compton, and H. M. Levy, "A new W-band coplanar waveguide test fixture," in *IEEE MTT-S International Microwave Symposium Digest*, Long Beach, CA, USA, June 13-15, 1989, pp. 1203-1204.
- [151] V. S. Möttönen, "Wideband coplanar waveguide-to-rectangular waveguide transition using fin-line taper," *IEEE Microwave and Wireless Components Letters*, vol. 15, no. 2, pp. 119-121, Feb. 2005.
- [152] T. Kiuru, V. S. Möttönen, and A. V. Räsänen, "W-band waveguide impedance tuner utilizing dielectric-based backshorts," *IEEE Transactions on Microwave Theory and Techniques*, vol. 55, no. 8, pp. 1659-1665, Aug. 2007.
- [153] T. Kiuru, K. Dahlberg, J. Mallat, A. V. Räsänen, and T. Närhi, "EH impedance tuner with dielectric-based backshorts for millimeter wave diode testing," in *Proceedings of 40th European Microwave Conference*, Paris, France, Sept. 28-30, 2010, pp.1357-1360.
- [154] T. Kiuru, K. Dahlberg, J. Mallat, A. V. Räsänen, and T. Närhi, "Noncontacting multiwaveguide-band backshort for millimeter wave applications," *IEEE Microwave Theory and Wireless Component Letters*, vol. 20, no. 9, pp. 483-485, Sept. 2010.
- [155] A. V. Räsänen, "Experimental studies on cooled millimeter wave mixers," *Acta Polytechnica Scandinavica*, Electrical Engineering Series, No. 46, Helsinki, Finland, 1980, available at: <http://lib.tkk.fi/Diss/198X/isbn9512283727/> (8th May 2014).
- [156] R. Trambarulo and H. S. Berger, "Conversion loss and noise temperature of mixers from noise measurements," in *IEEE MTT-S International Microwave Symposium Digest*, Boston, MA, USA, May 31-June 3, 1983, pp. 364-365.
- [157] B. Thomas, A. Maestrini, and G. Beaudin, "Design of a broadband sub-harmonic mixer using planar Schottky diodes at 330 GHz," in *Conference Digest of the 2004 Joint 29th International Conference on Infrared and Millimeter Waves, and 12th International Conference on Terahertz Electronics*, Karlsruhe, Germany, Sept. 27 – Oct. 1., 2004, pp. 457-458.
- [158] T. Newman, W. L. Bishop, K. T. Ng, and S. Weinreb, "A novel planar diode mixer for submillimeter-wave applications," *IEEE Transactions on Microwave Theory and Techniques*, vol. 39, no. 12, pp. 1964-1971, Dec. 1991.
- [159] I. Oprea, A. Walber, O. Cojocari, H. Gibson, R. Zimmermann, and H. L. Hartnagel, "183 GHz mixer on InGaAs Schottky diodes," in *Proceedings of 21th International Symposium on Space Terahertz Technology*, Oxford, UK, Mar. 23-25, 2010, pp. 159-160.

- [160] T. Waliwander, M. Crowley, M. Fehilly, D. Lederer, J. Pike, L. Floyd, and D. O'Connell, "Sub-millimeter wave 183 GHz and 366 GHz MMIC membrane sub-harmonic mixers," in *IEEE MTT-S International Microwave Symposium*, Baltimore, MD, USA, June 5-10, 2011, 4 p.
- [161] S. Marsh, B. Alderman, D. Matheson, and P. de Maagt, "Design of low-cost 183 GHz subharmonic mixers for commercial applications," *IET Circuits Devices Systems*, vol. 1, no.1, pp. 1-6, Feb. 2007.
- [162] D. Porterfield, J. L. Hesler, T. W. Crowe, W. L. Bishop, and D. Woolard, "Integrated terahertz transmit / receive modules," in *Proceedings of 33rd European Microwave Conference*, Munich, Germany, Oct. 7-9, 2003, pp.1319-1322.
- [163] B. Alderman, H. Sanghera, C. Price, B. Thomas, and D. N. Matheson, "Fabrication of reproducible air-bridged Schottky diodes for use at frequencies near 200 GHz," *Joint 32th International Conference on Infrared and Millimeter Waves and 15th International Conference on Terahertz Electronic*, Gardiff, UK, Sept. 2 -9, 2007, pp. 848-849.
- [164] I. Mehdi, S. M. Marazita, D. A. Humphrey, T. -H. Lee, R. J. Dengler, J. E. Oswald, A. J. Pease, S. C. Martin, W. L. Bishop, T. W. Crowe, and P. Siegel, "Improved 240-GHz subharmonically pumped planar Schottky diode mixers for space-borne applications," *IEEE Transactions on Microwave Theory and Techniques*, vol. 46, no. 12, pp. 2036-2042, Dec. 1998.
- [165] B. Thomas, A. Maestrini, and G. Beaudin, "A low-noise fixed-tuned 300-360 GHz sub-harmonic mixer using planar Schottky-diodes," *IEEE Microwave and Wireless Components Letters*, vol. 15, no. 12, pp. 865-867, Dec. 2005.
- [166] P. J. Sobis, N. Wadefalk, A. Emrich, and J. Stake, "A broadband, low noise, integrated 340 GHz Schottky diode receiver," *IEEE Microwave and Wireless Components Letters*, vol. 22, no. 7, pp. 366-368, July 2012.
- [167] J. L. Hesler, "Broadband fixed-tuned subharmonic receivers to 640 GHz," in *Proceedings of 11th International Symposium on Space and Terahertz Technology*, Ann Arbor, MI, USA, May 1-3, 2000, pp. 172-178.
- [168] J. Treuttel, B. Thomas, A. Maestrini, H. Wang, B. Alderman, J. V. Siles, S. Davis, and T. Närhi, "A 380 GHz sub-harmonic mixer using MMIC foundry based Schottky diodes transferred onto quartz substrate," in *Proceedings of 20th International Symposium on Space and Terahertz Technology*, Charlottesville, VA, USA, April 20-22, 2009, pp. 251.
- [169] B. Thomas, J. Siles, E. Schlect, A. Maestrini, G. Chattopadhyay, C. Lee, C. Jung, I. Mehdi, and S. Gulkis, "First results of a 1.2 THz MMIC sub-harmonic mixer based on GaAs Schottky diodes for planetary atmospheric remote sensing," in *Proceedings of*

23rd International Symposium on Space and Terahertz Technology, Tokyo, Japan, April 2-4, 2012, pp. 100-102.

Errata

Publication II

In the second paragraph of section IV A. it should read “The reflection coefficients of the match, short, and open standards are calculated from the measured raw data, based on the preliminary extra information about the thru and match, given by Cascade Microtech.”

Publication VI

In Figure 1. terms “H-plane tuner backshort” and “E-plane tuner backshort” have switched places.

Millimeter wave and THz technologies are quickly developing fields. The majority of the applications are still scientific, but also commercial applications become gradually available. The on-wafer S-parameter measurements performed with a vector network analyzer are significant part of the development process of the devices, but the high frequency and on-wafer environment introduce challenges for the calibration and the measurements. One of the most important components in the millimeter wave and THz frequency applications is a Schottky diode. The design of the millimeter wave and THz diode mixers relies heavily on the extracted parameters from the traditional characterisation measurements, e.g. S-parameter measurements. In addition to the traditional characterisation a mixer-based characterisation could be profitable to obtain comprehensive characterisation of Schottky diodes. This thesis focuses on development of on-wafer calibration methods for S-parameter measurements and Schottky diode characterisation at millimeter wave and THz frequencies.



ISBN 978-952-60-5830-6
ISBN 978-952-60-5831-3 (pdf)
ISSN-L 1799-4934
ISSN 1799-4934
ISSN 1799-4942 (pdf)

Aalto University
School of Electrical Engineering
Department of Radio Science and Engineering
www.aalto.fi

**BUSINESS +
ECONOMY**

**ART +
DESIGN +
ARCHITECTURE**

**SCIENCE +
TECHNOLOGY**

CROSSOVER

**DOCTORAL
DISSERTATIONS**